UNIVERSIDADE D
COIMBRA

Petra Catarina Frazão Albuquerque

SYNTHETIC RECEPTORS FOR OPTICAL DETECTION OF DMMP (SARIN SIMULANT)

Dissertação no âmbito do Mestrado em Química Forense, orientada pelo Professor Doutor João Manuel Ferreira Pita Batista Pina e pelo Professor Doutor Guzmán Gil-Ramírez e apresentada no Departamento de Química

July of 2023

Petra Catarina Frazão Albuquerque

Synthetic receptors for optical detection of DMMP (sarin simulant)

Dissertação apresentada para provas de Mestrado em Química Forense

Supervisors:
Professor Guzmán Gil-Ramírez
Professor João Manuel Ferreira Pita Batista Pina

July of 2023

UNIVERSIDADE D
COIMBRA

"Do not think of today's failures, but of the success that may come tomorrow."
Helen Keller

Acknowledgments

I start for acknowledge everyone that helped me personally and professionally in the two years of my Master's in Forensic Chemistry.

First of all, I want to thank to the University of Coimbra and all the professors that gave me lectures in my first year, and a special thank you to Professor Maria Ermelinda da Silva Eusébio, manager of the master's and to the Professor João Manuel Ferreira Pita Batista Pina, my co-supervisor during my second year, for all the patience and advice.

Secondly, thanks to the University of Lincoln, United Kingdom, for having warmly welcomed me to their University so that I could carry out the necessary research for the writing of this project. An especial thank to my supervisor Professor Guzmán Gil-Ramírez for his tireless and crucial help during this last year. Not only his support in the project but also his advice for my integration in another country.

Related to the latest a group of people helped me to grown in another language and country, thank you to, Professor Jose Gonzalez-Rodriguez, my co-workers, friends, flatmates, and my stunt group of my cheerleading team. From them I want to give an especial acknowledgment to, James Disley, Jake Tomlinson, Mohammad Baqer, Roberta Carusone and Elizabeth Brigden. Can't forget to thank my Portuguese friends with an especial thank you to Pedro Matias for his readiness to help me when I need it.

Last but not least important, I would like to acknowledge my family, whom without I couldn't never do my master's or even go in an adventure of doing research in another country. Thank you for all the love, support and mainly for believing in me. Thank you mom, thank you grandma.

General Index

Figures Index

Tables Index

Schemes Index

Abbreviations and nomenclature

The nomenclature used in this project are the one followed by the scientific community and the IUPAC rules, having also included abbreviations to facilitate the reading of the project.

Abs. – absorbance

ACh – Acetylcholine

AChE – Acetylcholinesterase

BODIPY – Boron-dipyrromethene

$CHCl_3$ – Chloroform

$CHCl_3$-d – Deuterated $CHCl_3$

CN – Cyanide

CWA – Chemical Warfare Agents

CWC – Chemical Weapons Convection

DCM – Dichloromethane

DEPT – Distortionless Enhancement by Polarization Transfer

DFT – Density Functional Theory

DMMP – Dimethyl Methylphosphonate

DMSO – Dimethylsulfoxide

DMSO-d_6 – deuterated DMSO

eq. – equivalent

ESI-MS – Electrospray Ionization-Mass Spectroscopy

Et_3NH – Triethylamine

EtOH – ethanol

$Eu(OTf)_3$ – europium (III) trifluoromethanesulfonate

Exp. no – experiment number

G – Guest

GA – Tabun

GB – Sarin

GC-MS – Gas Chromatography – Mass Spectrometry

GD – Soman

GF – Cyclosarin

H – Host

H-bonds – Hydrogen bonds

I1 to I3 – Italian's ligand 1 to 3

IUPAC – International Union of Pure and Applied Chemistry

K– binding constant (M)

L – Luminescence

L1 to L3 – Ligands 1 to 3

LC_{50} – Lethal Concentration to kill 50 % of the population

LD – Lethal Dose

LG – Leaving Group

Ln – Lanthanides

LoD – Limit of Detection

LPA – Lysophosphatidic Acid

MeCN – Acetonitrile

MeCN-d_3 – Deuterated MeCN

MeOH – methanol

MIP – Molecularly Imprinted Polymer

ML_2 – 1 metal : 2 ligand

ms – milliseconds

NAs – Nerve Agents

NMR – Nuclear Magnetic Resonance

NT – Neurotransmitter

OPCs – Organophosphorus Compounds

OPCW – Organization of Prohibition of Chemical Weapons

OPIDP – Organophosphate-Induced Delayed Polyneuropathy

PPh_4 – tetraphenylphosphonium

PPh_4Br – tetraphenylphosphonium bromide

QY – Quantum Yield (%)

r. t. – room temperature

SAW – Surface Acoustic Wave

SD – Standard Deviation

SE – Standard Error

SiNR-FETs – Silicon Nanoribbon Field-Effect Transistors

UO_2 – uranyl

UV-Vis – Ultraviolet-Visible

WWI – World War I

$Zn(AcO)_2$ – Zinc acetate

The symbols used in this project are the followings:

Δ – right-handed rotation of the helix in the ligands **L1** to **L3**

ε – molar absorption coefficient (M^{-1} cm^{-1})

Λ – left-handed rotation of the helix in the ligands **L1** to **L3**

τ – lifetime (ms)

The abbreviations, nomenclature and units related to the NMR experiments are the followings:

br – broad

^{13}C – carbon-13

COSY – ^{1}H-^{1}H Correlation Spectroscopy

d – doublet

dd – doublet of doublets

^{1}H – proton

HMBC – Heteronuclear Multiple Bond Correlation

HSQC – Heteronuclear Single Quantum Coherence

Hz – Hertz

J – Coupling constant

m – multiplet

ppm – part per million

ROE – Rotating-frame Overhauser Effect

s – singlet

t – triplet

td – triplet of doublets

Resumo

Apesar da origem e da demanda de destruição das reservas de *Chemical Warfare Agents* (CWA) até 2007 ter sido acordada, estes ainda se encontram ligados a atividades criminais. Foram usados para cometer suicídios em 13.7% dos casos no mundo entre 2010 e 2014, estando associados a ataques terroristas como forma de espalhar o pânico ou como declaração política, tendo ocorrido assassinatos de pessoas em países como Iraque, Japão, Irão, Malásia, Síria e Inglaterra.

CWA dividem-se em diferentes grupos, dentre os quais se encontram os *Nerve Agents* (NAs), estes são compostos organofosforados (OPCs) que podem levar a vários problemas de disfunções, tais como do miocárdio, cognitivas ou neuropsiquiátricas, culminando eventualmente em morte. No entanto, encontram-se na literatura alguns tipos de tratamentos como *bioscavengers*, que apenas atuam como neutralizadores das reações destes. Um dos mais nefastos e o que será o analito deste projeto é o Sarin (GB), um agente da série G (uma das quatro séries de NAs).

Desde a descoberta do seu nível de toxicidade, tem vindo a ser feitos diversos estudos como contramedidas, na área de tratamento e métodos de destruições das suas reservas. Os métodos de destruição das reservas de GB usados atualmente são o de inceneração ou neutralização com solução aquosa de hidróxido de sódio.

No entanto, apesar das proibições estabelecidas pela *Chemical Weapon Convection* (CWC), ainda continuam a ser reportados ataques usando CWA, incluindo o uso de GB. Isto continua a acontecer provavelmente devido ao processo relativamente simples de síntese, portanto continua a ser necessária a pesquisa por detetores rápidos, robustos, precisos, portáteis e fácil de utilizar.

Neste projeto foi usado como analito o *dimethyl methylphosphonate* (DMMP) para mimetizar o Sarin, devido à impossibilidade de trabalho com o próprio Sarin. Foram então sintetizados uma série de ligandos capazes de formar complexos metálicos e posterior avaliação do comportamento de ligação dos complexos metálicos de zinco (Zn) e európio (Eu) relativamente ao DMMP. A estrutura dos ligandos foi realizada com diferentes variantes dos ligandos salen. Recetores de ligandos similares ao salen tem sido atualmente descritos como sensores de DMMP promissores devido à sua afinidade.

Mantida a estrutura do sensor (ligandos salen) foram realizadas substituições do centro metálico de Zn por Eu, testando diferentes quiralidades, grupos substituintes e contra-iões, estabelecendo-se numa estequiometria de 2:1 em vez de 1:1 (ligando : metal). Sendo assim criadas duas famílias de complexos, **L1** e **L2** apresentando o Eu como metal e a família **I1** e **I2** com o Zn como metal. A alteração do centro metálico tem como propósito tirar proveito da luminescência característica dos lantanídeos. Do európio em específico por apresentar uma luz vermelha sob radiação ultravioleta. As sínteses no geral foram bem sucedidas, tendo-se realizado titulações de UV-Vis, RMN e fluorescência.

Os dados recolhidos das diferentes titulações demonstram uma constante de ligação mais alta para a família de complexos **L1** e **L2** com Eu do que as relatadas na literatura para os compostos da família **I1** e **I2**.

Para além dos valores altas das constantes de ligação dos complexos sintetizados, estes compostos não apresentam mais seletividade do que aqueles relatados na literatura.

Palavras-chave: CWA, DMMP, európio, titulações, sensor

Abstract

Despite the genesis of Chemical Warfare Agents (CWA) and the demand of dismantling of the stockpiles by 2007 they are still involved with criminal activity. They were used in 13.7% of the total suicides in the world between 2010 and 2014, associated with terrorist attacks to spread panic or as a politic statement murdering people in some countries like Iraq, Japan, Iran, Malaysia, Syria and England.

CWA can be subdivided in different groups, being one of them the Nerve Agents (NAs), that are organophosphorus compounds (OPCs). The exposure to them can lead to several health problems like myocardial, cognitive, and neuropsychiatric malfunctions, and ultimately to death. However, is already in literature some types of treatment like bioscavengers, that only lead to a neutralization of their reaction. One of the most dangerous and the analyte of this project is Sarin (GB), a G-agent (one of the four series of NAs).

Since the discovery of its toxicity has been made several countermeasure studies, for treatment and method of destruction of the stockpiles. For GB the destruction is by incineration or neutralization with aqueous sodium hydroxide.

However, besides the prohibitions of Chemical Weapons Convection (CWC), the use of CWA, especially GB continues to be reported, probably due to the relatively simple process of synthesis. Justifying the need to continue the research for quick, reliable, accurate, portable, and easy to use detectors.

In this project dimethyl methylphosphonate (DMMP) was used as a simulant of Sarin, due to the impossibility of working with Sarin itself. A series of ligands capable of forming metal complexes were synthesized and the binding behaviour towards DMMP of their metal complexes with Zn and Eu was evaluated. The ligand's backbone was based on variants of salen ligands. The similar zinc receptors have been currently described as promising sensors for DMMP due to their affinity.

It was made a replacement in the metal center from Zn to Eu and kept the backbone of the sensor (salen ligand), testing different chiralities, substituent groups and counterions, establishing a 2:1 stoichiometry instead of a 1:1 (ligand : metal). It was made two family of complexes, Eu as the metal for **L1** and **L2** and Zn as the metal for **I1** and **I2**. The change of the metallic center is to use the distinct feature of the luminescence of the lanthanides. Specifically, Eu that presents a red colour under the UV light. The synthesis was overall successful, being able to be realized UV-Vis, NMR, and fluorescence titrations.

The data collected from the various titrations indicate a larger binding constant in the family of complexes **L1** and **L2** with Eu, than the ones reported in the literature, and from the family of complex **I1** and **I2**.

Besides the large values of the binding constant the complexes synthesized do not show more selectivity from the ones reported in the literature.

Keywords: CWA, DMMP, europium, titrations, sensor

Chapter 1

Introduction

1.1 CWA and their history

Throughout the centuries human race has been in war between themselves, only changing the means and scale of violence. However, the XX century marks an important development in the means used in the war. Prior the World War I (WWI) was already some exploitation of chemicals to use in war but it was only in WWI the first massive use of chemicals and war, that later would be called chemical warfare agents (CWA).[1]

While the development of these weapons was happening, it was also being researched about defensive countermeasures, entering in a circle of producing deadlier chemicals. However, the most known and toxic CWA wasn't discovered with that purpose in the beginning. For better understanding, the CWA is a wide class of compounds, so they can be classified in three different ways. Based on their main effect when in realistic concentrations, by their physicochemical properties or the most common way based on the physiological effects. Following this last one, they can be classified in 6 types: vesicants (blister agents), lung injurants (choking agents), blood agents, irritants (skin, eye and respiratory), incapacitants, and nerve agents (NAs).[1]

The NA are the most dangerous of the synthetic chemical derivates, and they are all organophosphorus compounds (OPCs). However, not all OPCs are NAs, these ones have a potent action in the nervous system of our body, mainly on the acetylcholinesterase (AChE).[2, 3, 4, 5] They can be divided into four different types: G-agents (German-agents), V-agents (Venomous-agents), GV-agents and A-agents or Novichock-agents.[4]

After WWI, 1936, in Germany the scientist Gerhardt Schrader who worked in an industrial laboratory was developing new organophosphorus insecticides when created a more toxic than expected compound, than later would be called Tabun. After his discovery it was presented to the military, starting secretly working on new compounds to be weaponized.[1] Two years before was created a more potent compound, Sarin,[2] name given by the scientists involved, Gerhard Schrader, Otto Ambros, Gerhard Ritter, and Hans-Jürgen von der Linde[1]. By the end of 1948 they already had developed two more of this type of G-agents.[2] This first series of NA agents has then four different agents, Tabun (GA), Sarin (GB), Soman (GD) and Cyclosarin (GF). They are non-persistent and have a lethal concentration (LC_{50}) of 2 ppm, 1.2 ppm and 0.9 ppm respectively for the first three.[5]

Later were developed the V-agents in which theirs structures mimics the natural neurotransmitter (NT) of the body[1] to increase affinity for enzymes, that could lead to an anaphylactic shock. In this category are included VE, VG, VM, VX and this last one can be subdivided as Chinese VX and Russian VX. They are one of the important persistent agents.[1, 5]

The third type of agent series are the GV that is a combination of the structures of the Tabun and Sarin with V-agents.[1, 5]

The fourth one is the Novichock or A agents,[5] some of that agents are A230, A232, A234, Novichok-5. Initially they were just unitary agents (just the active agent) but the last one it's already binary (with two agents, one being the precursors that activates the second one)[4], what would help to increase the stability of storage of the compound. The same was tried to do with others NAs. They were release in the 70s with the aim of compromise the defensive countermeasure that were been made.[1]

The G and V-agents are the most known, and so they have distinct features. The G are less toxic and non-persistent (more volatile) as it was already mentioned, and the V are in part more toxic because they are also persistent (takes more time to completely volatile). However, they both release volatile fluoride when the hydrolysis occurs and have a stereogenic phosphorus that makes stereoisomers compounds. The agents of both series present two enantiomers, excluding the soman that have more than two enantiomers because it has two, and not just one, chiral atoms. The chirality of these compounds is very important for determination and detection of toxicity.[4]

Getting back again specifically to the G-agents, they have a very simple structure as can be seen on the ***figure 1*** below.

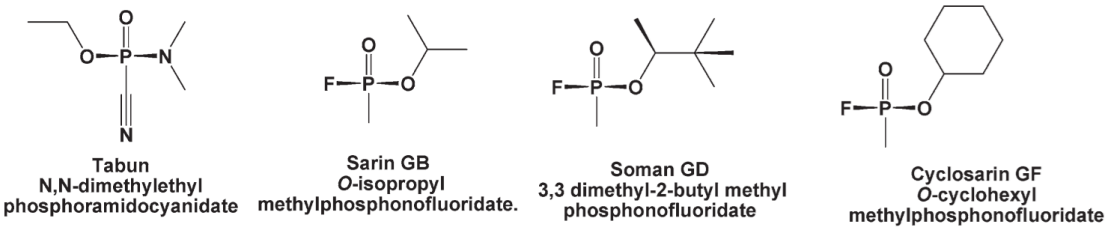

Figure 1. *Structure of G-agents and the respective IUPAC names.*[2]

Excluding the Tabun, that is the less effective and eventually became redundant[1], the other three only present differences in the group attached to the single bond O-P. The key feature of these compounds is the fluorine (F) because of its capacity to be a good leaving group (LG).

The most common way of OPCs to enter the human body is by respiration or skin and eyes absorption. They cross the respiratory epithelial and dermal membrane facilitating the distribution, that can also reach the fat tissues and in cases of suicide the gastric muscles.[4]

The dissemination method is also very important and will affect the effectiveness of CWA. For example, in the attack of the subway in Tokyo by the religious cult Aum Shinrikyo (also known as Supreme Truth) they had 20 Kg of crude Sarin. Because of the crudeness of the compound, it was a slow dissemination and only twelve people killed despite all the casualties. The attack could had been worse if it would have been released in gaseous form.[1, 6]

After these compounds enter the human body, they will interact mainly with the enzyme AChE, suffering biotransformation that generates their active form.[4] This enzyme is responsible for

the degradation of the acetylcholine (ACh), a NT involved with path in the central and peripherical neuronal system, such as the contraction/relaxation of muscles. When the OPCs find the AChE, they will conduct a selective and catalytic chemical reaction between the residues of aminoacids of the binding site, forming, most of them, an irreversible bond[1, 3, 4, 5] as shown in the ***figure 2***. The process of the unavailability of the binding site, is called "aging" of the enzyme. It involves reaction of OPCs with a serine residue at the binding site of the AChE. That reaction will phosphorylate the enzyme, instead of acetylation that occurs when the reaction is with the ACh.[2] As a result the enzyme gets trapped in an irreversible inactive state caused by the loss of the LG from the OPC (normally a halogen like F or cyanide, CN[1]), becoming impossible to hydrolyse ACh. This process can have different rates depending on the stereochemistry of the NA used.[4] Due to the stereogenic phosphorus of the NA, different stereoisomers react with AChE at different rates what will result in also different toxicological properties.[1]

As a result, the accumulation of ACh will arrive to the post-synaptic neuron and cholinergic receptors, muscarinic and nicotinic, saturating them in a permanent way. This leads to a cholinergic crisis that originates severe health issues, as neuromuscular paralysis culminating in dead due anaphylactic shock.[1, 3]

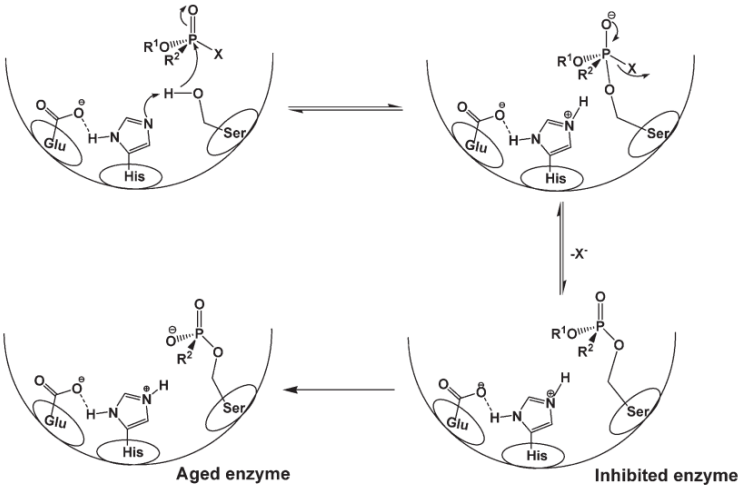

Figure 2. *Scheme of the reaction of OPCs with the binding site of AChE.*[2]

Besides AChE inhibition being the most well-known way of NA interaction, not all symptoms could be explained through this pathway. To account for them, the theory of the non-cholinergic effects appeared.[1,3] One of the non-cholinergic pathways could be explained by the hyperstimulation of the endocannabinoid system. Triggering a retrograde signaling pathway causing a delay on the saturation of the cholinergic receptors and creating non-cholinergic toxicity.[1] Other non-cholinergic effects may display other types of neurotoxicity such as organophosphate-induced delayed polyneuropathy (OPIDP), oxidative stress, and the inhibition of other enzymes, as esterases.[4]

Due to all the consequences displayed above, some countries developed an organization to prevent the use of warfare agents known as The Organization of Prohibition of Chemical Weapons (OPCW). This organization drafted the CWC in 1992, being signed in 1993, an in April of 1997 [2] started to be implemented, as a way to globally supervise chemical weapons in a way to permanently eliminate and check them.[4] Whoever they persist around the world and need our attention and study.[7]

1.2 Properties of G-agents and simulants

The series of G-agents started in Germany with Tabun, and then Sarin, a more volatile and potent compound that was developed after multiple molecular modifications. Soman was developed after the Sarin and is less volatile than it, and lastly the Cyclosarin that has an intermediate volatility of the last two and wasn't weaponised just alone. Other countries like the USA tried to develop similar compound but were less potent than Tabun. Decades after they developed the V-agents in partnership with Canada, and the Soviet Union developed similar compounds around the same time.[1]

The G-agent Sarin and the V-agents VX and RVX (V-agent designed by the Soviet Union) are the favorites of the arsenals in the modern era. That's due not only to the relatively simple process of production[8] but also related to the close physicochemical properties to the ideal for an agent.[1]

The V-agents are persistent and act in hours, these types of agents, as the G ones, are easily volatilized once they are mixed with water or most of the others organic solvents. More specifically the G-agents are highly volatile with 576-22 000 mg/m^3 at 25ºC, and the V agents have just 3-30 mg/m^3 at the same temperature.[5, 9] What makes the G-agents, as Sarin easier to disseminate compared to the V ones.[1]

Sarin is a compound with a boiling point of 150ºC and 18 700 mg/m^3 at 25ºC, depending on the temperature to volatilize and characterized by his moderate to high vapor pressure (2.10 mmHg at 20ºC and 16 4000 to 22 000 mg/m^3 at 25ºC)[2]. Its best way of dissemination is in gas form, near to the ground and in the morning. The reason is because in the morning the cold air lays near the ground, preferentially with no turbulence, to maximize the damage. It was tried a technique called thickening (basically the increase of the viscosity) in the Sarin to allow use it in munitions, also making the decontamination more difficult.[1] However not only the temperature but the pH can alter the half-life (time that takes to evaporate 50% of the compound) of this compound. For instance, at 25ºC and pH = 6.5, its half-life is 237h and at pH = 7.5 it drops to 24h. However when the temperature drops to 0ºC and the half-time increases, reaching 8 300h.[2]

In 2001 were reported 15 thousand tonnes of Sarin to the OPCW from stockpiles, the second most large number, only losing to RVX.[1] The destruction of the stockpiles of CWA is an on-going task[2] and because of the fast advances in life sciences the concern about the development of new agents is growing.[1] Due to it and the report of the first evidence of use of Sarin made in the middle

east only four years after its attack[1], proves that this type of research is still worth it, at least to help give answers, closer, and rest to the mind of people.

Not only the destruction of CWA, or the development of sensors (as will be explained below) have the attention of the scientific community. There is also a part that researches on treatment strategies, like using bioscavengers (biopharmaceuticals that inactivate highly toxic compounds), that can be three types: stoichiometric, catalytic or pseudocatalytic.[4]

After realizing the small lethal dose (LD) limit and the nefarious and extreme effects of these compounds, can't be used NAs, not even for research purposes. That only makes harder the progress of science in the way of finding cures and ways of detection. In consequence, a group of compounds called mimics/simulants/surrogates were developed. These compounds usually are less expensive, and have a lower toxicity[2], they have a similar geometry but a very important change that make them of lower risk that is the change on the removal of a good leaving group (LG), the fluorine (F) and the cyanide (CN).[5] The simulants can be known pesticides too, but the most well-known, the best one, and one that is used the most in studies is the dimethyl methylphosphonate DMMP (***figure 3***).[2, 3, 5] The DMMP is still a OPC and toxic, not as much as GB, because for example, the methoxy group is less of a good leaving group than fluorine. Even with this change and the change of the other bulk substitute for only a methyl group, losing the compound the chirality, the surrogate is still able to react with the AChE and so inhibit it[10].

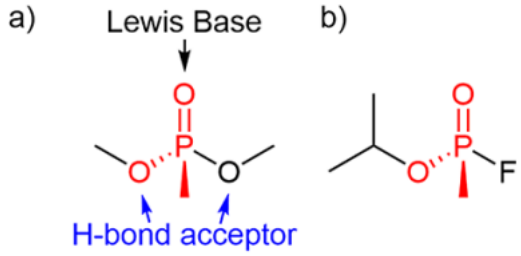

Figure 3 *Structure of a) DMMP and b) sarin, and at orange the common structure. Adapted from Disley et al.[10]*

1.3 Detection, salen ligands and metals

The detection of CWAs and simulants has gained relevance in the scientific literature in the last few years using different methods, better suited to field situations. In contrast to time consuming and expensive techniques such as gas chromatography or mass spectroscopy, which are highly sensitive useful techniques it has been developed portable sensors as a better strategy that can be carried to the field.[9]

In the recent years, different methods for the chemical detection of OPCs have been developed based on: chemical sensors based on silicon nanoribbon field-effect transistors (SiNR-FETs), surface acoustic wave (SAW) devices, coordination complexes containing ligands, chemiresistive sensors and mesoporous silica material containing BODIPY derivatives. More

recently, a focus for these two approaches has grown: a covalent approach and a supramolecular approach.[5] The first one is based on a covalent reaction between the P = O group of the analyte and the sensors, and this bond can be quantified after the interaction through emission fluorescence spectroscopy or ultraviolet-visible (UV-Vis) absorption.[3, 5, 9] It has some limitations like for example the fact that each sensor is only able to do one detection because it gets destroyed once in touch with the detection device, but it still presents a low selectivity because of the false positives.[3] The second approach it's more recent and also less developed.[9] This one will be explored in the context of this project and focus on the use of sensors working with recognition of reversible non-covalent interactions. It does present an advantage over the former approach, because the sensors can be reused after being exposed to the simulant.[5] These non-covalent interactions can be just one or combination of several in what is known as multi-topic recognition. This is an extreme advantage to distinguish different analytes, since it can be a more selective approach, although more difficult to achieve.[9]

Some of the more relevant non-covalent interactions for OPCs are hydrogen bond interactions and Lewis acid-base interactions, these interactions are going to be between the P=O group of the simulant and a Lewis acidic (an acceptor of a pair of electrons) with the metal center in the sensors.[9]

This supramolecular approach has gained attention recently, in particular using metal complexes with salen-type ligands. A literature survey shows results of aluminum salen complexes for sarin and soman detection through electrospray ionization – mass spectroscopy (ESI-MS)[5], and more recently using uranyl-salen complexes, that make two interactions, that being between the uranyl and the oxygen from the P=O bond and small hydrogen-bond interactions. However, the uranyl ion cause quenching to the free ligand fluorescence, making difficult using fluorescence spectroscopy, uranyl was replaced for Zinc (II).[3]

Metal-salen complexes are known in literature as catalysts and supramolecular hosts, the acidic metallic centre can be used for recognition with Lewis bases. The latest ability it will be relevant to this work.[9]

There are a couple of derivates of salen ligand complexes are reported in the literature for detection of DMMP, e.g., based in uranyl (UO_2), and zinc (Zn), which can coordinate to different salen ligands, with different substituents, like Zn-5but or Zn-3OH (***figure 4***)[3], or Zn oligomers in different lengths (***figure 5***)[9].

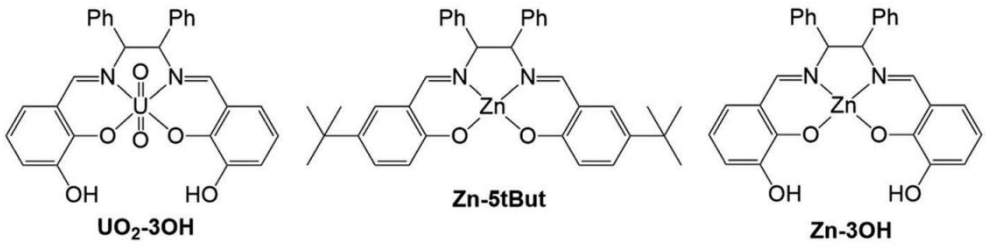

Figure 4. *Structures of different types of salen ligands complexes. Adapted from Puglisi et al.*[3]

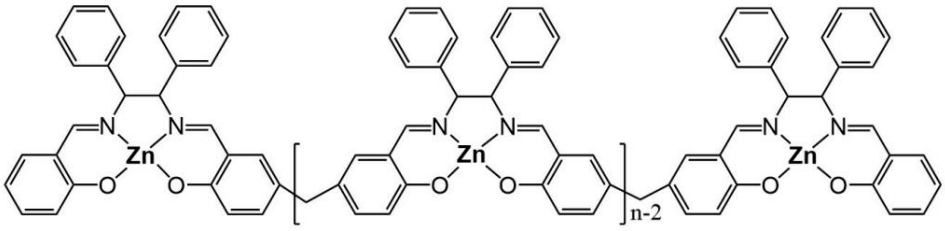

Figure 5. *Oligomers of salen ligands with zinc as a metal. Adapted from Puglisi et al.* [9]

Puglisi *et al.* reported that receptor UO_2-3OH (***figure 4***) interacts with the P=O group of the DMMP forming two hydrogen-bonds (H-bonds) between the sensor (host) and the analyte, DMMP (guest), which couldn't be easily monitored using luminescence due to the quenching ability of the uranyl group. In consequence, the uranyl was substituted for Zn and modifications of the salen ligand were performed, for testing the importance of the H-bonds. The new host, Zn-3OH, had better results than the uranyl-ligand, with a binding constant of log *K* of 5.04, the highest value to recognize DMMP, compared to other two derivatives having values of log *K* 4.35 and 4.33. Consequently they gained an easy way to detect and selectivity.[3] They were also carried out some experiments, with some positive results, in selectivity and competitive experiments with atmospheric air, however, it should be done with some real interferences of compounds with P=O bonds, like pesticides for example. They weren't reported any value for limits of detection (LoD) by Puglisi *et al.* The promising results of the binding constant were corroborated by a ROE (Rotating-frame Overhauser Effect, an NMR technique) that DMMP stablish two types of contact with the Zn-3OH complex, counting three binding sites. The main one is the interaction of the oxygen from the P=O with the metal (Zn) and the other two are the hydrogen bonds of the hydroxyl groups with the phosphodiesteric oxygens of the DMMP.[3]

In 2019, the same authors reported a modification of the receptor with two major differences. The first one was removing the possibility of H-bonds due to the ligand not having the hydroxyl groups, and in the second one the hosts were made in a non-monomeric way, three oligomers with different lengths. They have LoD of 1μM[9] for the receptors with the possibility to detection DMMP in the order part per million (ppm). All the oligomers showed affinity for the

DMMP while the largest affinity was displayed by the oligomer with the 4 units (n=4), with a binding constant log *K* of 5.69 which is higher than the ones previously reported for the monomers. They also carried out the same type of experiments with atmospheric air, with an equally positive outcome, not having any effect on emission profile of the experiments. These studies are thought for detection in solid state.[9]

As showed in the previous examples, in the scientific community has been growing an interest for the study of metal-containing systems to incorporate in a sensor. Metals can be useful in the achievement of selectivity and simultaneously perform degradative processes, due to their catalytic properties even at a low temperature.[2]

Rare earth elements (lanthanides, scandium and yttrium) since the discovery of their singular feature of distinct and stable emission colours[11] were extensively studied and made part of very different fields, presenting themselves well described in literature.[12] Rare earths have a wide range of applications in magnetic and optical devices, since as catalysts in organic synthesis,[13] luminesce probes in biosciences, until security inks and telecommunications.[12]

One of the key features of this type of compounds, is their photoluminescence properties. Luminescence is the emission of light by a compound or material after being irradiated with photons. There is two competitive types of luminescence, fluorescence, or phosphorescence, the former being a fast and spin-allowed process and the latter a slow and spin-forbidden process. Both types can be observed in lanthanide (Ln) ions, even at the same time. Lanthanide ions display very low luminescence ($L = QY \times \varepsilon$), being L the luminescence, due to their forbidden f-f transitions which result in low quantum yields (QY) and low molar absorption coefficient (ε) from direct excitation.[12] Herein a way that was developed to bypass it was to attach ligand to the ions. The stable and characteristic colours of these compounds are then due to the Ln ions, but their intensity is due to the aromatic organic ligands since they are involved in a process called photo-antenna effect or luminescence sensitization with the Ln ions.[11, 12] This process in the excitation of the electronic levels of the ligand that will act as an energy donor[11] and transfer that energy, intramolecularly, to the metal ion[12], as shown in ***figure 6***.

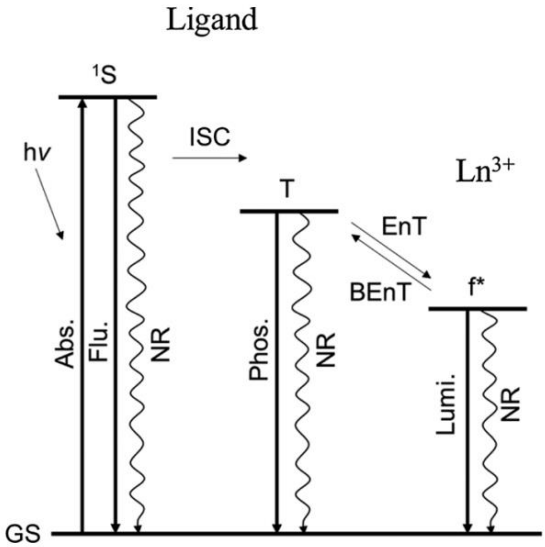

Figure 6. *Illustration of the excitation of the ligand followed by the intersystem crossing to the triplet state, followed too by the energy transfer of the ligand to the trivalent lanthanide ion and his luminescence. All this processes are competitive with the non-radiative processes and emit light in different ways as is represented.*[11]

As shown in the ***figure 6*** the orbitals excited in the group of the lanthanides are the f ones, although these ones are not the outer shells. The outer shells are the 5d and 6s orbitals, making the 4f orbitals the inner shells and in consequence better shielded from the environment. Which explains why each element of the lanthanide group has a well-defined colour that does not vary much even with the changes of the chemical environment brought by different ligands attached to them.[14] The colours shown under irradiation are characterized by very sharp peaks in the emission spectra, which often displays smaller peaks for the less probability transitions (***figure 7*** *a)*).[11]

For this project it was chosen to work with the lanthanide in the position 63 of the periodic table, Europium (Eu). This element can have two different configurations in the ground state [Xe] $4f^6\ 5d^1\ 6s^2$ or [Xe] $4f^7\ 5d^0\ 6s^2$, being the last one the most stable. Due to this ability, it can be transformed in a trivalent ([Xe] $4f^6\ 5d^0\ 6s^0$) or bivalent ion ([Xe] $4f^7\ 5d^0\ 6s^0$), and the most stable one is the Eu^{III}.[11] It is shown in ***figure 7*** *a)* the red colour of the strong red luminescence attached to the transitions of the europium ion, and the respective transitions from the ground state level of Eu ($^5D_0$). The $^5D_0$ level corresponds to the level created by the energy transfer from the ligand. In ***figure 7*** *b)* is shown the unique splitting for Eu^{3+}, seeing that every lanthanide has their own splitting and different type of transitions.[11]

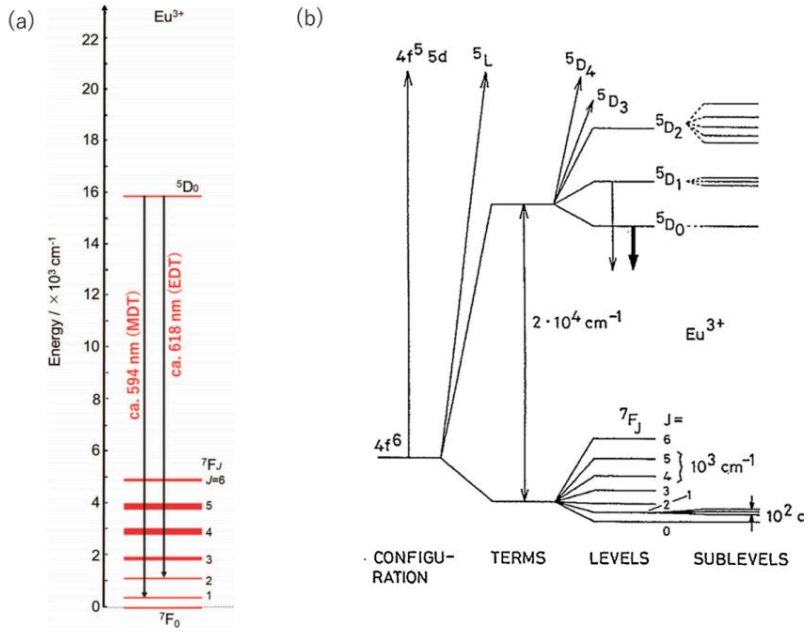

Figure 7. *Representation of the luminescence energy levels of the trivalent europium ion in a) and the respective partial energy diagram showing the splitting of the levels. Adapted from Hasegawa et al.* [11]

Along with luminescence there are a series of deactivation process that will rapidly deactivate the pathways that lead to luminescence in lanthanides. One way to minimize these deactivation processes is by having a rigid environment around the metal protecting the lanthanide ion from solvent interactions.[12] The process of suppression of the luminescence, is called quenching. Oxygen dissolved is one of the best quenchers, making water the solvent that more decreases the lifetimes due to the large solubility of oxygen in water. Nevertheless, it was proved that if the hydroxyl group of water will be involved in strong intra or intermolecular H-bonding the quenching will be minor.[12] However, Ln can have an stability in solution, like for example gadolinium Gd^{III} complexes that can be used in magnetic resonances as a contrast agent.[13]

There are multiple reports in literature of organic lanthanides complexes presenting luminescence characteristics, implying they can be used as sensors for different groups of compounds, like for instance nitrate explosives.[15]

Lanthanides also present other characteristics that can be useful in the sensing. For instance, the inherent fingerprint luminescent properties; making them easy to differentiate,[2] and their long luminescence lifetimes and bandwidths of only a few nanometers.[8] In some studies it was shown that ethanol is the organic solvent displaying the most intense fluorescence and that the Eu^{III}, forms successful interaction/bonds with carbonyl groups.[15]

Another example of Ln used in detection are the lanthanum and europium, used to detect neutral acids, glycolipids, and phospholipids, when they are in complexes or soluble in water. This is possible due to the cooperative complexation between the metallic center and the groups of the before refereed analytes. This ability is very useful because the Eu complexes can be used to detect

biomarkers of various pathologies, like in the case of the LPA (lysophosphatidic acid) biomarker for ovarian cancer.[16]

The lanthanide compounds together with the salen ligand can introduce colorimetric systems and fluorescent signals as methods of sensing. From the survey in the literature were found calculational studies that proved that OPCs can bind to lanthanides forming ML_2 complexes.[2]

One of the reasons why lanthanides are chosen is due to their optical transduction, explained in their spectroscopy properties. It was tried to develop a type of MIP (molecularly imprinted polymer) with Eu^{III} to detect products of the hydrolysis of Sarin and Soman. They showed low LoD and referred the performance of interference tests with others organophosphorus pesticides and insecticides. The structure of the polymer was based on dimethyldipyridyl due to the knowledge of pyridine rings to enhance the luminescence of the lanthanides. Jenkins *et al.* tried to develop a sensor portable enough to carry to the field that could give results that can be trusted, however that was not accomplished.[8] Many years after, that is still the main goal, the development of cheap, easy to work with, portable and reliable sensors that can be carry to the field.

The relationship between NAs and simulants is not well understood but if it was[2], it would help to diminish the probability of error when the translation of knowledge is made, because the difference in bonds behaviour could be significative, and that makes the choose of the simulant challenging. Even with the DMMP (best surrogate for sarin) and sarin there is a difference in the chirality. Sarin is chiral and DMMP is non-chiral, that seems a difference overlooked that can be important when it is done the translation of results from the simulant to the CWA. That gap in translation of knowledge between surrogates and CWA is due to most of the laboratories and scientists don't have clearance to work directly with this type of compounds, what forces the use of the simulants that have structural differences, owing that to the low LC_{50} and high toxicity of CWA.

An ideal portable sensor should be not only reliable, reusable, and with high sensitivity or selectivity, but also should have a short time response, a low false alarm rate, have a low cost, maintain consistence over time and over a range of temperatures and a good resistance to aging.[2]

1.4 Aims and objectives

The aim of this work is, to develop a sensor, sensitive enough for trace amounts of DMMP, that can be used as an easy-to-use portable sensor showing the presence of the analyte.

The first section reports a preliminary study with some different salen type ligands in different chiralities using molecular modelling to see the influence of the chirality and the importance of the position of the groups and which groups enhance better the possibility of forming H-bonds.

In the next section it is reported the synthesis of a series of Zn complexes with similar structure of the complex Zn-3OH synthesized by Puglisi *et al.* (2018)[3]. Since this complex has the highest binding constant with DMMP reported in the literature (the best surrogate described in

literature for Sarin). Based on the structure of Zn-3OH, changes in the structure of the salen type ligands were developed to improve the hydrogen bonds of the complex with the DMMP, forming the **I1** to **I3** family, as shown in the figure below (***figure 6***).

Finally, another family of salen type ligands **L1** to **L3** is presented, as shown in the ***figure 7***. Followed by their complexation with europium, as a new metal.

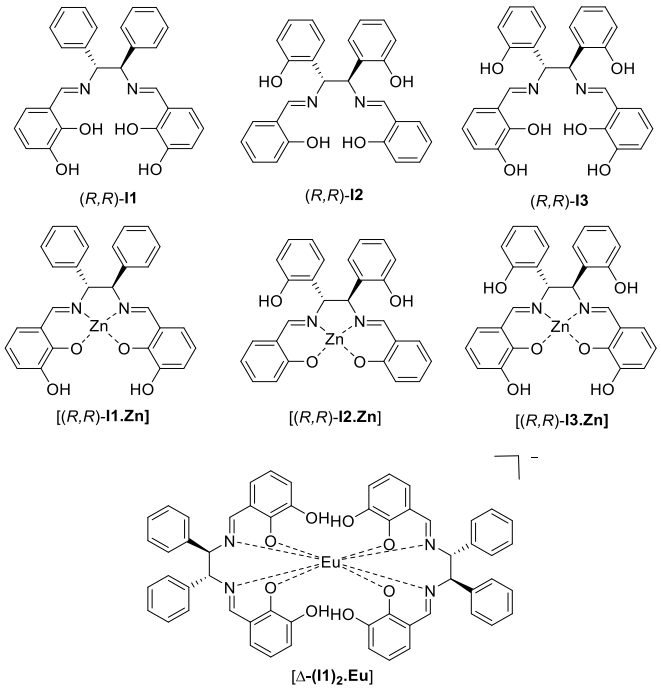

Figure 8. *Structure of the family of the compounds italian's **I1** to **I3** and respective complexes with Zn and Eu.*

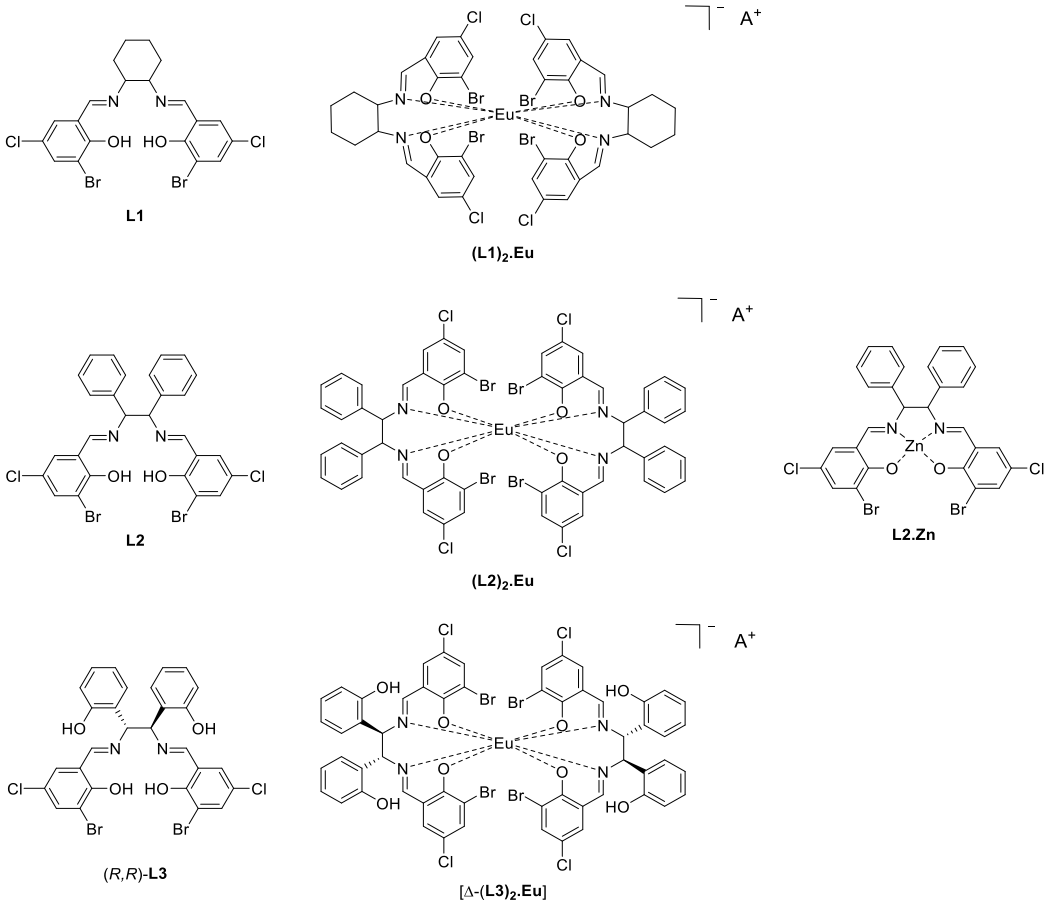

Figure 9. *Structures of the family of salen tyle ligands **L1** to **L3** and the respective complexes with Eu and Zn. **L1** and **L2** salen ligands were made in both chiralities (R,R) and (S,S) and the respective complexes with Eu were made in both chiralities. Each compound was synthesized with two different counterions, represented as A^+, that being Et_3N^+ and PPh_4^+.*

The ligands and compounds synthetized will be characterized using a combination of spectroscopic techniques (NMR, absorption, emission). Finally, the binding ability of these receptors with DMMP will be tested by performing titrations in NMR, UV-Vis, and fluorescence to test the effectiveness of complexes as detectors for DMMP. The strength of binding will be assessed by calculating the binding constants from the fitting of the data taken from the spectra.

Chapter 2

Results and Discussion

2.1 Molecular modelling

Molecular modelling is a way of saving time and resources using computational databases and mathematical functions. In this case to predict the probability of interaction of different ligands complexes and our analyte, DMMP. For that was used Density Functional Theory (DFT) method, an quantum mechanical computational method to calculate the predict of interactions and more stable conformations between compounds.

The structures chosen are showed in ***figure 10*** and were performed in a way to improve the multi-topic approach through maximizing H-bonds interactions, having different positions of hydroxyl groups in the diamines and different chirality to see their influence in the final energy.

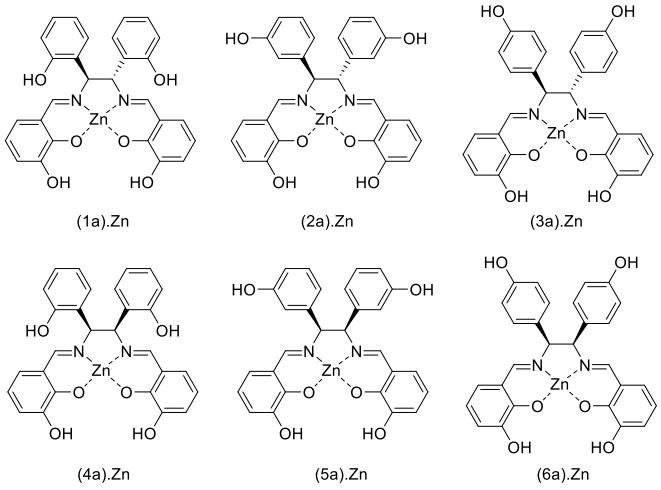

Figure 10. *Structures of the variation of the complexation of Zn with salen ligand a. Ligand a has a 2,3-dihydroxylbenzaldehyde as the aldehyde, changing the position of the hydroxyl groups in the diamine (orto, meta and para, respectively 1/4, 2/5, 3/6), and changing the chirality (S,S for 1 to 3 and S,R for 4 to 6).*

Meanwhile were performed some others complexes with changes in the aldehydes (ligand b and ligand c) as shown in ***figure 11*** and ***figure 12***. With the same changes in the diamines and the chirality to see the influence of the aldehyde groups.

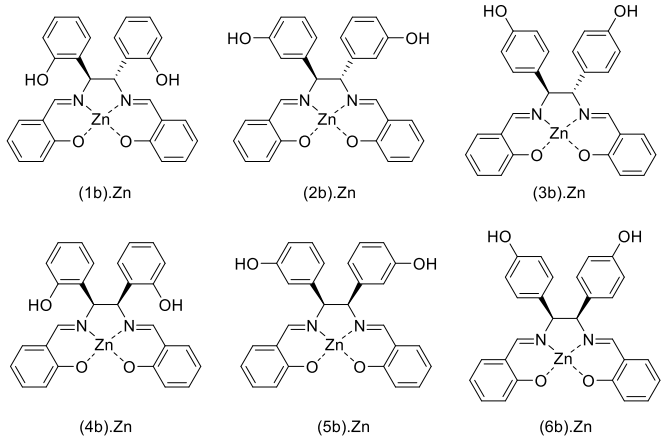

Figure 11. *Structures of the variation of the complexation of Zn with salen ligand b. Ligand b has salicylaldehyde as the aldehyde, having the same changes in hydroxyl groups and chirality as the ligand a.*

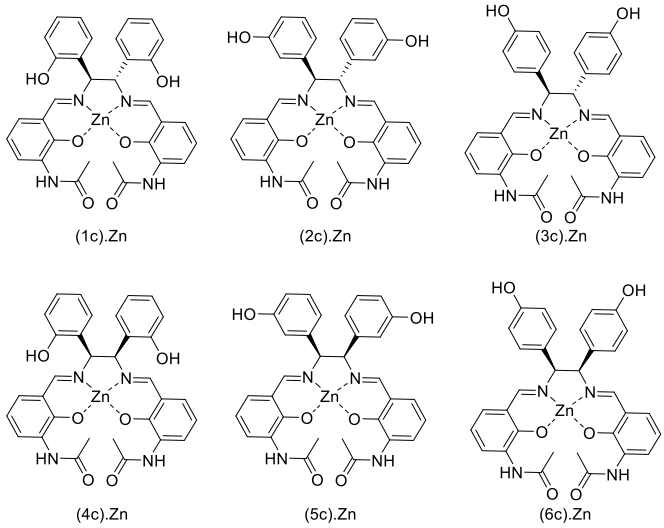

Figure 12. *Structures of the variation of the complexation of Zn with salen ligand c. Ligand c has N-(3-formyl-2-hydroxyphenyl) acetamide as the aldehyde, having the same changes in hydroxyl groups and chirality as the ligand a and b.*

Calculations about the final value of energy of the interaction of the complex with DMMP and the number of the bonds that were made with it, were also performed. The values are presented in ***table 1***.

The best value of the final energy is the one that is more negative, because indicates a more stable conformation, a more probable bond to occur. However, analyzing the data from the computational, do not present as a trend, not having a clear answer of which family of compounds should be best. To understand it better, were then performed two types of alterations to the initials modes of molecular modelling. The first one was forcing the bond of the P=O of DMMP with the zinc from the complex to study how many bonds will form and how stable that structure would be. This ones were only made with (1a).Zn and (1c).Zn to evaluate if their significative changes to proceed for the rest of the compounds. The (1b).Zn was not tried as well, because has less groups to

stablish H-bonds. The results are represented also in ***table 1*** with a *. It gave a more negative final energy, what was positive, but had a smaller number of hydrogen bonds.

It was then performed another change in the way the molecules were positioned. The four bonds of the ligand to the zinc were frozen and then the molecules of DMMP were positioned and the calculations were made. The compounds chosen for this were the (1a).Zn, (1b).Zn, (4a).Zn and (4b).Zn to see the influence of the chirality and if the groups in the aldehyde hindered the approximation of the DMMP. They are also presented in ***table 1*** with a **.

The results for the family of the 1 were much better than before, having the (1a**).Zn the best result, by having two hydrogen bonds and a more negative result than the others two tries, (1a).Zn and (1a*).Zn. Overall, the conclusions were that the best chirality was the (S,S) or (R,R) compounds, and not the (R,S) or (S,R) form ones, being the family of the first compounds more promising then the fourth.

The results of the molecular modelling were not as enlightening as expected but helped to choose in just synthesized enantiomer compounds (*R,R*) and (*S,S*), and a way to simplifying the synthesis, it was chosen to pursuit the path of the small alterations of the Zn-3OH from Puglisi *et al.*[3], by synthesizing (1a).Zn and (1b).Zn.

Table 1. *Table of the final energies of the optimization of the complex with DMMP, and the respective interactions (H-bonds). * - calculations made forcing the coordination bond between P=O and Zn, ** - calculations made with the angles from the Zn bonds frozen.*

Molecule		Final energy (kJ/mol)	Number of H-bonds
1	**a**	-38.787	0
	a*	-67.436	0
	a**	-82.246	2
	b	-15.351	0
	b**	-35.565	1
	c	-34.279	1
	c*	-88.913	0
2	**a**	-22.949	0
	b	-83.100	1
	c	-97.994	1
3	**a**	-31.385	1
	b	-52.397	1
	c	-31.188	1
4	**a**	-29.773	1

Table 1. *Continuation.*

	a**	-25.974	1
	b	-55.535	1
	b**	-19.413	0
	c	-130.871	0
5	**a**	-32.414	1
	b	-38.314	1
	c	-92.383	1
6	**a**	-30.430	1
	b	-28.941	1
	c	-17.993	0

2.2 DMMP receptors based on Zn complexes

2.2.1 Synthesis and characterization of the complexes

Ligands **I1–I3** were synthesized in good yields using the approaches outlined in section 4.1.3.[3] Imine condensation of the corresponding aldehyde derivate with the corresponding diamine gave salen type ligands **I1**, **I2** and **I3** in 72% 20% and 40% yields respectively. Ligands **I1** and **I2** were transformed into the corresponding Zn complex by adding zinc acetate to obtain monometallic complexes **I1**.Zn and **I2**.Zn in 69% and 40% yields respectively. Attempts to form the **I3**.Zn complex were unsuccessful, likely due to the difficulty in complexation with the right hydroxyl groups and the possibility of oligomeric complexes (***figure 13***).

The C_2-symmetry of ligands **I1 – I3** results in a similar ^{1}H NMR in DMSO-d_6. They have some similarities between them in chemical shifts from the aromatic rings protons appearing between 6.55 to 7.35 ppm. The imine protons appearing between 8.34 to 8.48 ppm and the H_g protons between 5.08 to 5.56 ppm. Due to the different number and positions of hydroxyl groups, **I1** has two hydroxyl groups what is represented in the NMR by two broad signals of H_a and H_b at 13.39 and 9.08 ppm, respectively. **I2** has two hydroxyl groups have the following chemical shifts of H_a and H_h 13.62, 9.68 ppm, respectively. The hydroxyl protons at **I3** are H_a, H_h, H_b at 13.71, 9.72 and 8.96 ppm. After the complexation with Zn, the ligand C_2-symetry structures were confirmed once more with ^{1}H NMR. The signals experience a slight shift ($\Delta\delta_{max.} \approx 0.4$ ppm), but the major difference is the disappearance of the hydroxyl protons signal that is lost due to the formation of the metal complex. In the case of the **I1**.Zn a less broad signal for the hydroxyl protons was observed due to the loss of one of the two types of the hydroxyl groups that the ligand **I1** has. The H_a from the hydroxyls groups were making

a bound with the zinc, hindering the protons (H_b) of the other hydroxyl groups to change between them, originating then a sharper signal. Unfortunately, the synthesis for complex **I3**.Zn was unsuccessful (for more details see **4.1.3**).

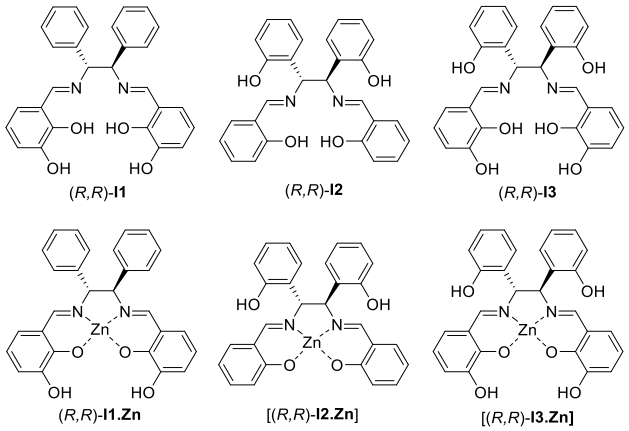

Figure 13. *Structures of the salen ligand italian's 1, 2 and 3 (**I1**, **I2** and **I3**), and the three the respective complexations with zinc. The ligand **I1** only has hydroxyl groups in the aldehyde, **I2** only have hydroxyl groups in the diamine and the ligand **I3** has two hydroxyl groups both diamine and aldehyde.*

2.2.2 UV-Vis titrations

The binding behaviour of compound **I1**.Zn with DMMP was initially tested in order to assess reproducibility with the reported method by Puglisi *et al.*[3] A UV-Vis titration with DMMP was performed in DMSO maintaining the concentration of host = 18.2 μM constant, while adding stepwise aliquots of DMMP with a range of [DMMP]/[**I1**.Zn] 0 – 6 (see ***table 9*** for more details). The UV-Vis spectral changes upon the titration of [(*R,R*)-**I1**.Zn] with DMMP in DMSO was performed multiple times (***figure 14***), disagreeing the profile of the titration with what was previously reported in the literature.[3] However Puglisi *et al.* reported a binding constant of log *K* 5.04, which was similar to the value obtained, log *K* 5.71, by fitting our data (***figure 16***).

Each addition of DMMP produced a noticeable change in the titration spectra (***figure 14***). The titration presented three isosbestic points (wavelength at which the absorbance of the mixture doesn't change) at 288 nm, 322 nm and 353 nm. Since the first addition can be seen a change of the spectra, indicating the initiation of a process. The decrease of the intensity of the band at 383 nm is followed by an increase of intensity at 335 nm, being more evident this transition after the addition of 18.8 μM of guest, due to the appearance of the isosbestic points (***figures 14 and 15***). The certainty of what process was happening needed to be backed up with more data information.

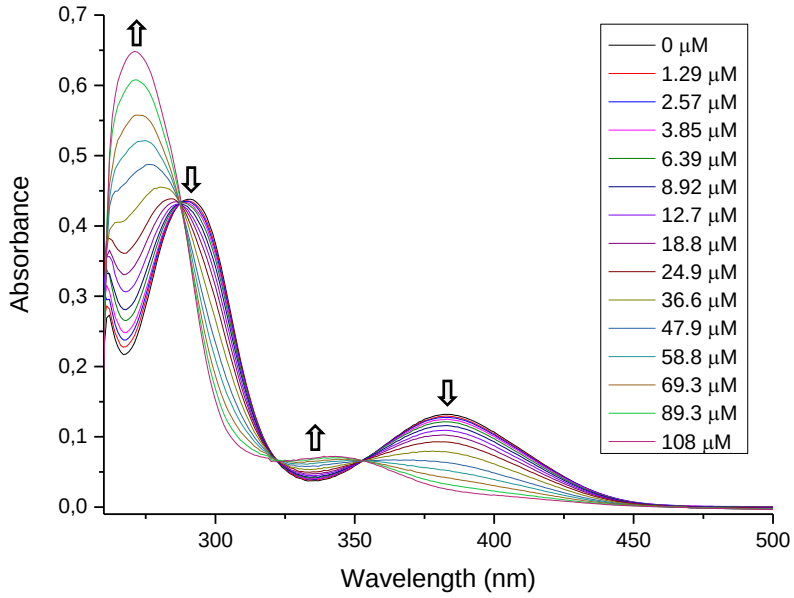

Figure 14. *Absorption spectral change of [(R,R)-**I1**.Zn] in DMSO at r.t. upon the titration with DMMP (1.29-108 μM). Concentration of [(R,R)-**I1**.Zn] constant at 18.2 μM.*

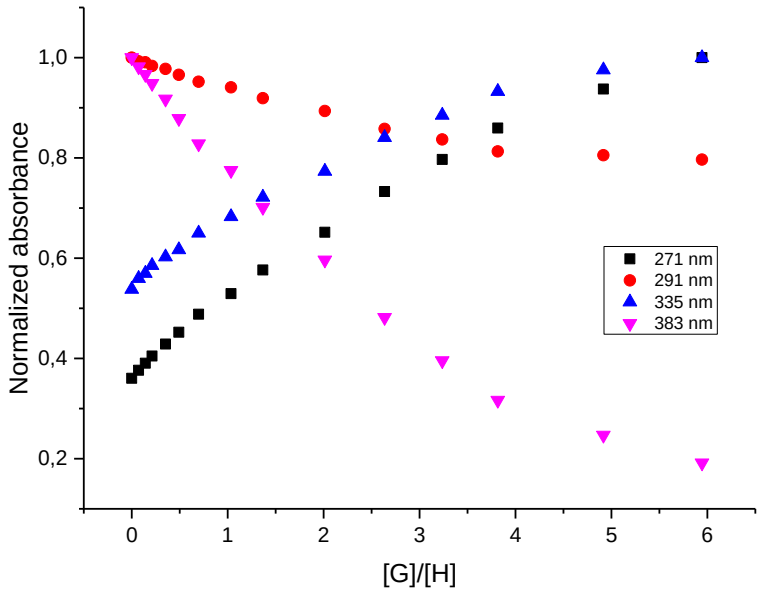

Figure 15. *Plot of the absorbance of two wavelengths in function of the number of the equivalents, related to the UV-Vis titration of [(R,R)-**I1**.Zn].*

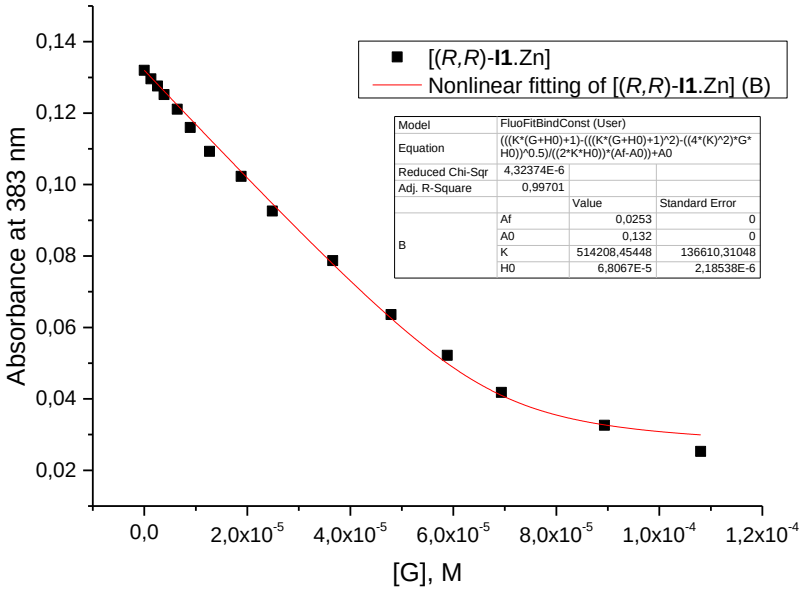

Figure 16. *Nonlinear fitting to a 1:1 stoichiometry of [(R,R)-**I1**.Zn] and DMMP in DMSO.*

Once the behaviour of the reported receptor was assessed, it was decided to study the new receptor **I2**.Zn, in which the hydroxyl substituent was moved from the salicylaldehyde ring to the diamine aromatic rings. The same line of thought was pursuit for this compound. A UV-Vis titration of [(*R,R*)-**I2**.Zn] in DMSO with DMMP was performed, with number of equivalents 0-6 eq. (for more details see ***table 10***). The spectra obtained is represented below in ***figure 17***.

These spectra showed only one isosbestic point, at 340 nm, due to the shift of the band from the host at 366 nm to 324 nm for the complex. The appearance of a new band at 324 nm indicates that initially the guest was complexing with the host and then after the addition of 12.7 μM of guest another process formed a new specie that has a different absorbance wavelength. This was known because in the first experiment, the solution only had host, and that was the only band that appeared (366 nm). After the addition of guest, that same band decreased in intensity, explained by the complexation of the host with the guest, since the guest does not absorb in that region. However, at the same time, the intensity of a band at 324 nm slowly started to increase the intensity, having in the end that new specie the one in excess in the solution. That new process can be a demetallation of the host in free ligand, or a formation of a new complex other than guest–host, due to the decomplexation of the guest-host complex already formed. This thesis is corroborated in the ***figure 18***, however without more data information, cannot have certainty of which process is taking place. It should had been done a spectrum of the free ligand and one from the free host too to compare with the shape of the titration spectra's that are presented.

Although, other information can be taken from the data presented in ***figures 17*** and ***18***. The intersection point occurs after seven experiments (after six additions of solution with DMMP),

meaning that the new process happens after the addition of 12.7 mM of guest. After reaching near 3 equivalents, it seems that the addition of more guest does not change the spectra, indicating that the compound that was complexing with DMMP reached saturation.

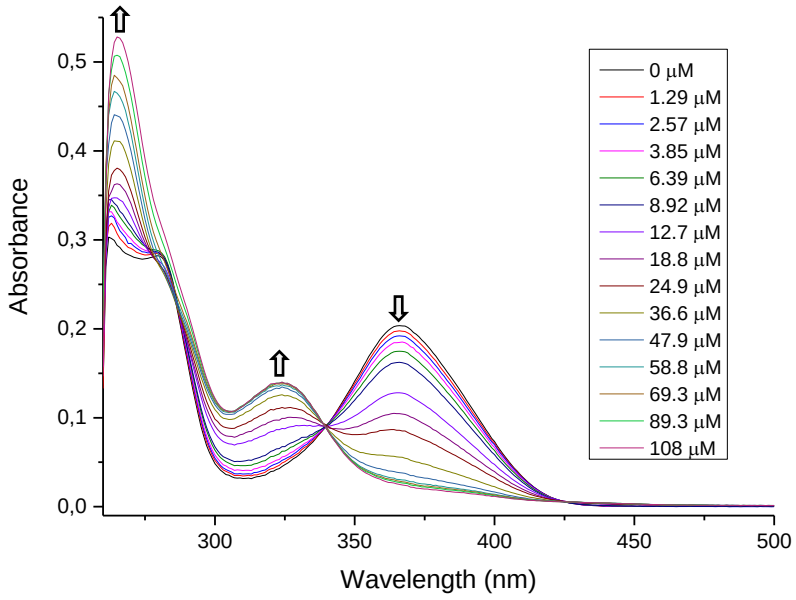

Figure 17. *Absorption spectral change of [(R,R)-**I2**.Zn] in DMSO at r.t. upon titration with DMMP (1.29-108 mM). Concentration of [(R,R)-**I2**.Zn] maintained constant at 18.2 μM.*

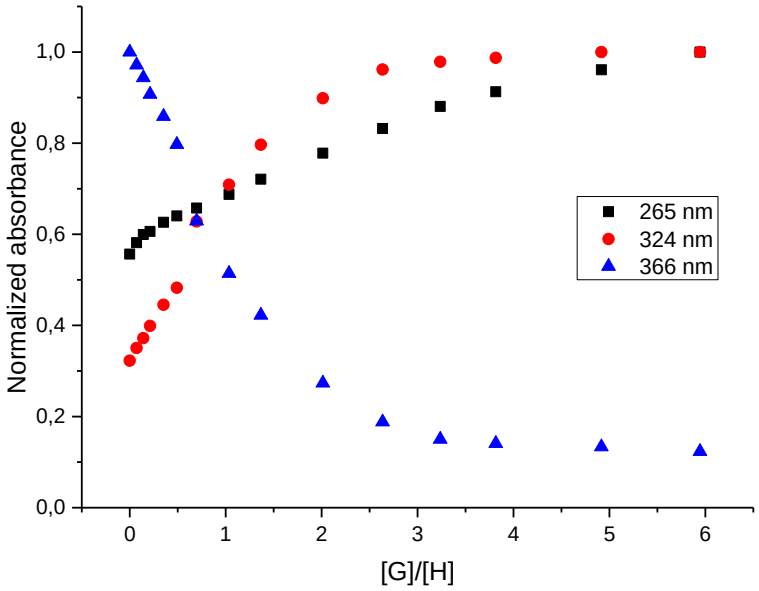

Figure 18. *Plot of the normalized absorbance of three wavelengths in function of the number of the equivalents, related to the UV-Vis titration of [(R,R)-**I2**.Zn].*

Nevertheless, it was made a calculation of binding constant in a plot of absorbance at 366 nm in function of the concentration of the guest, ***figure 19***.

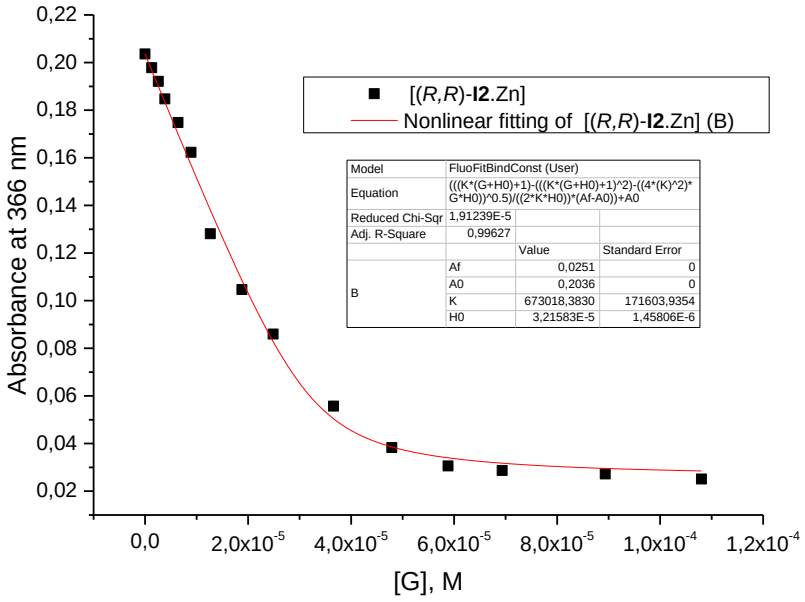

Figure 19. *Nonlinear fitting to a 1:1 stoichiometry of [(R,R)-**I2**.Zn] and DMMP in DMSO.*

Table 2. *Table with the comparation of the values of the binding constant reported in literature and performed with the zinc complexes **I1** and **I2**. The reports from Puglisi et al. only report the value of the standard deviation (SD), and the ones performed in this project were only calculated the standard errors (SE).*

Complex	*K*	Log *K*	SD or SE
Zn-3OH	---	5.04[3]	0.4084[3] (SD)
[(*R*,*R*)-**I1**.Zn]	514208.45	5.71	1.37E5 (SE)
[(*R*,*R*)-**I2**.Zn]	673018.38	5.83	1.72E5 (SE)

The value of the binding constant of [(*R*,*R*)-**I1**.Zn] should be the same as reported in Puglisi *et al.*, but this result was expected based on the slight inconsistency between the behaviour of the both UV-Vis spectra. However, accepting the log *K* 5.71 as reference, the complex **I2**, presents a slight high value, what could be promising if they didn't seem the same due to the error.

To better understand the why behind the difference on the binding constant of [(*R*,*R*)-**I1**.Zn] it was needed more time, and it was also needed to perform NMR and fluorescence titrations to guarantee reproducibility. After that the same type of procedure should be applied to the [(*R*,*R*)-**I2**.Zn], to better compare the results.

2.3 DMMP receptors based on Eu complexes

2.3.1 Synthesis and characterization of the complexes

Ligands **L1–L3** were synthesized in good yields using the approaches outlined in section 4.1.3.[17] In brief, imine condensation of 3-bromo-5-chloro-2-hydroxybenzaldehyde with the corresponding diamine gave salen type ligands **L1–L3**. Ligands **L1** and **L2**, were obtained in both chiralities (*S,S* and *R,R*) in 20 %, quant., 79 % and 87 % yields respectively, while **L3** was only obtained as the *R,R* enantiomer in 65 % yield. Ligands **L1** and **L2** were subsequently transformed into the corresponding Eu complex by adding europium (III) trifluoromethanesulfonate in MeOH solution to obtain monometallic complexes [Λ-(**L1**)$_2$.Eu][Et_3NH] (81 %), [Δ-(**L1**)$_2$.Eu][Et_3NH] (90 %), [Λ-(**L1**)$_2$.Eu][PPh_4] (86 %), [Δ-(**L1**)$_2$.Eu][PPh_4] (86 %), [Λ-(**L2**)$_2$.Eu][Et_3NH] (19 %), [Δ-(**L2**)$_2$.Eu][Et_3NH] (72 %), [Λ-(**L2**)$_2$.Eu][PPh_4] (quant.), [Δ-(**L2**)$_2$.Eu][PPh_4] (73 %), with their respective yields. Ligand **L2** was transformed into the corresponding Zn complex upon the addition of zinc acetate obtaining [(*S,S*)-**L2**.Zn] (68 %), [(*R,R*)-**L2**.Zn] (81 %) with their respective yields. Attempts to form the **L3**.Eu complex were unsuccessful, probably due to the presence of other hydroxyl groups and their proximity to the nitrogen what could difficult the complexation between the right groups. The complexation of ligand **I1** and europium (III) trifluoromethanesulfonate was attempted but proved also unsuccessful, likely because the presence of additional hydroxyl groups enables the formation of oligomeric Eu species.

The rationale behind the introduction of bromide and chloride (heavier elements) in the aldehyde is to increase the probability of intersystem crossing to emphasize the indirect excitation of the europium. Additionally, it was intended to study the influence of π interactions by replacing the phenyl rings (**L2**) of the diamine group for a cyclohexane (**L1**) (***figure 20***).

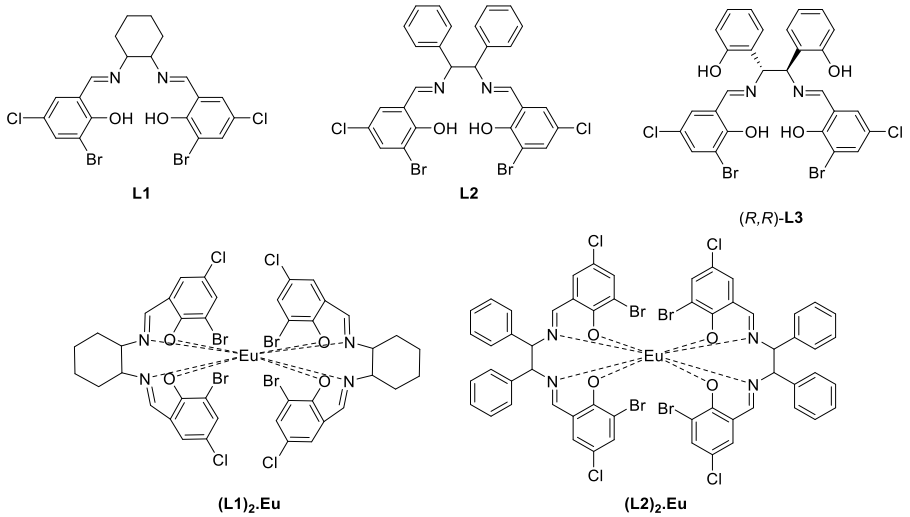

Figure 20. *Structure of the salen ligands **L1**, **L2** and **L3** in their respective complexes.*

The **L1** and **L2** ligands were synthesized in both chiralities (*S,S*) and (*R,R*), and how it was expected they have the same ^{1}H NMR spectrum (for more details see **4.1.3**), since the only thing that should change is which side they turn under polarized light. The hydroxyl protons were between 14.27-14.44 ppm, the aromatic protons between 7.11-8.35 ppm, the protons for the H_e can be found at 5.11 ppm for **L2** and at 3.36 ppm for **L1**, however due to the cyclohexane **L1** has signals more upfield between 1.42-1.99 ppm. The **L3** ligand was just synthesized in (*R,R*) chirality, having signals around the same region then **L2**, but having different couplings due to the hydroxyl group introduced.

The four **L1** and **L2** ligands were complexed with Eu, in a stoichiometry 2:1 (ligand : metal). The chirality were then called "lambda" Λ, or "delta" Δ. This is because the 2:1 stoichiometry, generates a bidentate complex. The complex that turn counterclockwise the light, are left-handed and then "lambda", this happened to the (*S,S*) ligands. The (*R,R*) ligands, rotate clockwise or right-handed, generating the "delta" enantiomer of the complexes.[18] This procedure was made with the counterions Et_3NH, and followed by the salt metathesis, changing the counterion for PPh_4. The salt metathesis was made to test the influence of the counterion, being the second one more bulked and so should have a lower probability of interaction with the center, what should be better. However, were also made some studies with the first counterion too, to see if the aromatic rings of the PPh_4 could interact with the aromatic rings from the complexes.

The ^{1}H NMR spectra of these complexes are a little bit different from what happened in the Zinc complexes, due to the paramagnetic feature of the Eu. This feature cause the broadening of the protons near to the metal and spreads the signals over a much wider window of ppm. This makes more difficult the assignment of the signals. However, a characteristic that appeared in all the spectrum done with Eu was a signal at negative upfield, normally between -7.87 and -7.78 ppm.

As referred before a way to characterized lanthanides is to give the information of the QY (***table 3***) and ε (***table 4***), for that were performed fluorescence quantum yields studies and absorbance titrations with only host to calculate the molar absorption coefficient (for more detailed information see **4.1.8**).

Table 3. *Quantum Yield (%) of the eight different complexes of **L1** and **L2** with Eu and their counterions changes, followed by the SD of the calculated with base of different concentrations.*

Compounds	Concentration (M)	Quantum Yields (QY/%)	Standard Deviation (SD)
[Λ-(**L1**)$_2$.Eu][Et_3NH]	10^{-5}	0.46	0.085
	10^{-4}	0.63	
[Δ-(**L1**)$_2$.Eu][Et_3NH]	10^{-5}	0.72	0.12
	10^{-4}	0.96	

Table 3. *Continuation.*

[Λ-(**L1**)$_2$.Eu][PPh$_4$]	10^{-5}	1.09	0.0386
	10^{-4}	1.18	
	10^{-3}	1.16	
[Δ-(**L1**)$_2$.Eu][PPh$_4$]	10^{-5}	1.24	0.0236
	10^{-4}	1.29	
	10^{-3}	1.29	
[Λ-(**L2**)$_2$.Eu][Et$_3$NH]	10^{-5}	3.08	0.222
	10^{-4}	2.86	
	10^{-3}	2.54	
[Δ-(**L2**)$_2$.Eu][Et$_3$NH]	10^{-5}	3.45	0.0409
	10^{-4}	3.50	
	10^{-3}	3.40	
[Λ-(**L2**)$_2$.Eu][PPh$_4$]	10^{-5}	3.72	0.103
	10^{-4}	3.47	
	10^{-3}	3.56	
[Δ-(**L2**)$_2$.Eu][PPh$_4$]	10^{-5}	3.83	0.0946
	10^{-4}	3.62	
	10^{-3}	3.64	

As stated, before Ln don't usually have high QY. That said the **L2** complexes have a higher value, what is more promising, what could help in increasing having higher values of luminescence. The other facto that determines that is the values of the molar absorption coefficients.

It shouldn't be any difference of the value of the coefficients between different enantiomers of the same complex. However, that happened and can be explained, in the ones with the Et$_3$NH as a counterion, by the different levels of purity in the synthesis. The ones with the other counterion have a bigger difference, that not even with the high vacuum or the repetition of the experiments and neither the use of the different measurements significantly changed the final results. For a better understanding needed to be done more and different experiments. Although these results are not key for the purpose of the project, being then put aside. However, comparing the average of the values of [(**L1**)$_2$.Eu][Et$_3$NH] and [(**L2**)$_2$.Eu][Et$_3$NH], the complex **L2** presents itself as a slightly higher molar absorption coefficient. Adding this results with the previous ones of the QY, this corroborates the thesis that the complex **L2** will have a higher luminescence.

Table 4. *Molar absorption coefficient of the eight different complexes of **L1** and **L2** with Eu and their counterions changes. The respective excitation wavelengths and the R^2 of the plots.*

Compounds	Molar absorption coefficient (ε) (M^{-1} cm^{-1})	λ (nm)	R^2
[Λ-(**L1**)$_2$.Eu][Et_3NH]	28625	364	0.999
[Δ-(**L1**)$_2$.Eu][Et_3NH]	26035	364	0.999
[Λ-(**L1**)$_2$.Eu][PPh_4]	22292	364	0.999
[Δ-(**L1**)$_2$.Eu][PPh_4]	29505	364	0.999
[Λ-(**L2**)$_2$.Eu][Et_3NH]	29532	366	0.999
[Δ-(**L2**)$_2$.Eu][Et_3NH]	30877	366	0.999
[Λ-(**L2**)$_2$.Eu][PPh_4]	38301	366	0.999
[Δ-(**L2**)$_2$.Eu][PPh_4]	29024	366	0.999

2.3.2 UV-Vis titrations

As previously done, the first study performed was an UV-Vis titration with DMMP in acetonitrile. Starting by the titration of the [Δ-(**L1**)$_2$.Eu][PPh_4], following by the [Δ-(**L2**)$_2$.Eu][PPh_4] titration (see ***tables 13*** and ***14***, respectively, for more information).

The titration with [Δ-(**L1**)$_2$.Eu][PPh_4] shown below in ***figure 21*** presents two different isosbestic points, at 347 nm and 408 nm. With the data presented in both ***figure 21*** and ***figure 22*** it was clear that after six additions of guest, the shape of the spectrum and plot changes. First, happened the formation of a new complex between the guest and the host, shown by the decrease of the intensity of the band at 364 nm. Secondly after addition of 11.7 mM of guest the band at 364 nm decreases significantly and with that appears one at 337 nm, that does not correspond exactly (after normalizing it) with the spectra of the free ligand, (*S,S*)-**L1**, band also represented in the spectra (in a pink ticker line, ***figure 21***). With the appearing of the new band, it shown a small band at 437 nm from the new species that was formed, originating the second isosbestic point.

This interpretation of the data allows to put the hypothesis that after 11.7 mM of guest instead of having the demetallation of the host, a new complex was being formed with the P=O bond from DMMP.

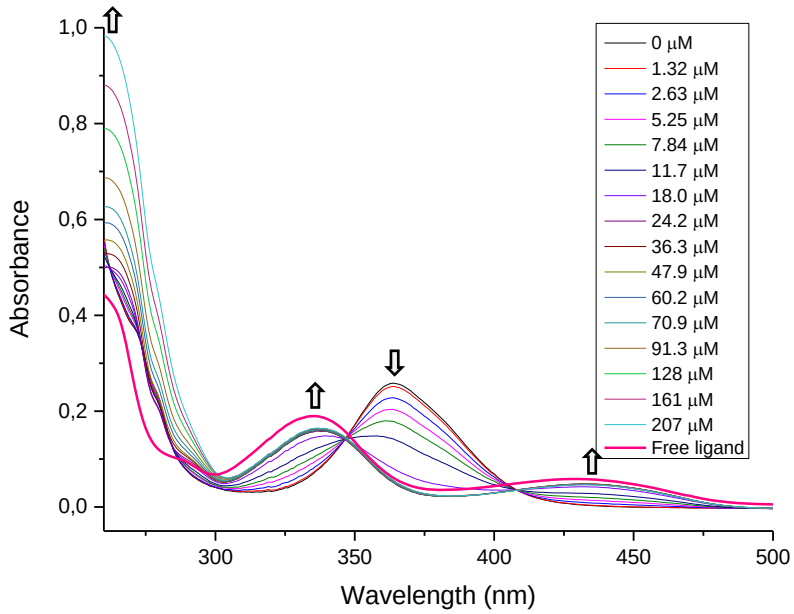

Figure 21. *Absorption spectral change of [Δ-(**L1**)$_2$.Eu][PPh$_4$] in acetonitrile at r.t. upon titration with DMMP (1.32-207 µM). Concentration of [Δ-(**L1**)$_2$.Eu][PPh$_4$] constant at 13.2µM, and concentration of the free ligand ((R,R)-**L1**) of 25.93 µM.*

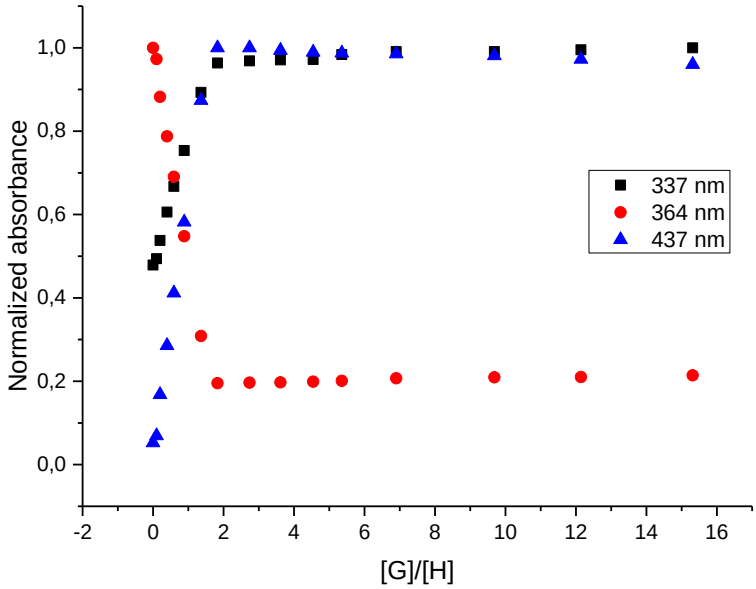

Figure 22. *Plot of the normalized absorbance of three wavelengths in function of the number of the equivalents, related to the UV-Vis titration of the complex [Δ-(**L1**)$_2$.Eu][PPh$_4$].*

The ***figure 22*** shows a steep slope, indicative of a strong binding, that was corroborated by the calculation of the binding constant in ***figure 23.***

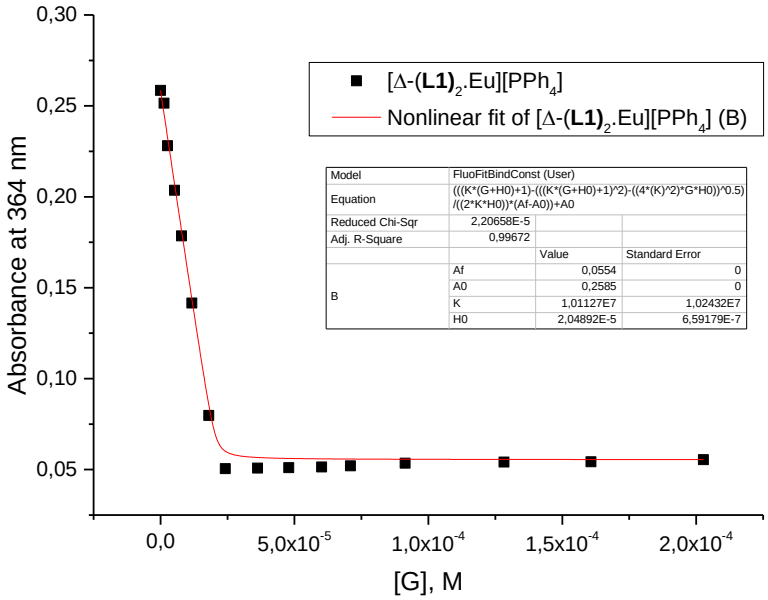

Figure 23. *Nonlinear fitting of [Δ-(**L1**)$_2$.Eu][PPh$_4$] and DMMP in MeCN.*

Additional to this titration were performed ^{1}H NMR and fluorescence titrations of this compound that will be shown in **2.3.3** and **2.3.4** sections, respectively.

The same titration (same guest and host concentration) was made with the host being [Δ-(**L2**)$_2$.Eu][PPh$_4$], data represented in ***figure 24*** and ***figure 25***.

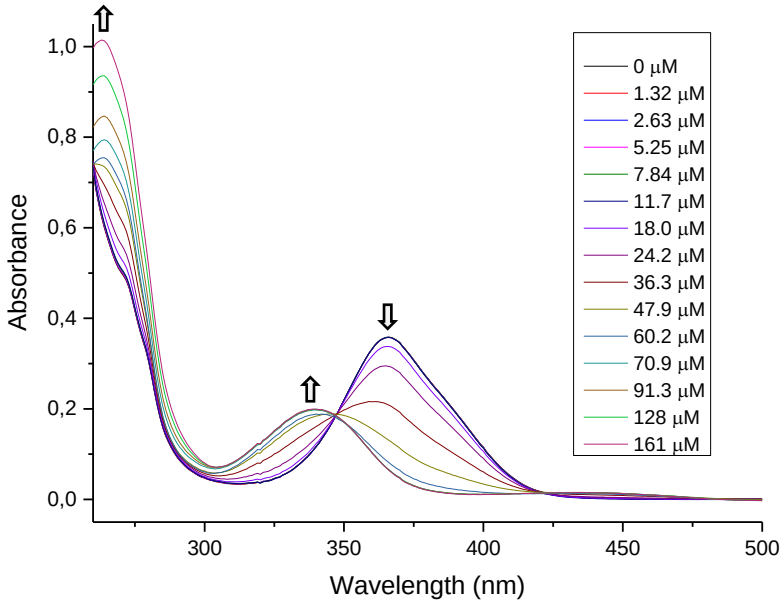

Figure 24. *Absorption spectral change of [Δ-(**L2**)$_2$.Eu][PPh$_4$] in acetonitrile at r.t. upon titration with DMMP (1.32-161 μM). Concentration of [Δ-(**L2**)$_2$.Eu][PPh$_4$] constant at 13.3 μM.*

The data shows the existence of only one isosbestic point at 347 nm (same as the previous complex), and very likely one at 422 nm, however the difference in the absorbance is not high enough to consider it. The profile of the spectrum was very similar as the previous one ([Δ-(**L1**)$_2$.Eu][PPh$_4$]), like the maximum of the bands and even the trending of the experiments. However, looking closely for the data profiled at ***figure 25*** can be seen a slightly different behavior. The shape of the curve is presented a sigmoidal, that is a behaviour found in systems with negative cooperativity (the binding of the first DMMP does not change the behaviour, needed more molecules of DMMP bind to the complex to see change). Explaining why it seemed that nothing happened during the first six experiments, due to the spectra having the same shape for that long. For that it needs to have two binding sites, no longer being in the presence of a 1:1 binding. This can explain why the fitting is not the appropriated, as could be seen by the shape of the fitting curve, and the very large standard deviation (***figure 26***). Two processes could had happened in this case, the first was that more than one molecule of DMMP is binding to the complex or the addition of DMMP detaches the ligand, forming just 1:1 complex of host having the Eu possibility to form bonds with more than only one molecule of DMMP. To better understand which process happened it was also performed an NMR titration of this host, as will be described in section **2.3.3.**

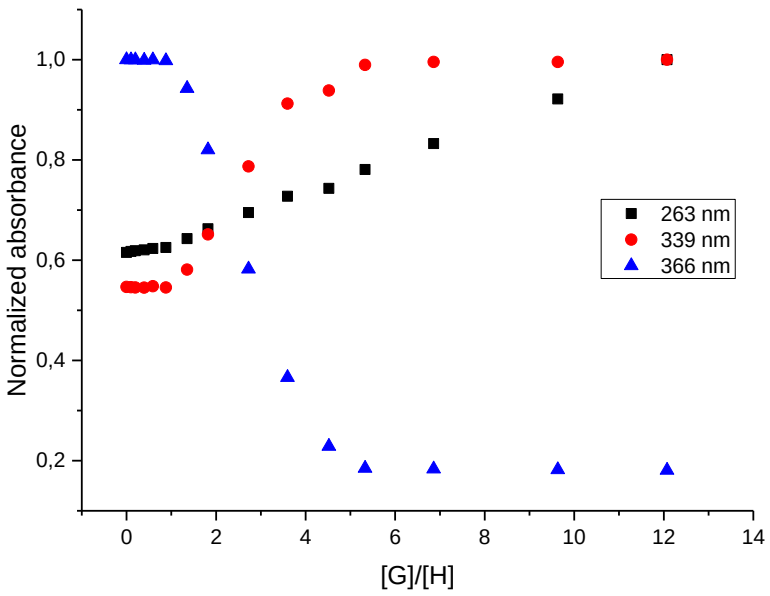

Figure 25. *Plot of the normalized absorbance of three wavelengths in function of the number of the equivalents, related to the UV-Vis titration of the complex [Δ-(**L2**)$_2$.Eu][PPh$_4$].*

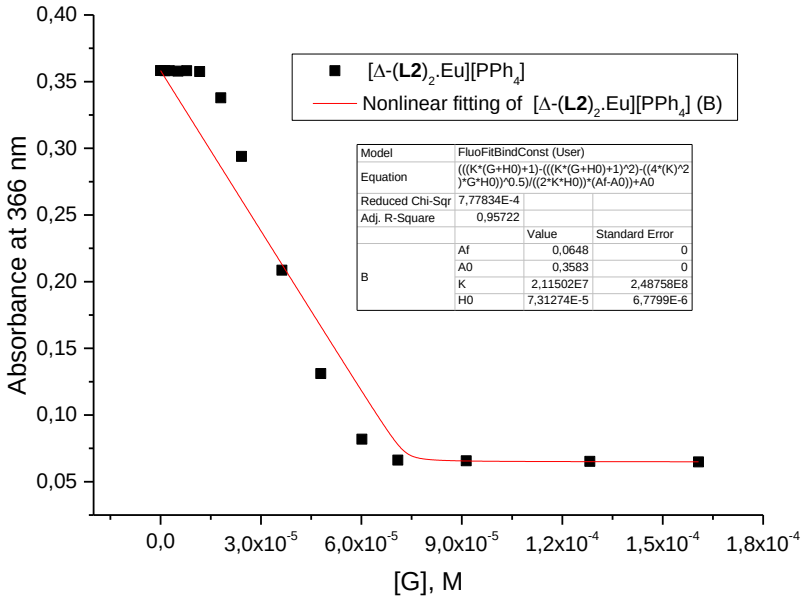

Figure 26. *Nonlinear fitting of [Δ-(**L2**)$_2$.Eu][PPh$_4$] and DMMP in MeCN.*

It was also performed an UV-Vis titration with the complex [(*R,R*)-**L2**.Zn] and DMMP. However, there was no time to perform all the studies needed do take meaningful interpretations of the results.

2.3.3 ^{1}H NMR titrations

To better understood the mechanism behind the behaviour observed in the UV-Vis titration the system was studied by NMR titration. NMR is powerful spectroscopic technique capable of providing structural information on the binding event. Following the chemical shifts of the protons and their environments upon the addition of DMMP provided valuable information of the structure of the complexes formed.

It were tried to be made four ^{1}H NMR titration in MeCN-d$_3$, [Δ-(**L1**)$_2$.Eu][Et$_3$NH], [Δ-(**L1**)$_2$.Eu][PPh$_4$], [Δ-(**L2**)$_2$.Eu][Et$_3$NH], [Δ-(**L2**)$_2$.Eu][PPh$_4$]. However, the [Δ-(**L1**)$_2$.Eu][Et$_3$NH] titration was unsuccessful due to the instable solubility of the complex in deuterated acetonitrile in the amounts needed to perform the titration, being just performed the other three ^{1}H NMR titrations.

The first titration was the [Δ-(**L1**)$_2$.Eu][PPh$_4$] complex represented in ***figure 27*** and ***figure 28*** (see ***table 8*** for more information).

From the first experiment, that only has host, to the second one, it appeared a couple of signals that correspond to the protons from the DMMP molecule. They are two major doublets, one at 1.40 ppm (J = 17.38 Hz) with a shift of Δδ = 0.03 ppm (ΔJ = 0.08 Hz), and other at 3.64 ppm (J = 10.97 Hz) with a shift of Δδ = 0.04 ppm (ΔJ = 0.23 Hz), all the shifts were towards the upfield.

There is a negative signal generated due to the paramagnetic feature of the Eu, making one of the protons close to the bonds where it is involved be at, in this case -7.80 ppm suffered a shift until -7.82 ppm during the first seven experiments because after that it disappeared the signal. To have a better understanding of the stack plots all the signals before 4 ppm are going to be out of the chosen window.

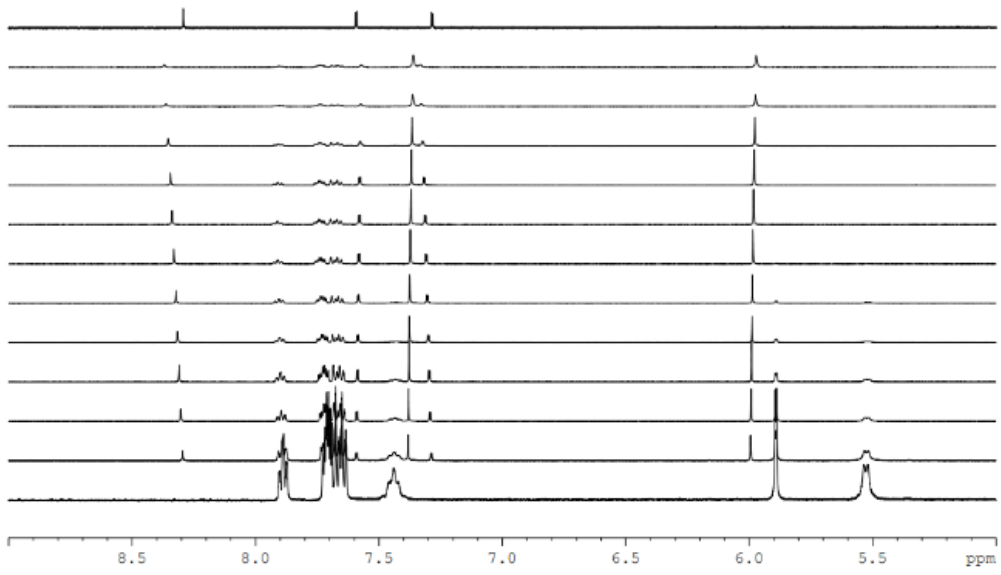

Figure 27. *Selected region of ^{1}H NMR titration of [Δ-(**L1**)$_2$.Eu][PPh$_4$] with DMMP in MeCN-d$_3$. Number equivalents between 0 and 3.07. Being the first experiment without DMMP, and start adding from the bottom to the top, being the top ^{1}H NMR from the free ligand ((R,R)-**L1**).*

The signals between 7.62 and 7.93 ppm belong to the counterion, PPh_4, what corroborate the thesis of consecutive dilution of the sample with the additions. However, that can be seen protons like the single signal starting at 8.30 ppm, going to downfield, that does not match the signal at 8.29 ppm from the free ligand. Another signal that only appears after the first addition of DMMP and does not match any signal from the free ligand is the one at 6.00 ppm, that suffers a shift of $\Delta\delta$ = 0.03 ppm upfield. The first signal could indicate the bond of a proton from the host with DMMP, and the second proton could indicate a DMMP proton that for making a new bond appears at a different chemical shift then the ones referred before.

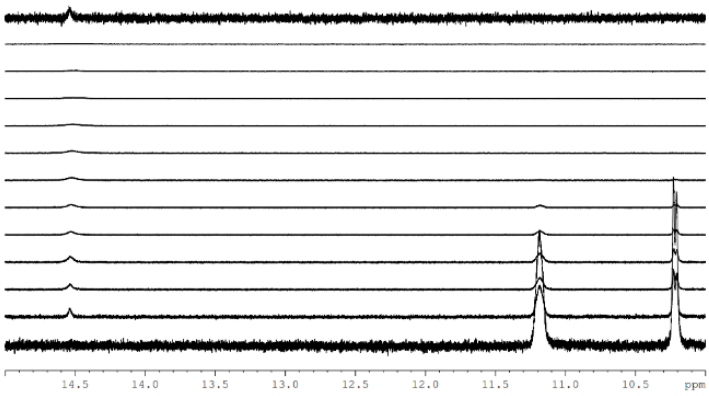

Figure 28. *Selected region of ^{1}H NMR titration of [Δ-(**L1**)$_2$.Eu][PPh$_4$] with DMMP in MeCN-d$_3$. Number equivalents between 0 and 3.07. Being the first experiment without DMMP, and start adding from the bottom to the top, being the top ^{1}H NMR from the free ligand ((R,R)-**L1**).*

The second ^{1}H NMR was the [Δ-(**L2**)$_2$.Eu][Et$_3$NH] complex, represented in ***figure 29*** (see ***table 9*** for more information).

The appearance of the DMMP signals after the first addition of guest as expected has the same behaviour as the previous compound.

The negative signal at -8.37 ppm suffered a shift of $\Delta\delta$ = 0.05 ppm towards the upfield side, disappearing this signal after the first nine additions. To have a better understanding of the stack plots all the signals before 4 ppm are going to be out of the chosen window.

Signals of low intensity like the ones at 8.34, 7.62, 7.27 and 5.11 ppm do not belong to the complex, being then impurities. However, they do not disappear with the titration, and they maintain the intensity, even with the factor of dilution, what makes it believe that could be breaking the host complex to form the free ligand. This theory is followed by the complete disappearance of all the signals from the host complex protons, by the tenth addition of guest. To corroborate this thesis, in the ***figure 30*** is a selected window (14 to 15.5 ppm) that shows the disappearance of the protons at 15.02 ppm from the host complex, and the slight increase of intensity of the protons at 14.43 ppm from the free ligand, that belongs to the hydroxyl group only present in that compound.

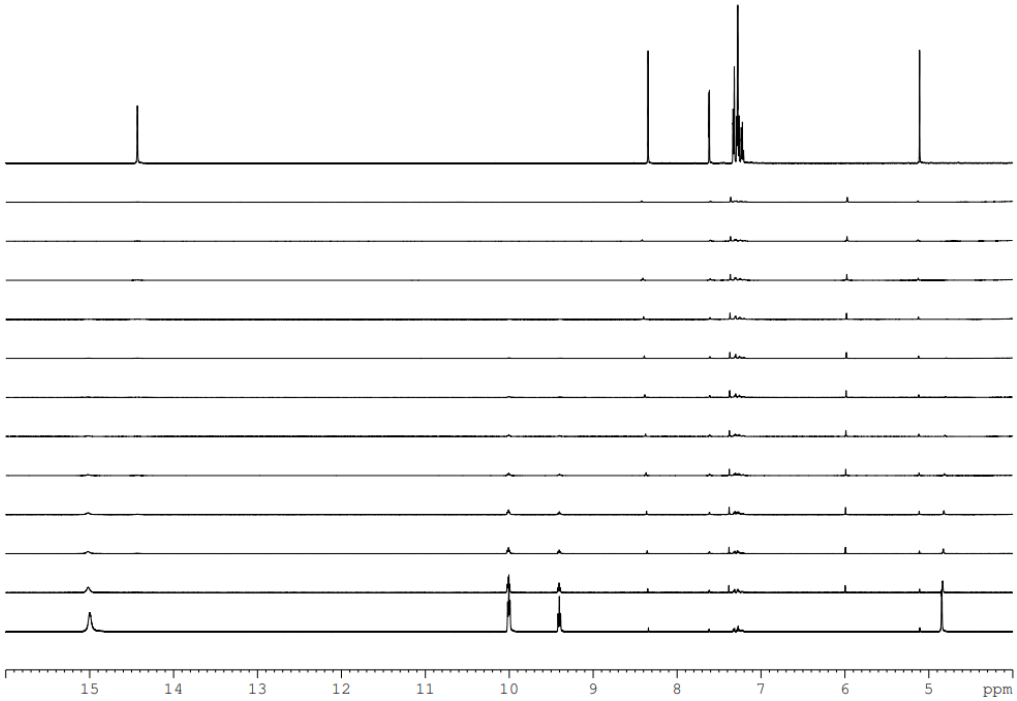

Figure 29. *Selected region of ^{1}H NMR titration of [Δ-(**L2**)$_2$.Eu][Et_3NH] with DMMP in MeCN-d_3. Number equivalents between 0 and 3.17. Being the first experiment without DMMP, and start adding from the bottom to the top, being the top ^{1}H NMR from the free ligand ((R,R)-**L2**).*

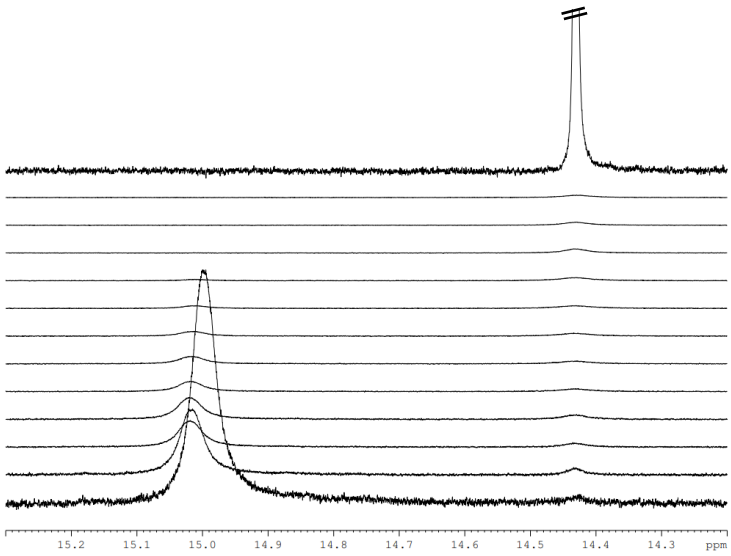

Figure 30. *Selected region of ^{1}H NMR titration of [Δ-(**L2**)$_2$.Eu][Et_3NH] with DMMP in MeCN-d_3. Number equivalents between 0 and 3.17. Being the first experiment without DMMP, and start adding from the bottom to the top, being the top ^{1}H NMR from the free ligand ((R,R)-**L2**).*

Besides the signals already referred can be found other signals that indicates the presence of free ligand, however due to the small impurities with starting material (free ligand) in the first experiment, cannot affirm with certainty this results. The same cannot be said by the proton that again appears at 6 ppm, what reenforces the idea that the DMMP is in fact makings bonds.

The [Δ-(**L2**)$_2$.Eu][PPh$_4$] ^{1}H NMR titration was successful and gave the stack plots represented in ***figure 31*** (see ***table 10*** for more information).

The appearance of the DMMP signals has the same behaviour as the previous two experiments. There is also a negative signal, in this case appears at -8.35 ppm for the first experiment, going to -8.40 ppm until the seventh experiment, disappearing after. To have a better understanding of the stack plots all the signals before 4 ppm are going to be out of the chosen window, as before.

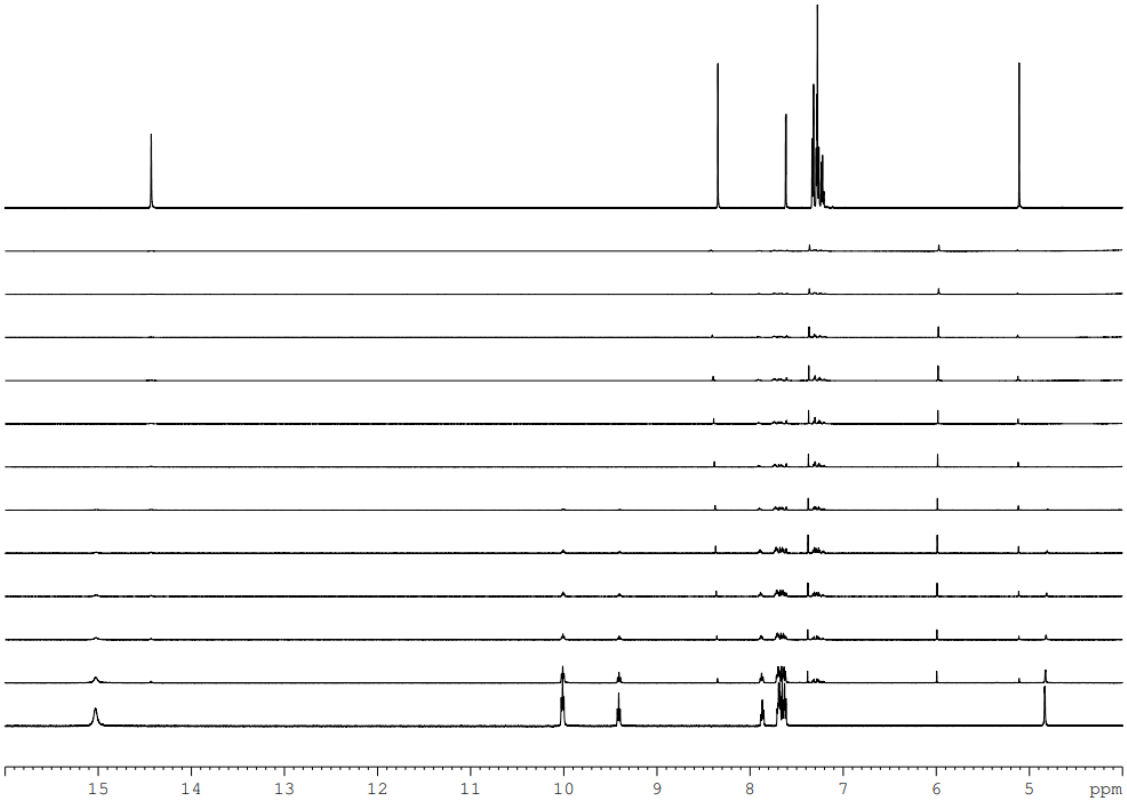

Figure 31. *Selected region of ^{1}H NMR titration of [Δ-(**L2**)$_2$.Eu][PPh$_4$] with DMMP in MeCN-d_3. Number equivalents between 0 and 3.26. Being the first experiment without DMMP, and start adding from the bottom to the top, being the top ^{1}H NMR from the free ligand ((R,R)-**L2**).*

This initial spectra do not present any impurities with the starting material and has presented the same behaviour as its enantiomer. Addressing the two hypothesis described for this compound, [Δ-(**L2**)$_2$.Eu][PPh$_4$], after the UV-Vis titration of it, it appears that the one that happened was the second one. It has the formation of the free ligand, evidence in the signals at 14.45, 8.35 and 5.11 ppm, and appearance of the peak at 6 ppm, indicates the formation of multiple bonds between the new 1:1 complex and DMMP.

This last two spectra of the enantiomers show that the counterion may not play an important role in the bonding of the DMMP, however more studies should be made due to the impurity of the one with Et$_3$NH and due to the discrepancy in the molar absorption coefficients between the enantiomers that hinders the comparation between the counterions, that in theory should be the same.

2.3.4 Fluorescence titrations

It was also performed two fluorescence titrations of the [Δ-(**L1**)$_2$.Eu][PPh$_4$] and [Δ-(**L2**)$_2$.Eu][PPh$_4$], with DMMP in acetonitrile (for more information see ***table 15*** and ***table 16***, respectively). The maximum wavelength of absorption of both complexes was at 364 and 366 nm respectively, so they were both excited 370 nm. Both plot of intensity in function of the number of equivalents were made based on the intensity collected at 612 nm, due that to be the most intense wavelength characteristic of the Eu ($^5D_0 \rightarrow {}^7F_2$) as can be proved by the ***figure 55*** and ***56***, respectively.

Both plots are shown in ***figure 32***, however it was needed to do new plots, in function only of the guest solution and not in order of [G]/[H], so could be fitted the data (as previously done for the UV-Vis data), to calculate the binding contestant, as is shown in ***figure 33*** for [Δ-(**L1**)$_2$.Eu][PPh$_4$] and in ***figure 34*** for [Δ-(**L2**)$_2$.Eu][PPh$_4$].

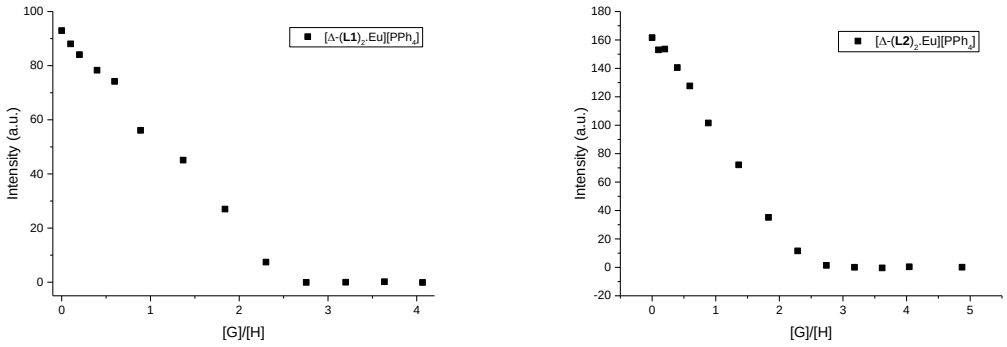

Figure 32. *Fluorescence spectra during the titration of left - [Δ-(**L1**)$_2$.Eu][PPh$_4$] with DMMP (0.668-27.1 μM) and right - [Δ-(**L2**)$_2$.Eu][PPh$_4$] with DMMP (0.668-32.6 μM). Concentration of the hosts constants left at 6.66 μM and right at 6.69 μM. Titration in acetonitrile at r.t. (λ_{ex} – 370 nm) at the wavelength of 612 nm.*

From the plots of ***figure 32*** we can interpretate it like having similar shapes, with a difference in intensity, agreeing that both present a strong binding.

It was made a table to compare the results of the logarithmic of the binding constants from the UV-Vis and fluorescence titrations of [Δ-(**L1**)$_2$.Eu][PPh$_4$] and [Δ-(**L2**)$_2$.Eu][PPh$_4$] (***table 5***).

All the values calculated gave values in between log *K* 7 and 8, these were too large to be accurately determined by techniques. This could be corroborated by the also large values of the standard error. Another incongruence is the fact that values for the binding constant for the complex [Δ-(**L1**)$_2$.Eu][PPh$_4$] gave almost an order of magnitude of difference. The results should give the same value. The hypothesis here is that the family of complexes **L1** and **L2** gave better results than **I1** and **I2**. However, should be performed more studies.

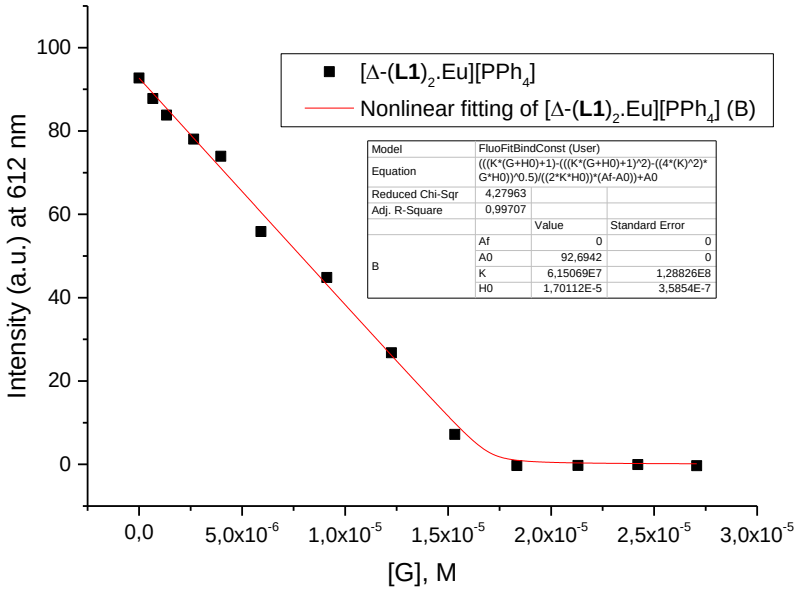

Figure 33. *Nonlinear fitting of [Δ-(**L1**)$_2$.Eu][PPh$_4$] and DMMP in MeCN.*

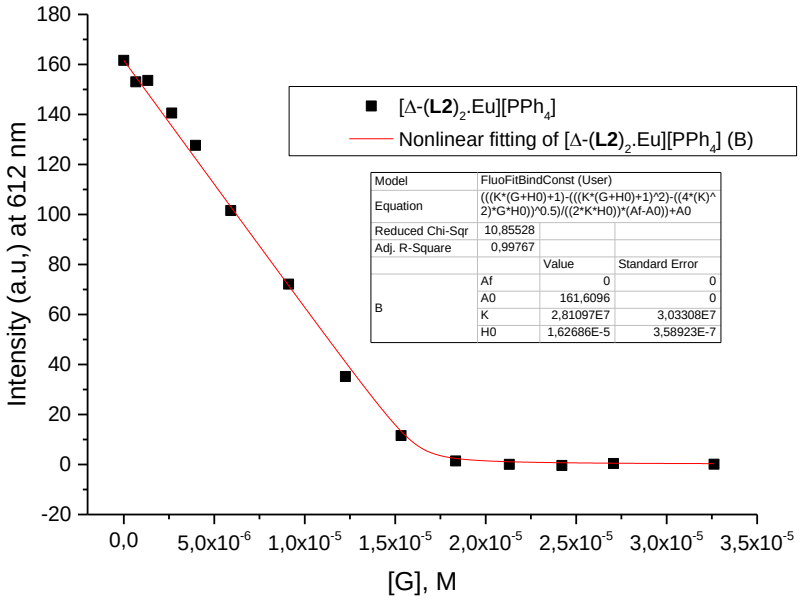

Figure 34. *Nonlinear fitting of [Δ-(**L1**)$_2$.Eu][PPh$_4$] and DMMP in MeCN.*

Table 5. *Table to compare the results of the binding constant of the host complexes with two different techniques, UV-Vis and fluorescence, with the respect standard errors.*

Complex	Technique	*K*	Log *K*	Standard Error
[Δ-(**L1**)$_2$.Eu][PPh$_4$]	UV-Vis	1.011E7	7.00	1.024E7
	Fluorescence	6.15E7	7.79	1.29E8
[Δ-(**L2**)$_2$.Eu][PPh$_4$]	UV-Vis	2.12E7	7.33	2.49E8
	Fluorescence	2.81E7	7.45	3.03E7

2.3.5 Lifetimes

The lifetimes studies were just performed in the "lambda" (Λ) chirality and with Et_3NH counterion the due to the similarities between both enantiomers in the molar absorption coefficient results and the congruence between enantiomers with that same counterion.

Table 6. *Lifetimes of the compounds [Λ-(**L1**)$_2$.Eu][Et$_3$NH] and [Λ-(**L2**)$_2$.Eu][Et$_3$NH] in milliseconds (ms), with the respective concentration and SD.*

Compounds	Solvent	Concentration (M)	Tau (τ, ms)	Standard Error, SD
[Λ-(**L1**)$_2$.Eu][Et$_3$NH]	MeCN	1.78E-05	0.0191	2.99E-4
	MeCN-d$_3$		0.0182	2.043E-4
	MeOH		0.0315	5.74E-4
	MeOH-d$_4$		0.0359	3.62E-4
	$CHCl_3$		0.0513	2.72E-03
	$CHCl_3$-d		0.0396	2.020E-03
[Λ-(**L2**)$_2$.Eu][Et$_3$NH]	MeCN	1.29E-05	0.0412	4.54E-4
	MeCN-d$_3$		0.0420	4.48E-4
	MeOH		0.135	9.75E-4
	MeOH-d$_4$		0.157	1.36E-3
	$CHCl_3$		0.0393	5.59E-4
	$CHCl_3$-d		0.0394	5.73E-4

The lifetimes results show that there is no significative difference between deuterated and non-deuterated solvents. This indicates that the solvent is not able to coordinate with the first coordination sphere, due to the non-accessible metal in any of these solvents.[12] However, the results for the experiments in both methanol solvents present a higher value of lifetime that was expected. The methanol solvents due to their ability to make H-bonds should perform quenching, decreasing the lifetime. This results are curious also because this phenomena only happens in the complex **L2**. It should be done more studies using a more sensitive instrument that also allows more scans.

Chapter 3

Conclusion and future perspectives

3.1 Conclusion

This project aimed to develop of a more sensitive and easier to use sensor to detect DMMP (simulant Sarin). Two families of compounds **I1**, **I2** and **L1**, **L2** were synthesized and their behaviour in the presence of DMMP was studied by UV-Vis, NMR and fluorescence titrations.

The synthesis of ligand **I1** and the complex **I1**.Zn was achieved with yields of 72 and 69 % respectively. The ligand **I2**, and its respective complex with Zn was obtained in 20 and 40 % yields respectively. A third ligand **I3** was synthesized (40 % yield) but attempts of synthesizing its Zn complex were unsuccessful. The second family of ligands **L1** and **L2** with their respective complexes with Eu were successfully obtained with yields ranging between 72 and 90 % yields, with the exception of (S,S)-**L1** (20 %) and [Λ-(**L2**)$_2$.Eu][Et_3NH] (19 %). Ligand, **L3**, that was successfully obtained in 65 % yield, however its complexation with Eu was not accomplished. The complexation of **L2** with Zn was successfully accomplished with 68 % yield.

To better interpretate the results of the UV-Vis and fluorescence titration, in ***table 7*** are the values of all the calculated binding constants for each complex, with the respective standard errors.

Table 7. *Table to compare the results of the binding constant of all the host complexes with two different techniques, UV-Vis and fluorescence, with the respect standard errors (SE). Zn-3OH is the highest value reported in literature host to detect DMMP, and it respective SD.*

Complex	Technique	*K*	Log *K*	SD or SE
Zn-3OH	UV-Vis	---	5.04[3]	0.4084[3] (SD)
[(*R*,*R*)-**I1**.Zn]		5.14E5	5.71	1.37E5 (SE)
[(*R*,*R*)-**I2**.Zn]		6.73E5	5.83	1.72E5 (SE)
[Δ-(**L1**)$_2$.Eu][PPh_4]		1.011E7	7.00	1.024E7 (SE)
	Fluorescence	6.15E7	7.79	1.29E8 (SE)
[Δ-(**L2**)$_2$.Eu][PPh_4]	UV-Vis	2.12E7	7.33	2.49E8 (SE)
	Fluorescence	2.81E7	7.45	3.033E7 (SE)

The results of the complex **I1**.Zn comparing with the ones described in the literature, show a change in the behaviour and a slightly higher binding constant. The complex **I2**.Zn displayed a slightly higher value compared to **I1**, what indicated that it could be more sensitive to the detection of DMMP.

The values of the binding constants for the family of complexes **L1**.Eu and **L2**.Eu were too large (> 1×10^7) to be accurately determined by these techniques. In the case of the complex **L1** the data collected from the UV-Vis, NMR and fluorescence indicates the formation of a new complex other than the simple bonding between the complex **L1** and the DMMP. In the case of the complex **L2** the data shown a typical negative cooperativity profile. Likely, this indicates a mechanism in which after the addition of DMMP, one of the ligands of $(\mathbf{L2})_2$.Eu detaches, producing ligand **L2** and a new 1:1 complex (ligand : europium) with the Eu coordination sites available. This 1:1 complex is able to bind more than one DMMP molecule forming a new complex. This complex looks promising due to the large values of the binding constant.

The results presented indicate that the complexes **L1** and **L2** are more promising than the **I1** and **I2** family, and that the counterion of the complexes does not affect the binding of the DMMP.

3.2 Future perspectives

Starting from the point of view of the synthesis that are interesting to be done is the one that were unsuccessful during this thesis, the **I1** with Eu, **I3** with Zn and **L3** with Eu. Could also be interesting the synthesis of the **I2** and **I3** with Eu. However, due to the conclusion that the initial complex of 2:1, ligand : europium, is breaking into forming a 1:1 complex and having free ligand would be interesting the pursuit of two different pathways of synthesis. The first one would it be to synthesize a more label ligand to increase the efficiency of binding the DMMP. However, this approach only makes the sensor more sensitive and nor specific as the initial aim of this project. With that in mind the second approach would be the search and synthesis of a more robust ligand that does not break after the addition of the DMMP, by maximizing the interaction between host and guest. The second approach is more challenging due to inability of some computational programmes to use calculations with lanthanides.

The experiment of the UV-Vis titration of the complex **I1**, due to the disparity of the value of the binding constant calculated with the one reported in the literature. To complement this comparation, with will be also needed the performance of the NMR and fluorescence titrations of the same complex. The same is applicable for the complex **I2** that will need the performance of the NMR titration to better understand the process that can be seen happening by the UV-Vis titration performed.

It is also needed the performance of different techniques to understand why it was the values of the binding constants of the complexes **L1** and **L2** so large, and a new fitting for the complex **L2** should be considered.

Also, it should be noted that only the performance of all three different titrations of all the complexes synthesized will gave the certainty if the change in counterion and the change in the chirality influence the outcome of the results.

Chapter 4

Experimental

4.1 Methods and materials

4.1.1 General Methods

Unless stated otherwise, all reagents were purchased from fluoro**chem** and used without further purification. NMR spectra were recorded on a Bruker TopSpin instrument with an Ascend™ 500. Chemical shifts were reported in parts per million (ppm) from high to low frequency and referred to the residual solvent resonance. Coupling constants (J) are reported in hertz (Hz). Were used the standard abbreviations indicating the multiplicity as referred in abbreviations (page xi and xii). UV-Vis spectra were obtained by using a Specord 50 plus from SciMed, analytikjena, and data collected with the program WinASPECT PLUS. The fluorescence spectra were recorded on a fluorescence spectrophotometer from Cary Eclipse, varian with data collect with the program Scan – Online. For this last two techniques were used quartz cells with a path length of 1 cm. The QY were performed in a different fluorimeter, Edinburgh instruments, FLS980.

All the data was processed using excel and OriginPro 9.1 64Bit, except the NMR spectra that was in Bruker TopSpin 4.2.0 on Desktop.

4.1.2 Molecular modelling

Using the ChemDraw 21.0.0 the structures of the compounds were made to be after uploaded in the Spartan '14 V1.1.4. In the software were made first the optimization of each compound isolated, and the same to the DMMP, before the final calculation with both compounds (complex and DMMP). The seatings of the computational calculations were the following, equilibrium geometry at ground state with density functional B3LYP 6-31G* in vacuum. Setting for a geometrycycle equal to 100000.

After individual geometry optimization similar calculations were performed with the salen ligand and DMMP together, to see their interactions.

4.1.3 Procedures of the synthesis

Ligand 1:

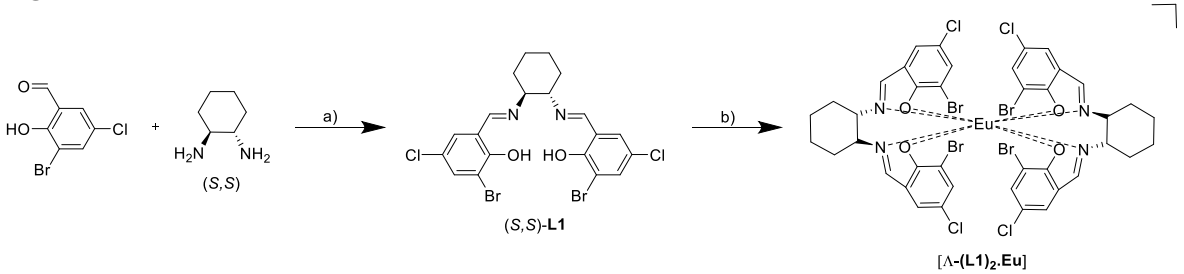

Scheme 1. *Scheme of the synthesis overview of ligand 1 and the respective complex. Reagents and conditions: a) EtOH, DCM/hexane; b) Eu(OTf)3, Et3N, MeOH.*

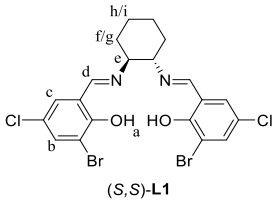

Figure 35. *Structure of the salen ligand (S,S)-**L1**.*

To the powders of 3-bromo-5-chloro-2-hydroxybenzaldehyde (0.218 g, 0.924 mmol, 2.0 eq) and (1S,2S)-(-)-1,2-cyclohexanediamine (0.052 g, 0.462 mmol, 1.0 eq) was added ethanol 99% (24 mL). The reaction mixture was stirred at 70°C for 3h. Cooled down to r.t., placed in an ice bath and the yellow solid recovered by filtration on high vacuum, washed with cold ethanol. Gave the title compound (*S,S*)-**L1** as a bright yellow powder (0.100 g, 0.182 mmol, 20%).

^{1}H NMR (500 MHz, $CHCl_3$-d) δ 14.29 (s, H_a), 8.15 (s, 2H, H_d), 7.52 (d, J = 2.48 Hz, 2H, H_c), 7.13 (d, J = 2.48 Hz, 2H, H_b), 3.36 (m, 2H, H_e), 1.93 (m, 2H, H_f), 1.71 (m, 2H, H_g), 1.47 (m, 4H, $H_{h/i}$).

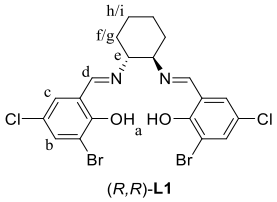

Figure 36. *Structure of the salen ligand (R,R)-**L1**.*

The experimental procedure followed was analogous to that of (*S,S*)-**L1** but starting from (1R,2R)-(+)-1,2-cyclohexanediamine. Gave the title compound (*R,R*)-**L1** as a bright yellow powder (quant., 0.256 g).

^{1}H NMR (500 MHz, $CHCl_3$-d) δ 14.29 (s, H_a), 8.15 (s, 2H, H_d), 7.52 (d, J = 2.48 Hz, 2H, H_c), 7.13 (d, J = 2.48 Hz, 2H, H_b), 3.36 (m, 2H, H_e), 1.93 (m, 2H, H_f), 1.71 (m, 2H, H_g), 1.47 (m, 4H, $H_{h/i}$).

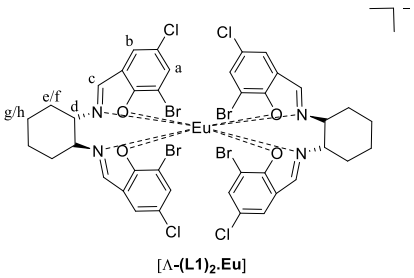

Figure 37. *Structure of the complex [Λ-(**L1**)$_2$.Eu].*

To a stirred solution of (*S,S*)-**L1** (0.088 g, 0.16 mmol, 2 eq) in Et_3N (0.067 mL, 0.48 mmol, 6 eq) was added MeOH (15 mL) until was fully dissolved. To the mixture was added $Eu(OTf)_3$ (0.047 g, 0.08 mmol, 1 eq) in powder. Reaction mixture stirred at 60°C for 1h, then was cooled to r. t. and stirred for another 48h. Cooled down to r.t., placed in an ice bath and the yellow solid recovered by vacuum filtration with a nylon membrane, washed with cold ethanol after the addition (3 mL) of distilled water dropwise. Gave the title compound [**Λ-(L1)$_2$.Eu**] as a pale-yellow powder (0.088 g, 0.065 mmol, 81 %).

^{1}H NMR (500 MHz, MeCN-d_3) δ 11.15 (s, 8H, $H_{g/h}$), 10.18 (d, J = 11.10Hz, 4H, H_e), 7.41 (t, J = 8.80 Hz, 4H, H_f), 5.90 (d, J = 2.54 Hz, 4H, H_b), 5.50 (d, J = 8.25 Hz, 4H, H_d), 3.03 (m, 6H, Et_3N), 2.57 (d, J = 2.54 Hz, 4H, H_a) 1.20 (t, J = 7.28 Hz, 9H, Et_3N), -7.85 (s, 4H, H_c).

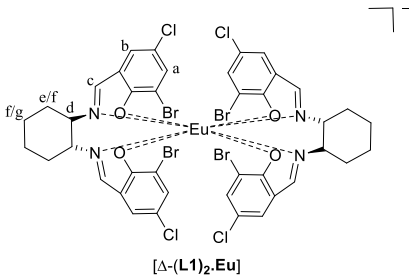

Figure 38. *Structure of the complex [Δ-(**L1**)$_2$.Eu].*

The experimental procedure followed was analogous to that of [**Λ-(L1)$_2$.Eu**] but starting from (*R,R*)-**L1**. Gave the title compound [**Δ-(L1)$_2$.Eu**] as a pale-yellow powder (0.097 g, 0.072 mmol, 90%).

^{1}H NMR (500 MHz, MeCN-d_3) δ 11.15 (s, 8H, $H_{g/h}$), 10.18 (d, J = 11.10Hz, 4H, H_e), 7.41 (t, J = 8.80 Hz, 4H, H_f), 5.90 (d, J = 2.54 Hz, 4H, H_b), 5.50 (d, J = 8.25 Hz, 4H, H_d), 3.03 (m, 6H, Et_3N), 2.57 (d, J = 2.54 Hz, 4H, H_a) 1.20 (t, J = 7.28 Hz, 9H, Et_3N), -7.85 (s, 4H, H_c).

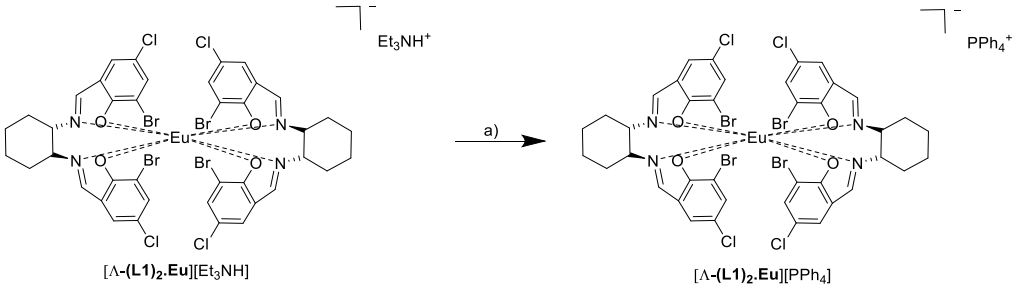

Scheme 2. *Scheme of the synthesis overview of the salt metathesis of the ligand 1 complex. Reagents and conditions: a)PPh_4Br, MeCN*

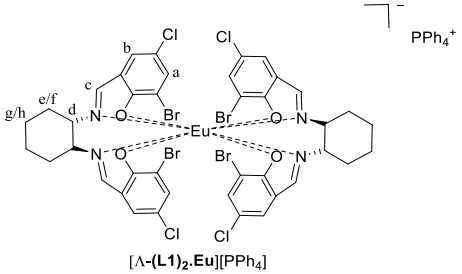

Figure 39. *Structure of the complex [Λ-(**L1**)$_2$.Eu][PPh_4].*

To a stirred solution of [Λ-(**L1)$_2$.Eu**][Et_3NH] (0.026 g, 0.019 mmol, 1 eq) in MeCN (1.83 mL), was added dropwise a solution of PPh_4Br (0.146 g, 0.349 mmol, 18 eq) in MeCN (1.36 mL). After stirred at r. t. for about 1h, the solid was dried washed with the minimum of cold MeCN, vacuum filtered with a nylon membrane. Gave the title compound [Λ-(**L1)$_2$.Eu**][PPh_4] as a pale-yellow powder (0.026 g, 0.016 mmol, 86 %).

^{1}H NMR (500 MHz, MeCN-d_3) δ 11.19 (s, 8H, $H_{g/h}$), 10.22 (d, J = 9.47 Hz, 4H, H_c), 7.90 (m, 8H, PPh_4), 7.70 (m, 12H, PPh_4), 7.44 (t, J = 8.42 Hz, 4H, H_f), 5.89 (d, J = 2.62 Hz, 4H, H_b), 5.53 (d, J = 8.26 Hz, 4H, H_d), 2.56 (d, J = 2.55 Hz, 4H, H_a), -7.80 (s, 4H, H_c).

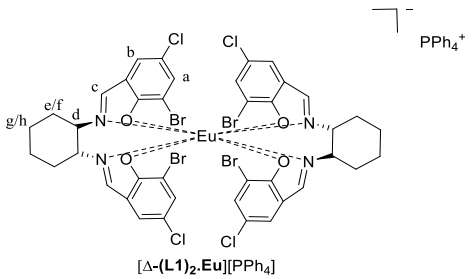

Figure 40*. Structure of the complex [Δ-(**L1**)$_2$.Eu][PPh_4].*

The experimental procedure followed was analogous to that of [Λ-(**L1)$_2$.Eu**][PPh_4] but starting from [Δ-(**L1)$_2$.Eu**][Et_3NH]. [Δ-(L1)$_2$.Eu][PPh_4] (0.026 g, 0.016 mmol, 86 %).

^{1}H NMR (500 MHz, MeCN-d$_3$) δ 11.19 (s, 8H, H$_{g/h}$), 10.22 (d, J = 9.47 Hz, 4H, H$_e$), 7.90 (m, 8H, PPh$_4$), 7.70 (m, 12H, PPh$_4$), 7.44 (t, J = 8.42 Hz, 4H, H$_f$), 5.89 (d, J = 2.62 Hz, 4H, H$_b$), 5.53 (d, J = 8.26 Hz, 4H, H$_d$), 2.56 (d, J = 2.55 Hz, 4H, H$_a$), -7.80 (s, 4H, H$_c$).

Ligand 2:

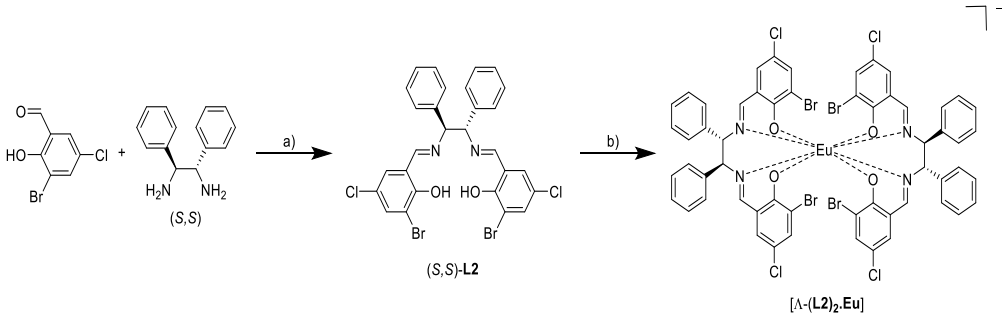

***Scheme 3**. Scheme of the synthesis overview of the ligand 2 and the respective complex . Reagents and conditions: a) EtOH; b) Eu(OTf)$_3$, Et$_3$N, MeOH.*

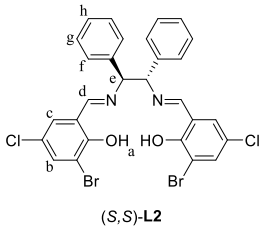

***Figure 41.** Structure of the salen ligand (S,S)-**L2**.*

To the powders of 3-bromo-5-chloro-2-hydroxybenzaldehyde (0.236 g, 1.0 mmol, 2.0 eq) and (1S,2S)-(-)-1,2-Diphenylethylenediamine (0.107 g, 0.5 mmol, 1.0 eq) was added ethanol 99% (8 mL) at room temperature (r. t.). The reaction mixture was stirred at r. t. for 24h. The solution was dried with a membrane vacuum filtration and washed with cold EtOH. Gave the title compound (*S,S*)-**L2** as a pale-yellow powder (0.257 g, 0.396 mmol, 79%).

^{1}H NMR (500 MHz, MeCN-d$_3$) δ 14.43 (s, 2H, H$_a$), 8.34 (s, 2H, H$_d$), 7.62 (d, J = 2.52 Hz, 2H, H$_c$), 7.32 (d, J = 7.00 Hz, 4H, H$_f$), 7.27 (m, 6H, H$_g$ and H$_b$), 7.22 (tt, J = 7.18, 1.75 Hz, 2H, H$_g$), 5.11 (s, 2H, H$_e$).

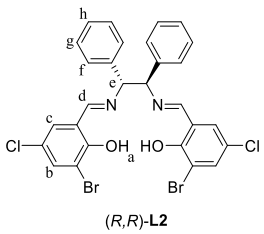

Figure 42.** Structure of the salen ligand (R,R)-**L2.

The experimental procedure followed was analogous to that of (*S,S*)-**L2** but starting from (1R,2R)-(+)-1,2-Diphenylethylenediamine. Gave the title compound (*R,R*)-**L2** as a pale-yellow powder (0.283 g, 0.437mmol, 87%).

^{1}H NMR (500 MHz, MeCN-d_3) δ 14.43 (s, 2H, H_a), 8.34 (s, 2H, H_d), 7.62 (d, J = 2.52 Hz, 2H, H_c), 7.32 (d, J = 7.00 Hz, 4H, H_f), 7.27 (m, 6H, H_g and H_b), 7.22 (tt, J = 7.18, 1.75 Hz, 2H, H_g), 5.11 (s, 2H, H_e).

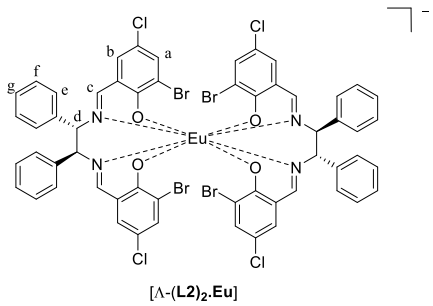

Figure 43. *Structure of the complex [Λ-(**L2**)$_2$.Eu].*

The experimental procedure followed was analogous to that of [**Λ**-(**L1)$_2$.Eu**] but starting from (*S,S*)-**L2**. Gave the title compound [**Λ**-(**L2)$_2$.Eu**] as a pale-yellow powder (0.024 g, 0.0153 mmol, 19%).

^{1}H NMR (500 MHz, MeCN-d_3) δ 15.02 (s, 4H, H_e), 10.01 (t, J = 7.12 Hz, 8H, H_f), 9.41 (t, J = 7.59 Hz, 8H, H_g), 4.84 (d, J = 1.69 Hz, 4H, H_b), 3.06 (m, 6H, Et_3N), 2.11 (s, 4H, H_a), 1.20 (t, J = 7.25 Hz, 9H, Et_3N), -8.37 (s, 4H, H_c). The proton H_d was missing, could be not in the window (-9 to 20 ppm) or just be overlapped with another signal.

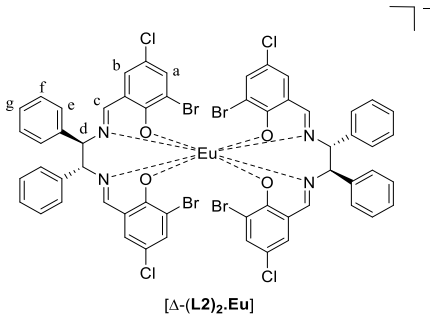

Figure 44. *Structure of the complex [Δ-(**L2**)$_2$.Eu].*

The experimental procedure followed was analogous to that of [**Λ**-(**L2)$_2$.Eu**] but starting from (*R,R*)-**L2**. Gave the title compound [**Δ**-(**L2)$_2$.Eu**] as a pale-yellow powder (0.089 g, 0.058 mmol, 72%).

^{1}H NMR (500 MHz, MeCN-d_3) δ 15.02 (s, 4H, H_e), 10.01 (t, J = 7.12 Hz, 8H, H_f), 9.41 (t, J = 7.59 Hz, 8H, H_g), 4.84 (d, J = 1.69 Hz, 4H, H_b), 3.06 (m, 6H, Et_3N), 2.11 (s, 4H, H_a), 1.20 (t, J = 7.25 Hz, 9H, Et_3N), -8.37 (s, 4H, H_c). The proton H_d was missing, could be not in the window (-9 to 20 ppm) or just be overlapped with another signal.

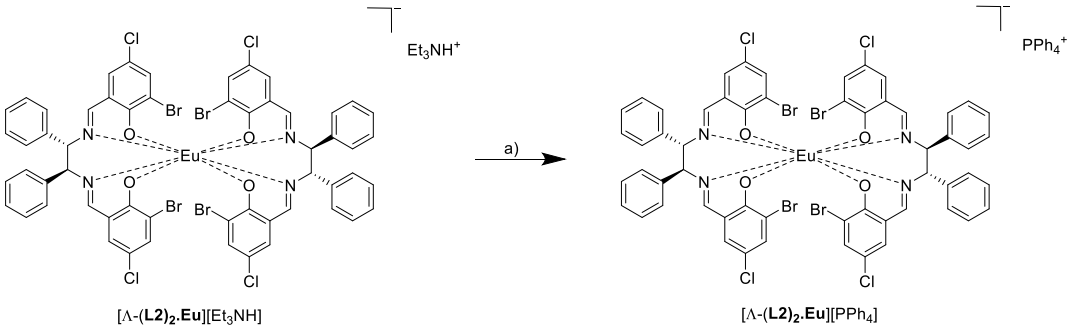

Scheme 4. *Scheme of the synthesis overview of the salt metathesis of the ligand 2 complex. Reagents and conditions: a)PPh_4Br, MeCN.*

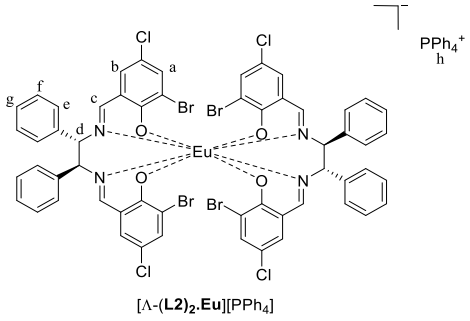

Figure 45. *Structure of the complex [Λ-(**L2**)$_2$.Eu][PPh_4].*

The experimental procedure followed was analogous to that of [Λ-(**L1)$_2$.Eu**][PPh_4] but starting from [Λ-(**L2)$_2$.Eu**][Et_3NH]. Gave the title compound [Λ-(**L2)$_2$.Eu**][PPh_4] as a pale-yellow powder (quant., 0.03 mg).

^{1}H NMR (500 MHz, MeCN-d_3) δ 15. 03 (s, 8H, H_e), 10.01 (t, J = 6.97 Hz, 8H, H_f), 9.41 (t, J = 7.72 Hz, 4H, H_g), 7.86 (t, J = 7.27 Hz, 4H, PPh_4), 7.64 (m, 16H, PPh_4), 4.83 (s, 4H, H_b), 2.10 (s, 4H, H_a), -8.36 (s, 4H, H_c). The proton H_d was missing, could be not in the window (-9 to 20 ppm) or just be overlapped with another signal.

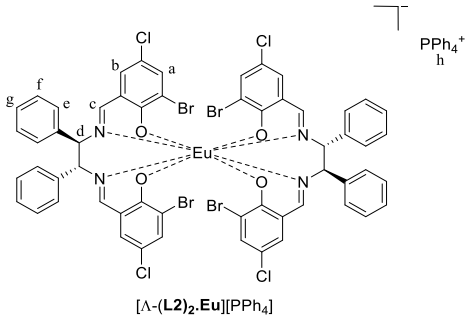

Figure 46. *Structure of the complex [Δ-(**L2**)$_2$.Eu][PPh4].*

The experimental procedure followed was analogous to that of [**Λ-(L2)$_2$.Eu**][PPh$_4$] but starting from [**Δ-(L2)$_2$.Eu**][Et$_3$NH]. Gave the title compound [**Δ-(L2)$_2$.Eu**][PPh$_4$] as a pale-yellow powder (0.025 g, 0.014 mmol, 73%).

^{1}H NMR (500 MHz, MeCN-d$_3$) δ 15. 03 (s, 8H, H$_c$), 10.01 (t, J = 6.97 Hz, 8H, H$_f$), 9.41 (t, J = 7.72 Hz, 4H, H$_g$), 7.86 (t, J = 7.27 Hz, 4H, PPh$_4$), 7.64 (m, 16H, PPh$_4$), 4.83 (s, 4H, H$_b$), 2.10 (s, 4H, H$_a$), -8.36 (s, 4H, H$_c$). The proton H$_d$ was missing, could be not in the window (-9 to 20 ppm) or just be overlapped with another signal.

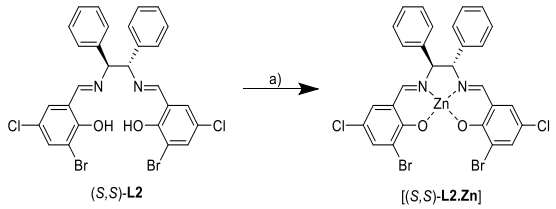

Scheme 5. *Scheme overview of synthesis of the complex [(S,S)-**L2**.Zn]. Reagents and conditions: a) Zn(AcO)$_2$, EtOH.*

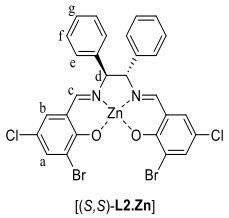

Figure 47. *Structure of the complex [(S,S)-**L2**.Zn].*

To a stirred solution of (*S,S*)-**L2** (0.103 g, 0.16 mmol, 1 eq) in EtOH (3 mL) was added a dissolved solution of Zn(AcO)$_2$ in EtOH (8 mL), Reaction mixture was stirred at ~90ºC with a Vigreux condenser on top during around 18h. The solution was dried with a membrane vacuum filtration and washed with cold EtOH. Gave the title compound [(*S,S*)-**L2.Zn**] as a yellow powder (0.0774g, 0.109 mmol, 68%).

^{1}H NMR (500 MHz, DMSO-d$_6$) δ 8.30 (s, 2H, H$_c$), 7.63 (d, J = 2.85 Hz, 2H, H$_b$), 7.39 (d, J = 7.12 Hz, 4H, H$_e$), 7.61 (t, J = 7.61 Hz, 4H, H$_f$), 7.28 (tt, J = 7.13, 1.67 Hz, H$_g$) 7.23 (d, J = 2.85 Hz, 2H, H$_a$), 5.15 (s, 2H, H$_d$).

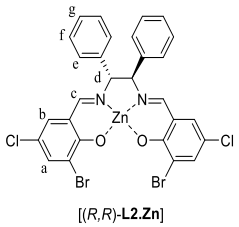

Figure 48. *Structure of complex [(R,R)-**L2**.Zn].*

The experimental procedure followed was analogous to that of [(*S,S*)-**L2.Zn**] but starting from (*R,R*)-**L2**. Gave the title compound [(*R,R*)-**L2.Zn**] as a yellow powder (0.0925 g, 0.130 mmol, 81 %).

^{1}H NMR (500 MHz, DMSO-d_6) δ 8.30 (s, 2H, H_c), 7.63 (d, J = 2.85 Hz, 2H, H_b), 7.39 (d, J = 7.12 Hz, 4H, H_e), 7.61 (t, J = 7.61 Hz, 4H, H_f), 7.28 (tt, J = 7.13, 1.67 Hz, H_g) 7.23 (d, J = 2.85 Hz, 2H, H_a), 5.15 (s, 2H, H_d).

Ligand 3:

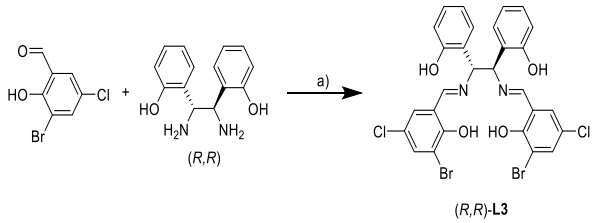

Scheme 6. *Scheme overview of the synthesis of the ligand 3. Reagents and conditions: a) EtOH.*

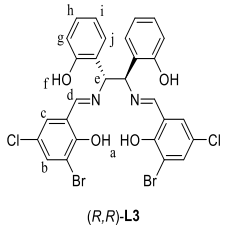

Figure 49. *Structure of the salen ligand (R,R)-**L3**.*

The experimental procedure followed was analogous to that of one following for ligand 3, but with 3-bromo-5-chloro-2-hydroxybenzaldehyde and (+)-2,2`-((1R,2R)-1,2-diaminoethane-1,2-diyl)-diphenol. The conditions of the rotary evaporation were adapted for this compound. After NMR was confirmation of presence of starting material. Was made a recrystallization in acetonitrile. Gave the title compound (*R,R*)-**L3** as an orange powder (0.2218 g, 0.327 mmol, 65%).

^{1}H NMR (500 MHz, MeCN-d_3) δ 14.75 (br, 2H, H_a), 8.28 (s, 2H, H_d), 7.60 (d, J = 2.55 Hz, 2H, H_c), 7.40 (br, 2H, H_f), 7.25 (dd, J = 7.75, 1.30 Hz, 2H, H_g), 7.22 (d, J = 2.55 Hz, 2H, H_b), 7.06 (td, J = 7.72, 1.60 Hz, 2H, H_i), 6.80 (d, J = 8.05 Hz, 2H, H_j), 6.75 (t, J = 7.48 Hz, 2H, H_j), 5.60 (s, 2H, H_e).

Italian's 1:

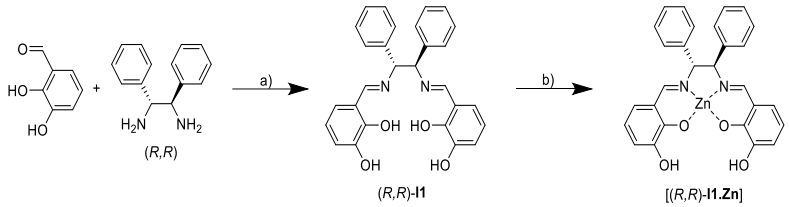

Scheme 7. *Scheme overview of the synthesis of the ligand italian's 1 and the respective complex. Reagents and conditions: a)EtOH; b) $Zn(AcO)_2$, EtOH.*

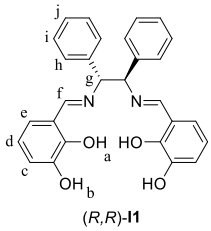

Figure 50. *Structure of the salen ligand (R,R)-**I1**.*

To the powders of 2,3-dihydroxylbenzaldehyde (0.138 g, 1.0 mmol, 2.0 eq) and (1R,2R)-(+)-1,2-Diphenylethylenediamine (0.106 g, 0.5 mmol, 1.0 eq) was added ethanol 99% (8 mL) at r.t. The reaction mixture was stirred at r.t. for 24h. The solution was dried using a rotary evaporation (35ºC,~250 mbar to ~50 mbar, ~30min). After completely dry gave the title compound (*R,R*)-**I1** as an orange solid (0.1623 g, 0.359 mmol, 72%).

^{1}H NMR (500 MHz, DMSO-d_6) δ 13.39 (br, 2H, H_a), 9.08 (br, 2H, H_b), 8.46 (s, 2H, H_f), 7.32 (d, J = 7.30 Hz, 4H, H_h), 7.26 (t, J = 7.55 Hz, 4H, H_i), 7.18 (t, J = 7.23 Hz, 2H, H_j), 6.82 (dd, J = 7.78, 1.38 Hz, 2H, H_e), 6.76 (dd, J = 8.00, 1.33 Hz, 2H, H_c), 6.64 (t, J = 7.75 Hz, 2H, H_d), 5.09 (s, 2H, H_g).

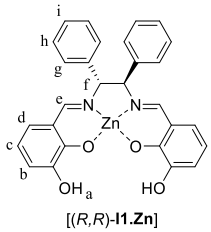

Figure 51. *Structure of the complex [(R,R)-**I1**.Zn].*

To a stirred solution of (R,R)-**I1** (0.0406 g, 0.0838 mmol, 1.0 eq) in EtOH (1.26 mL) was added dropwise a dissolved solution of $Zn(AcO)_2$ (0.01537 g, 0.0838 mmol, 1.0 eq) in EtOH (3.35 mL). Reaction mixture was stirred at ~90ºC with a Vigreux condenser on top during around 18h. The solution was dried with a membrane vacuum filtration and washed with cold EtOH. Gave the title compound [(*R,R*)-**I1.Zn**] as an orange powder (0.0297 g, 0.0576 mmol, 69%).

^{1}H NMR (500 MHz, DMSO-d$_6$) δ 8.24 (s, 2H, H$_a$), 7.88 (s, 2H, H$_e$), 7.40 (d, J = 7.30 Hz, 4H, H$_g$), 7.34 (t, J = 7.65 Hz, 4H, H$_h$), 7.26 (t, J = 7.28 Hz, 2H, H$_i$), 6.73 (dd, J = 7.30, 1.66 Hz, 2H, H$_d$), 6.53 (dd, J = 8.10, 1.65 Hz, 2H, H$_b$), 6.28 (t, J = 7.68 Hz, 2H, H$_c$), 5.14 (s, 2H, H$_f$).

Italian's 2:

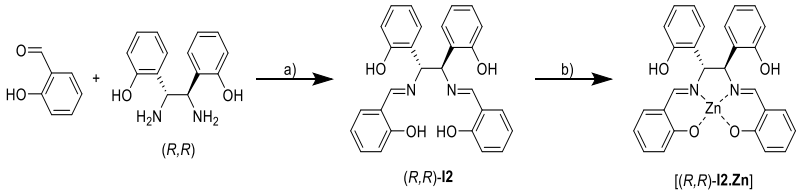

Scheme 8. *Scheme overview of the synthesis of the ligand italian's 2 and the respective complex. Reagents and conditions: a) EtOH, b) Zn(AcO)$_2$, MeOH.*

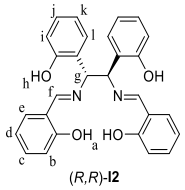

Figure 52. *Structure of the salen ligand (R,R)-**I2**.*

The experimental procedure followed was analogous to that of one following for ligand 3, but with 2,3-dihydroxylbenzaldehyde and salicylaldehyde. Do a recrystallization after the use of the rotary evaporation in MeCN. Gave the title compound (*R,R*)-**I2** as a yellow solid (0.0460 g, 0.102 mmol, 20%)

^{1}H NMR (500 MHz, DMSO-d$_6$) δ 13.62 (br, 2H, H$_a$), 9.68 (br, 2H, H$_h$), 8.42 (s, 2H, H$_f$), 7.32 (dd, J = 7.63, 1.67, 2H, H$_e$), 7.26 (m, 4H, H$_c$ and H$_j$), 6.97 (td, J = 7.66, 1.67 Hz, 2H, H$_d$), 6.81 (m, 4H, H$_b$ and H$_i$), 6.75 (dd, J = 8.10, 1.05 Hz, 2H, H$_l$), 6.65 (td, J = 7.46, 1.05 Hz, 2H, H$_k$), 5.52 (s, 2H, H$_g$).

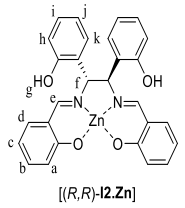

Figure 53. *Structure of the complex [(R,R)-**I2**.Zn].*

To a stirred solution of (*R,R*)-**I2** (0.0359 g, 0.0793 mmol, 1.0 eq) in EtOH (1.19 mL) was added dropwise a dissolved solution of Zn(AcO)$_2$ (0.0145 g, 0.0793 mmol, 1.0 eq) in EtOH (3.17 mL). Reaction mixture was stirred at ~90ºC with a Vigreux condenser on top during around 18h. volume of the solution was reduced to a $^1/_3$ on rotary evaporation, followed by an addition of 3

drops of distilled water and a membrane filtration. Gave the title compound [(*R,R*)-**I2.Zn**] as a yellow powder (0.0162 g, 0.0314 mmol, 40%).

^{1}H NMR (500 MHz, DMSO-d$_6$) δ 9.78 (br, 2H, H$_g$), 8.07 (s, 2H, H$_e$), 7.09 (m, 6H, H$_a$, H$_b$ and H$_i$), 6.95 (dd, J = 7.82 and 1.86 Hz, 2H, H$_d$), 6.81 (t, J = 7.90 Hz, 2H, H$_h$), 6.70 (t, J = 6.53 Hz, 2H, H$_c$) 6.62 (d, J = 8.72 Hz, 2H, H$_k$), 6.35 (t, J = 7.27 Hz, 2H, H$_j$), 5.30 (br, 2H, H$_f$).

Italian's 3:

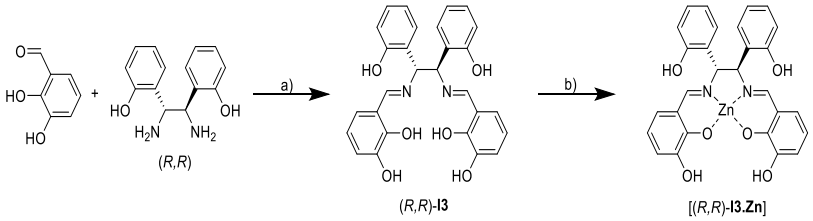

Scheme 9. *Scheme overview of the synthesis of the ligand italian's 3 and the respective complex. Reagents and conditions: a) EtOH, b) Zn(AcO)$_2$, MeOH.*

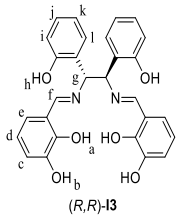

Figure 54. *Structure of the salen ligand (R,R)-**I3**.*

The experimental procedure followed was analogous to the one described for the ligand 2 but starting with 2,3-dihydroxylbenzaldehyde and (+)-2,2`-((1R,2R)-1,2-diaminoethane-1,2-diyl)-diphenol. To increase the yield, after the first filtration was added some drop of distilled water to the filtrate solution and made another filtration. Gave the title compound (*R,R*)-**I3** as an orange powder (0.0959 g, 0.198 mmol, 40%).

^{1}H NMR (500 MHz, DMSO-d$_6$) δ 13.71 (br, 2H, H$_a$), 9.72 (br, 2H, H$_h$), 8.96 (br, 2H, H$_b$), 8.36 (s, 2H, H$_f$), 7.23 (dd, J = 7.72, 1.49 Hz, 2H, H$_l$), 6.99 (td, J = 7.78, 1.67 Hz, 2H, H$_j$), 6.76 (m, 6H, H$_c$, H$_e$ and H$_i$), 6.66 (td, J = 7.48, 1.03 Hz, 2H, H$_k$), 6.57 (t, J = 7.77 Hz, 2H, H$_d$), 5.54 (s, 2H, H$_g$).

4.1.4. General Titration Procedure

To keep the concentration of the host (complex) constant through the experiments different stock solutions were prepared. Stock solution of the host (H), with the identity always being the complex salen ligand – metal. And a stock solution of guest (G), with identity always being DMMP. For the UV-Vis and fluorescence titrations, a working solution was also prepared. In the case of the

NMR titrations both solutions were mixed in the NMR tube, changing the concentration of H and G during the titration. The working solution consist in having the solvent, both stock solutions of guest and host in different proportions all mixed and from that solution is going to be taken proportions to add in the cuvettes. The experiment 1 is the addition correspondent to the aliquot from the stock solution H added to the working solution and then all the following experiments are aliquots from the working solution. All the solutions were stirred to maintain homogeneity and shielded from UV exposure wrapping the vials in aluminium foil due to the sensitivity of the host compounds.

4.1.5. NMR studies

The NMR studies were carried out after every synthesis that was made, to make sure that the compound that want to achieve was made or not, and if that was clean. When synthesized a new compound was made a full characterization of the compound, besides the ^{1}H includes: ^{13}C, DEPT, COSY, HSQC and HMBC to help in the accuracy of the characterization of the compounds.

Was taken a couple of milligrams (mg) of the synthesized compounds, added to an NMR tube and then added ~0.5 mL of the adequate deuterated solvent. It was made sure that everything was completely dissolved, sometimes it was needed to use the sonicator, heatgun or as last resource change the solvent.

Were carried out NMR titrations as described in the general titration procedure (**4.1.4.**).

Table 8. *Representative data for the NMR titration of the complex [Δ-(**L1**)$_2$.Eu][PPh$_4$].*

Exp no.	G add, µL	[H], M	[G], M	G/H (eq)	New ^{1}H δ (ppm)
1	0	1.79E-03	0	0.00	-----
2	20	1.72E-03	3.10E-04	0.18	5.9943
3	20	1.65E-03	5.97E-04	0.36	5.9923
4	20	1.60E-03	8.64E-04	0.54	5.9904
5	20	1.54E-03	1.11E-03	0.72	5.9886
6	20	1.49E-03	1.34E-03	0.90	5.9868
7	30	1.42E-03	1.66E-03	1.17	5.9844
8	30	1.35E-03	1.95E-03	1.43	5.9821
9	30	1.29E-03	2.22E-03	1.71	5.9801
10	50	1.21E-03	2.61E-03	2.16	5.9770
11	50	1.13E-03	2.96E-03	2.62	5.9741
12	50	1.06E.03	3.26E-03	3.07	5.9713

Table 9. *Representative data for the NMR titration of the complex [Δ-(**L2**)$_2$.Eu][Et$_3$NH].*

Exp no.	G add, μL	[H], M	[G], M	G/H (eq)	New ^{1}H δ (ppm)
1	0	1.73E-03	0	0.00	-----
2	20	1.66E-03	3.10E-04	0.19	5.9943
3	20	1.60E-03	5.97E-04	0.37	5.9921
4	20	1.54E-03	8.64E-04	0.56	5.9902
5	20	1.49E-03	1.11E-03	0.75	5.9883
6	20	1.44E-03	1.34E-03	0.93	5.9864
7	30	1.37E-03	1.66E-03	1.21	5.9838
8	30	1.31E-03	1.95E-03	1.49	5.9814
9	30	1.25E-03	2.22E-03	1.77	5.9792
10	50	1.17E-03	2.61E-03	2.24	5.9756
11	50	1.09E-03	2.96E-03	2.71	5.9727
12	50	1.03E-03	3.26E-03	3.17	5.9700

Table 10. *Representative data for the NMR titration of the complex [Δ-(**L2**)$_2$.Eu][PPh$_4$].*

Exp no.	G add, μL	[H], M	[G], M	G/H (eq)	New ^{1}H δ (ppm)
1	0	1.68E-03	0	0.00	-----
2	20	1.62E-03	3.10E-04	0.19	5.9941
3	20	1.56E-03	5.97E-04	0.38	5.9921
4	20	1.50E-03	8.64E-04	0.57	5.9901
5	20	1.45E-03	1.11E-03	0.77	5.9884
6	20	1.40E-03	1.34E-03	0.96	5.9867
7	30	1.34E-03	1.66E-03	1.24	5.9842
8	30	1.28E-03	1.95E-03	1.53	5.9819
9	30	1.22E-03	2.22E-03	1.82	5.9797
10	50	1.14E-03	2.61E-03	2.30	5.9765
11	50	1.07E-03	2.96E-03	2.78	5.9737
12	50	1.00E-03	3.26E-03	3.26	5.9708

4.1.6. UV-Vis studies

Table 11. *Representative data for the UV-Vis titration of the complex [(R,R)-**I1**.Zn] at a constant concentration of 1.82E-05M and a Guest concentration going from 1.29E-06M to 1.08E-04M.*

Exp no.	G add, µL	[G], M	G/H (eq)	Abs (271nm)	Abs (291nm)	Abs (335nm)	Abs (383nm)
1	60	0	0.00	0.2336	0.4381	0.0375	0.1320
2	5	1.29E-06	0.07	0.2441	0.4349	0.0390	0.1296
3	5	2.57E-06	0.14	0.2531	0.4340	0.0397	0.1276
4	5	3.85E-06	0.21	0.2624	0.4309	0.0408	0.1252
5	10	6.39E-06	0.35	0.2780	0.4282	0.0420	0.1211
6	10	8.92E-06	0.49	0.2932	0.4231	0.0430	0.1160
7	15	1.27E-05	0.70	0.3165	0.4170	0.0453	0.1093
8	25	1.88E-05	1.04	0.3431	0.4121	0.0476	0.1023
9	25	2.49E-05	1.37	0.3738	0.4027	0.0503	0.0926
10	50	3.66E-05	2.01	0.4225	0.3914	0.0539	0.0787
11	50	4.79E-05	2.64	0.4751	0.3758	0.0586	0.0636
12	50	5.88E-05	3.24	0.5167	0.3666	0.0617	0.0522
13	50	6.93E-05	3.82	0.5574	0.3561	0.0650	0.0418
14	100	8.93E-05	4.92	0.6077	0.3528	0.0680	0.0326
15	100	1.08E-04	5.94	0.6484	0.3490	0.0697	0.0253

Table 12. *Representative data for the UV-Vis titration of the complex [(R,R)-**I2**.Zn] at a constant concentration of 1.82E-05M and a Guest concentration going from 1.29E-06M to 1.08E-04M.*

Exp no.	G add, µL	[G], M	G/H (eq)	Abs (265nm)	Abs (324nm)	Abs (366nm)
1	60	0	0.00	0.2939	0.0452	0.2036
2	5	1.29E-06	0.07	0.3071	0.0491	0.1978
3	5	2.57E-06	0.14	0.3166	0.0521	0.1921
4	5	3.85E-06	0.21	0.3201	0.0559	0.1847
5	10	6.39E-06	0.35	0.3307	0.0624	0.1748
6	10	8.92E-06	0.49	0.3381	0.0676	0.1623
7	15	1.27E-05	0.70	0.3472	0.0880	0.1281
8	25	1.88E-05	1.04	0.3630	0.0993	0.1047

Table 12. *Continuation.*

9	25	2.49E-05	1.37	0.3807	0.1116	0.0860
10	50	3.66E-05	2.01	0.4109	0.1259	0.0557
11	50	4.79E-05	2.64	0.4395	0.1347	0.0383
12	50	5.88E-05	3.24	0.4650	0.1371	0.0306
13	50	6.93E-05	3.82	0.4820	0.1383	0.0287
14	100	8.93E-05	4.92	0.5075	0.1401	0.0272
15	100	1.08E-04	5.94	0.5281	0.1401	0.0251

Table 13. *Representative data for the UV-Vis titration of the complex [Δ-(**L1**)$_2$.Eu][PPh$_4$] at a constant concentration of 1.32E-05M and a Guest concentration going from 1.32E-06M to 2.03E-04M.*

Exp no.	**G add, µL**	**[G], M**	**G/H (eq)**	**Abs (337nm)**	**Abs (364nm)**	**Abs (437nm)**
1	30	0	0.00	0.0788	0.2585	0.0025
2	5	1.32E-06	0.10	0.0813	0.2515	0.0033
3	5	2.63E-06	0.20	0.0885	0.2281	0.0080
4	10	5.25E-06	0.40	0.0997	0.2036	0.0136
5	10	7.84E-06	0.59	0.1099	0.1785	0.0196
6	15	1.17E-05	0.88	0.1240	0.1416	0.0277
7	25	1.80E-05	1.36	0.1470	0.0798	0.0416
8	25	2.42E-05	1.83	0.1586	0.0505	0.0476
9	50	3.63E-05	2.74	0.1594	0.0508	0.0476
10	50	4.79E-05	3.62	0.1598	0.0510	0.0473
11	55	6.02E-05	4.54	0.1600	0.0514	0.0471
12	50	7.09E-05	5.36	0.1619	0.0520	0.0470
13	100	9.13E-05	6.90	0.1631	0.0535	0.0469
14	200	1.28E-04	9.69	0.1631	0.0541	0.0467
15	200	1.61E-04	12.14	0.1638	0.0543	0.0463
16	300	2.03E-04	15.31	0.1646	0.0554	0.0457

Table 14. *Representative data for the UV-Vis titration of the complex [Δ-(**L2**)$_2$.Eu][PPh$_4$] at a constant concentration of 1.33E-05M and a Guest concentration going from 1.32E-06M to 1.61E-04M.*

Exp no.	G add, µL	[G], M	G/H (eq)	Abs (263nm)	Abs (339nm)	Abs (366nm)
1	30	0	0.00	0.6245	0.1091	0.3583
2	5	1.32E-06	0.10	06263	0.1090	0.3582
3	5	2.63E-06	0.20	0.6278	0.1089	0.3582
4	10	5.25E-06	0.39	0.6296	0.1088	0.3579
5	10	7.84E-06	0.59	0.6323	0.1094	0.3582
6	15	1.17E-05	0.88	0.6344	0.1089	0.3576
7	25	1.80E-05	1.35	0.6524	0.1160	0.3378
8	25	2.42E-05	1.82	0.6723	0.1300	0.2939
9	50	3.63E-05	2.72	0.7052	0.1571	0.2086
10	50	4.79E-05	3.60	0.7381	0.1821	0.1311
11	55	6.02E-05	4.52	0.7542	0.1873	0.0819
12	50	7.09E-05	5.33	0.7924	0.1975	0.0662
13	100	9.13E-05	6.86	0.8446	0.1987	0.0657
14	200	1.28E-04	9.63	0.9352	0.1987	0.0652
15	200	1.61E-04	12.07	1.0146	0.1996	0.0648

4.1.7. Fluorescence studies

Table 15. *Representative data for the fluorescence titration of the complex [Δ-(**L1**)$_2$.Eu][PPh$_4$] at a constant concentration of 6.66E-06M and a Guest concentration going from 6.68E-07M to 2.71E-05M.*

Exp no.	G add, µL	[G], M	G/H (eq)	Intensity at abs (612.02 nm)
1	15	0	0.00	92.6942
2	5	6.68E-07	0.10	87.7961
3	5	1.33E-06	0.20	83.8113
4	10	2.65E-06	0.40	78.0580
5	10	3.97E-06	0.60	73.0580
6	15	5.91E-06	0.89	55.8536
7	25	9.11E-06	1.37	44.8529
8	25	1.22E-05	1.84	26.7815

Table 15. *Continuation.*

9	25	1.53E-05	2.30	7.1898
10	25	1.83E-05	2.75	-0.2936
11	25	2.13E-05	3.20	-0.2562
12	25	2.42E-05	3.64	-0.0624
13	25	2.71E-05	4.07	-0.3351

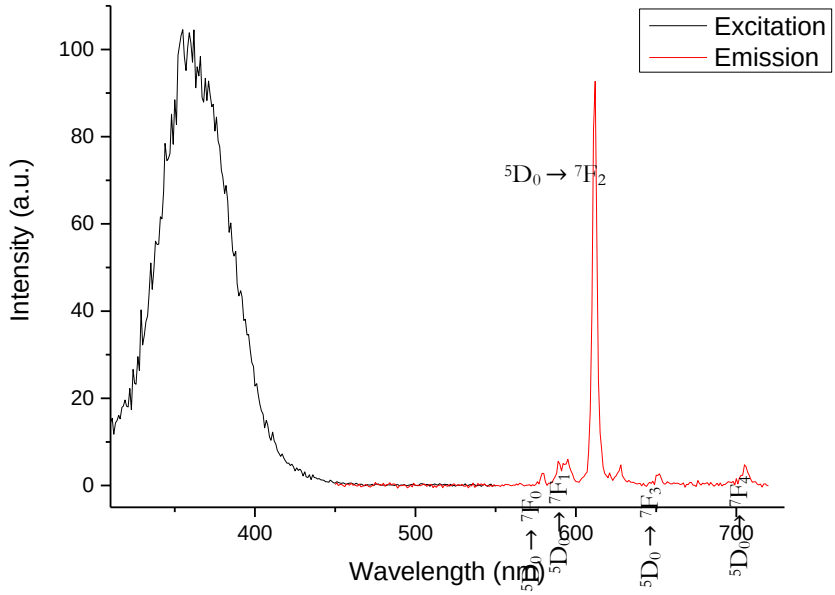

Figure 55. *Luminescence spectrum of the emission of the complex [Δ-(**L1**)$_2$.Eu][PPh$_4$] and posterior excitation collected at 612 nm.*

Table 16. *Representative data for the fluorescence titration of the complex [Δ-(**L2**)$_2$.Eu][PPh$_4$] at a constant concentration of 6.69E-06M and a Guest concentration going from 6.68E-07M to 3.26E-05M.*

Exp no.	G add, µL	[G], M	G/H (eq)	Intensity at abs (612.02 nm)
1	15	0	0.00	161.6096
2	5	6.68E-07	0.10	153.0241
3	5	1.33E-06	0.20	153.6207
4	10	2.65E-06	0.40	140.5668
5	10	3.97E-06	0.59	127.6429
6	15	5.91E-06	0.88	101.5622
7	25	9.11E-06	1.36	72.16192
8	25	1.22E-05	1.83	35.1444
9	25	1.53E-05	2.29	11.5997

Table 16. Continuation.

10	25	1.83E-05	2.74	1.4218
11	25	2.13E-05	3.18	0.0417
12	25	2.42E-05	3.62	-0.3823
13	25	2.71E-05	4.04	0.3757
14	50	3.26E-05	4.87	0.1211

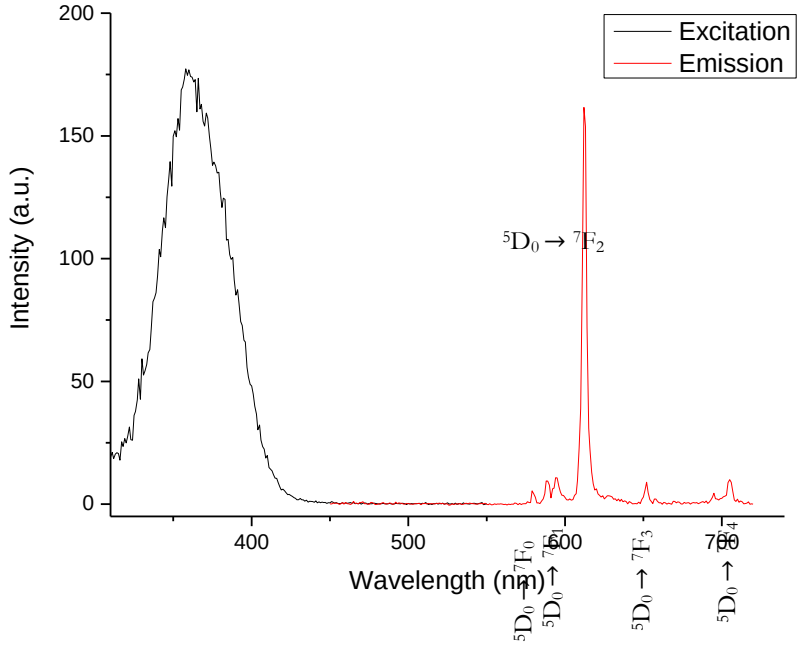

*Figure 56. Luminescence spectrum of the emission of the complex [Δ-(**L2**)$_2$.Eu][PPh$_4$] and posterior excitation collected at 612 nm.*

4.1.8. Characterization of L1 and L2 complexes

The QY were performed in by preparing three solutions with different concentration as showed before. Then just made a blank and run the experiment with a window 370 to 650 nm and an emission wavelength at 612 nm. XenonXe1 as source light path and slits and steps of 1 nm.

For the coefficient results were performed by preparing a solution in acetonitrile with the complex and adding consecutive amounts (as shown in the following tables) after ruining the blank. For all complexes at least two measurements were made, to be more accurate with the value of the constants. The calculations were made following the Beer-Lambert law, $A = \varepsilon lc$.

In the lifetimes experiments were made stock solutions of [Λ-(**L1**)$_2$.Eu][Et$_3$NH] and [Λ-(**L2**)$_2$.Eu][Et$_3$NH] complex in DCM (dichloromethane) due to his low boiling point. From this stock solution was taken aliquots of 0.2 mL and added the respective solvent (2 mL) in the moment before the measurement. For the calculation of the lifetimes was adjusted and following exponential decay $y = A_1 e^{(-t/\tau_1)} + c$, to the plot of intensity in function of the concentration.

Bibliography

(1) Black, R. Development, Historical Use and Properties of Chemical Warfare Agents. *Royal Society of Chemistry* **2016**, *Chapter 1*.

(2) Kim, K.; Tsay, O. G.; Atwood, D. A.; Churchill, D. G. Destruction and Detection of Chemical Warfare Agents. *Chem. Rev.* **2011**, *111* (9), 5345–5403. https://doi.org/10.1021/cr100193y.

(3) Puglisi, R.; Pappalardo, A.; Gulino, A.; Trusso Sfrazzetto, G. Supramolecular Recognition of a CWA Simulant by Metal–Salen Complexes: The First Multi-Topic Approach. *Chem. Commun.* **2018**, *54* (79), 11156–11159. https://doi.org/10.1039/C8CC06425C.

(4) Mukherjee, S.; Gupta, R. D. Organophosphorus Nerve Agents: Types, Toxicity, and Treatments. *Journal of Toxicology* **2020**, *2020*, 1–16. https://doi.org/10.1155/2020/3007984.

(5) Gangemi, C. M. A.; Rimkaite, U.; Pappalardo, A.; Trusso Sfrazzetto, G. Light-up Photoluminescence Sensing of a Nerve Agent Simulant by a Bis-Porphyrin–Salen–UO_2 Complex. *RSC Adv.* **2021**, *11* (22), 13047–13050. https://doi.org/10.1039/D1RA01397A.

(6) *Japan Marks 20 Years Since Subway Gas Attack*. NDTV.com. https://www.ndtv.com/world-news/japan-marks-20-years-since-subway-gas-attack-581645 (accessed 2022-12-10).

(7) Cave, H.; Ede, J. A.; Sambrook, M. R.; Dodd, H.; Fucassi, F.; Cragg, A. S.; Lansley, A. H.; Cragg, P. J. Hydrogen-Bonding Interactions in Crown-(Thio)Urea Complexes with Anions, Chemical Warfare Agents and Simulants. *Supramolecular Chemistry* **2019**, *31* (11), 703–712. https://doi.org/10.1080/10610278.2019.1659268.

(8) Jenkins, A. L.; Manuel Uy, O.; Murray, G. M. Polymer Based Lanthanide Luminescent Sensors for the Detection of Nerve Agents. *Anal. Commun.* **1997**, *34* (8), 221–224. https://doi.org/10.1039/a704220e.

(9) Puglisi, R.; Mineo, P. G.; Pappalardo, A.; Gulino, A.; Trusso Sfrazzetto, G. Supramolecular Detection of a Nerve Agent Simulant by Fluorescent Zn–Salen Oligomer Receptors. *Molecules* **2019**, *24* (11), 2160. https://doi.org/10.3390/molecules24112160.

(10) Disley, J.; Gil-Ramírez, G.; Gonzalez-Rodriguez, J. Chitosan-Based Molecularly Imprinted Polymers for Effective Trapping of the Nerve Agent Simulant Dimethyl Methylphosphonate. *ACS Appl. Polym. Mater.* **2023**, *5* (1), 935–942. https://doi.org/10.1021/acsapm.2c01859.

(11) Hasegawa, M.; Ohmagari, H.; Tanaka, H.; Machida, K. Luminescence of Lanthanide Complexes: From Fundamental to Prospective Approaches Related to Water- and Molecular-Stimuli. *Journal of Photochemistry and Photobiology C: Photochemistry Reviews* **2022**, *50*, 100484. https://doi.org/10.1016/j.jphotochemrev.2022.100484.

(12) Bünzli, J.-C. G. On the Design of Highly Luminescent Lanthanide Complexes. *Coordination Chemistry Reviews* **2015**, *293–294*, 19–47. https://doi.org/10.1016/j.ccr.2014.10.013.

(13) Miyamoto, R.; Sugai, T.; Sudoh, S. Spectroscopic Study of the Coordination Sphere of Gd(III) in Gd(III) Ã/M(II) Complexes with a Compartmental Ligand, Where the Local Environment around Gd(III) Is Controlled by (M(II) M(II) 0/Ni(II), Zn(II) and a Vacancy). **2002**.

(14) Eliseeva, S. V.; Bünzli, J.-C. G. Lanthanide Luminescence for Functional Materials and Bio-Sciences. *Chem. Soc. Rev.* **2010**, *39* (1), 189–227. https://doi.org/10.1039/B905604C.

(15) He, N.; Gao, M.; Shen, D.; Li, H.; Han, Z.; Zhao, P. Rapid Visual Detection of Nitroaromatic Explosives Using a Luminescent Europium-Organic Framework Material. *Forensic Science International* **2019**, *297*, 1–7. https://doi.org/10.1016/j.forsciint.2019.01.004.

(16) Alptürk, O.; Rusin, O.; Fakayode, S. O.; Wang, W.; Escobedo, J. O.; Warner, I. M.; Crowe, W. E.; Král, V.; Pruet, J. M.; Strongin, R. M. Lanthanide Complexes as Fluorescent Indicators for Neutral Sugars and Cancer Biomarkers. *Proc. Natl. Acad. Sci. U.S.A.* **2006**, *103* (26), 9756–9760. https://doi.org/10.1073/pnas.0603758103.

(17) Bolle, P.; Albrecht, N.; Amiaud, T.; Humbert, B.; Faulques, E.; Dessapt, R.; Serier-Brault, H. New Robust Luminescent Supramolecular Assemblies Based on $[Ln(Mo_8O_{26})_2]^{5-}$ (Ln = Eu, Sm) Polyoxometalates. *Inorg. Chem.* **2019**, *58* (24), 16322–16325. https://doi.org/10.1021/acs.inorgchem.9b02941.

(18) *Optical Isomers in Inorganic Complexes*. Chemistry LibreTexts. https://chem.libretexts.org/Bookshelves/Inorganic_Chemistry/Supplemental_Modules_and_Websites_(Inorganic_Chemistry)/Coordination_Chemistry/Structure_and_Nomenclature_of_

Coordination_Compounds/Isomers/Optical_Isomers_in_Inorganic_Complexes (accessed 2023-06-22).

Appendix

Fluorescence:

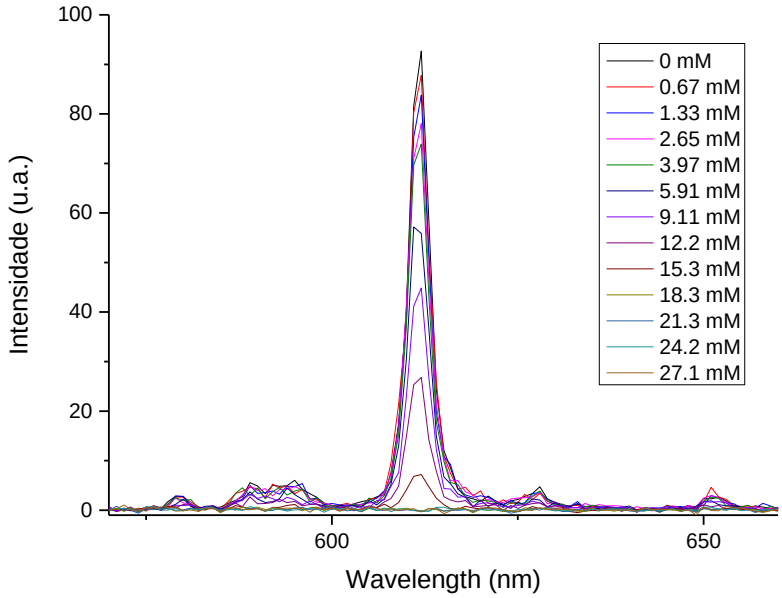

Figure 57. *Fluorescence spectra during the titration of [Δ-(**L1**)$_2$.Eu][PPh$_4$] with DMMP (0.67-27.1 mM) in acetonitrile at r.t. (λ_{ex} – 370 nm). Concentration of [Δ-(**L1**)$_2$.Eu][PPh$_4$] constant at 6.66 μM.*

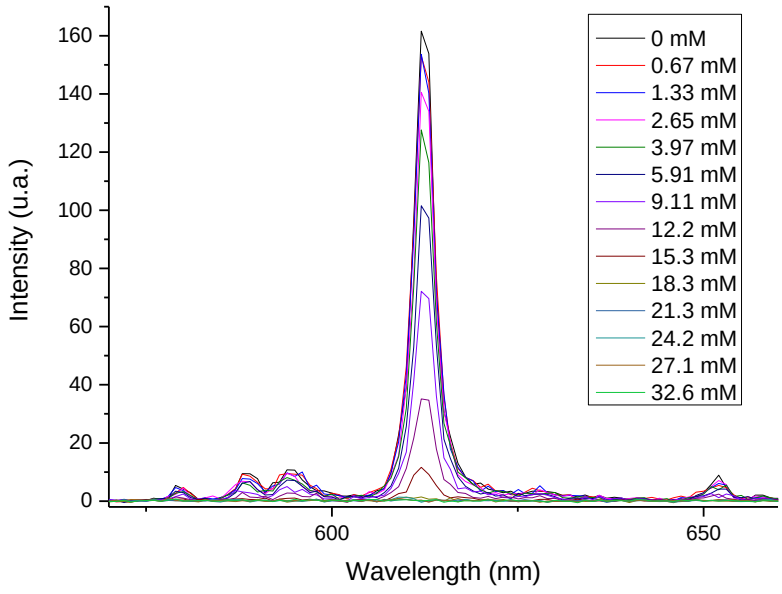

Figure 58. *Fluorescence spectra during the titration of [Δ-(**L2**)$_2$.Eu][PPh$_4$] with DMMP (0.67-32.6 mM) in acetonitrile at r.t. (λ_{ex} – 370 nm). Concentration of [Δ-(**L2**)$_2$.Eu][PPh$_4$] constant at 6.69 μM.*

NMR:

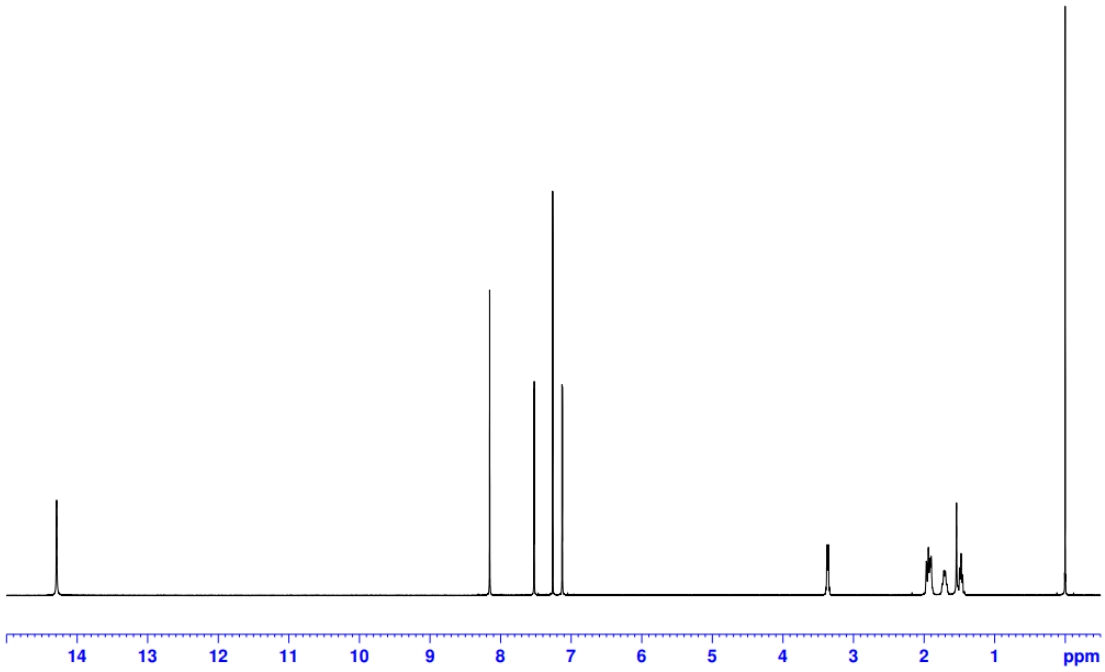

Figure 59. *^{1}H NMR spectrum of the ligand (S,S)-**L1** in $CHCl_3$-d.*

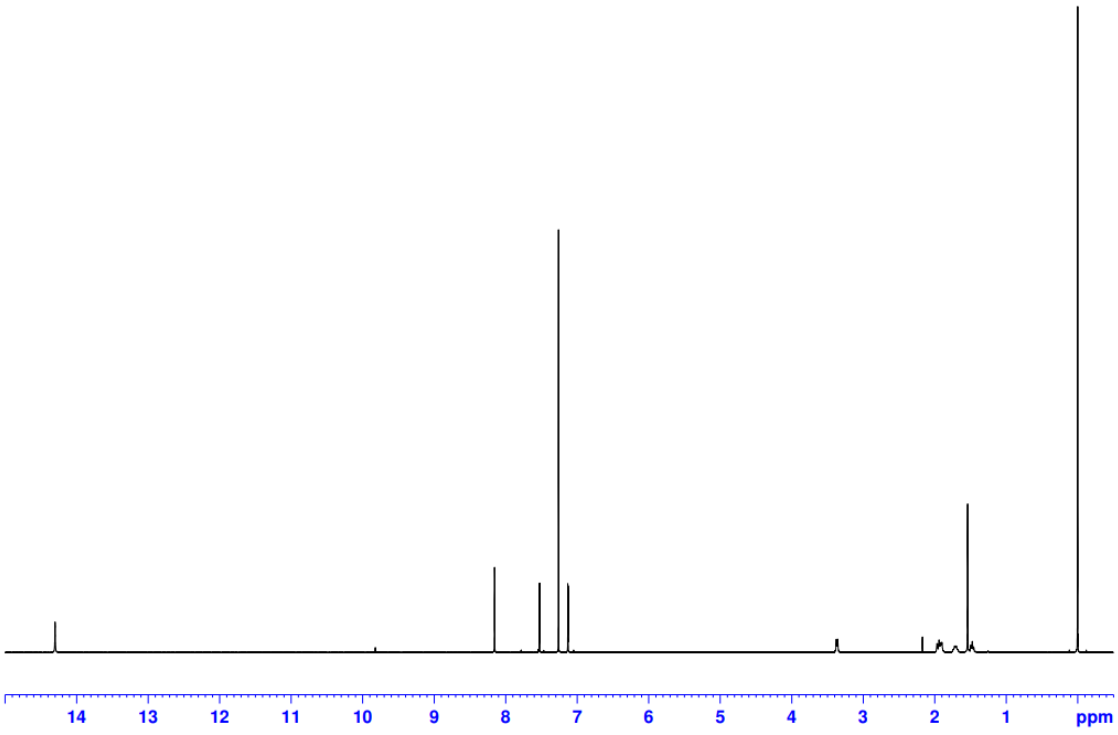

Figure 60. *^{1}H NMR spectrum of the ligand (R,R)-**L1** in $CHCl_3$-d.*

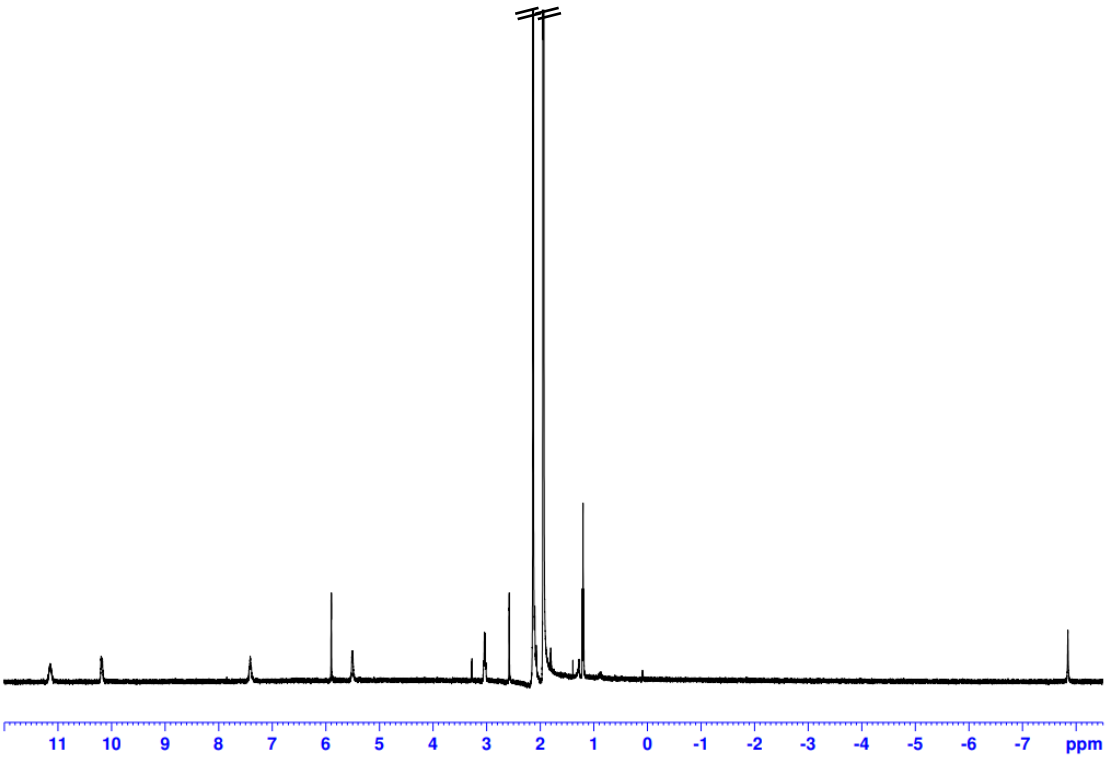

Figure 61. *^{1}H NMR spectrum of the complex [Λ-(**L1**)$_2$.Eu][Et$_3$NH] in MeCN-d$_3$.*

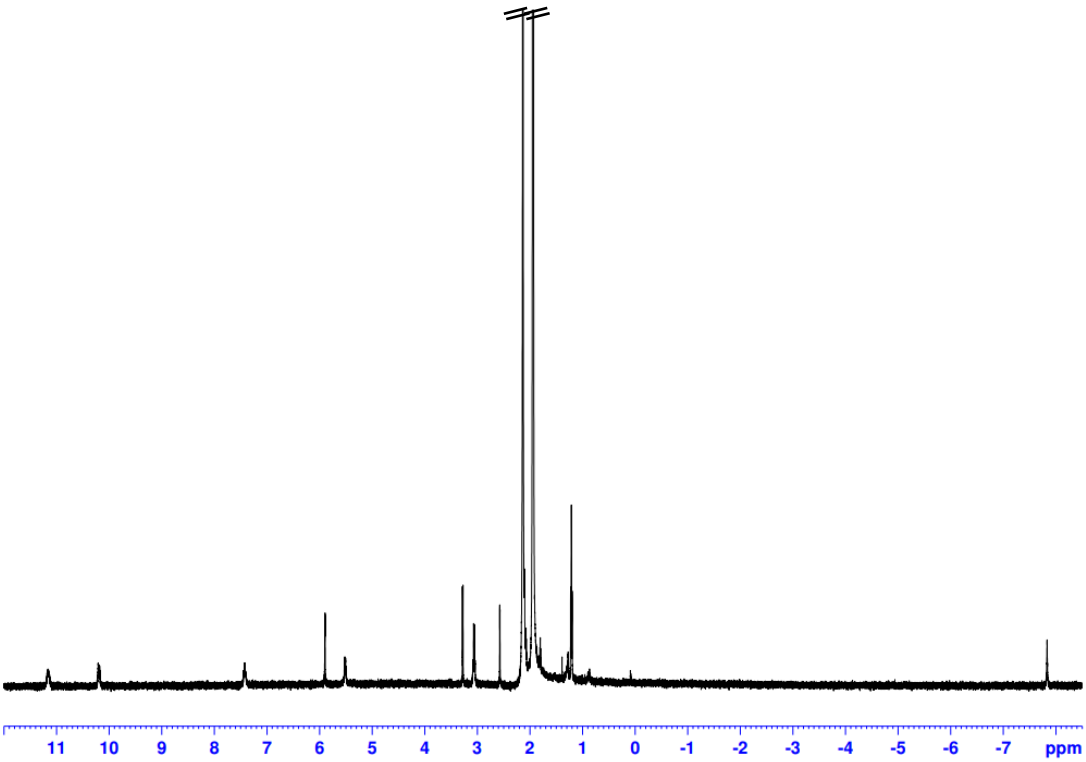

Figure 62. *^{1}H NMR spectrum of the complex [Δ-(**L1**)$_2$.Eu][Et$_3$NH] in MeCN-d$_3$.*

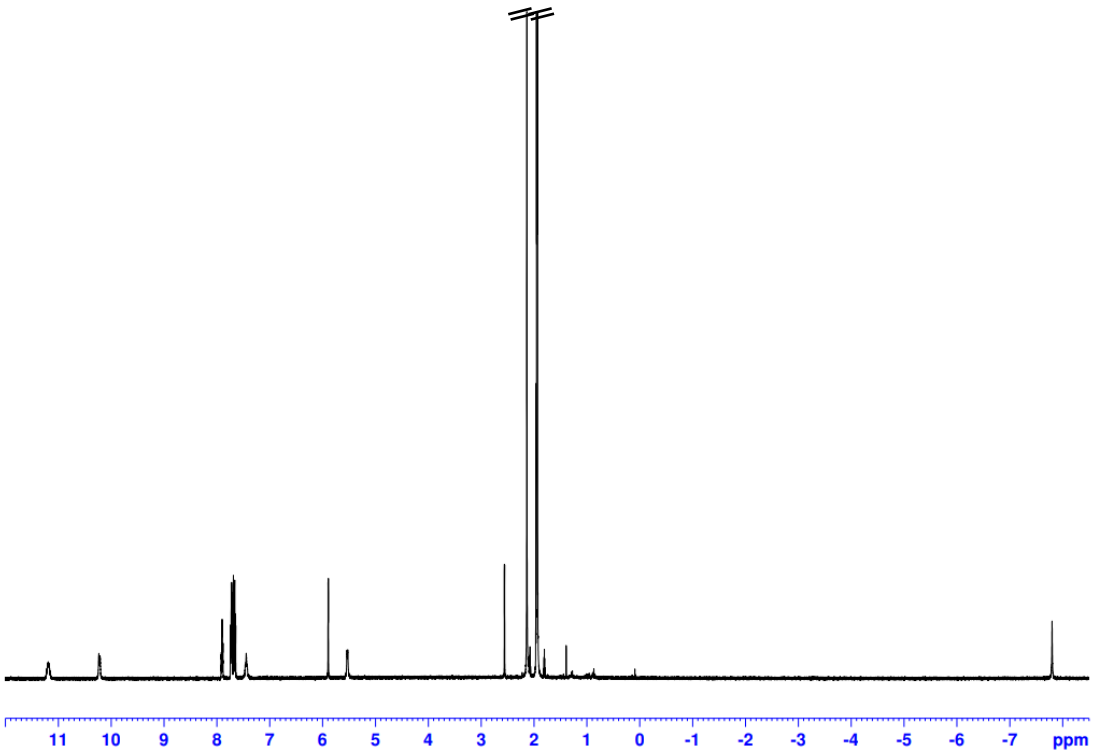

Figure 63. *^{1}H NMR spectrum of the complex [Λ-(**L1**)$_2$.Eu][PPh$_4$] in MeCN-d$_3$.*

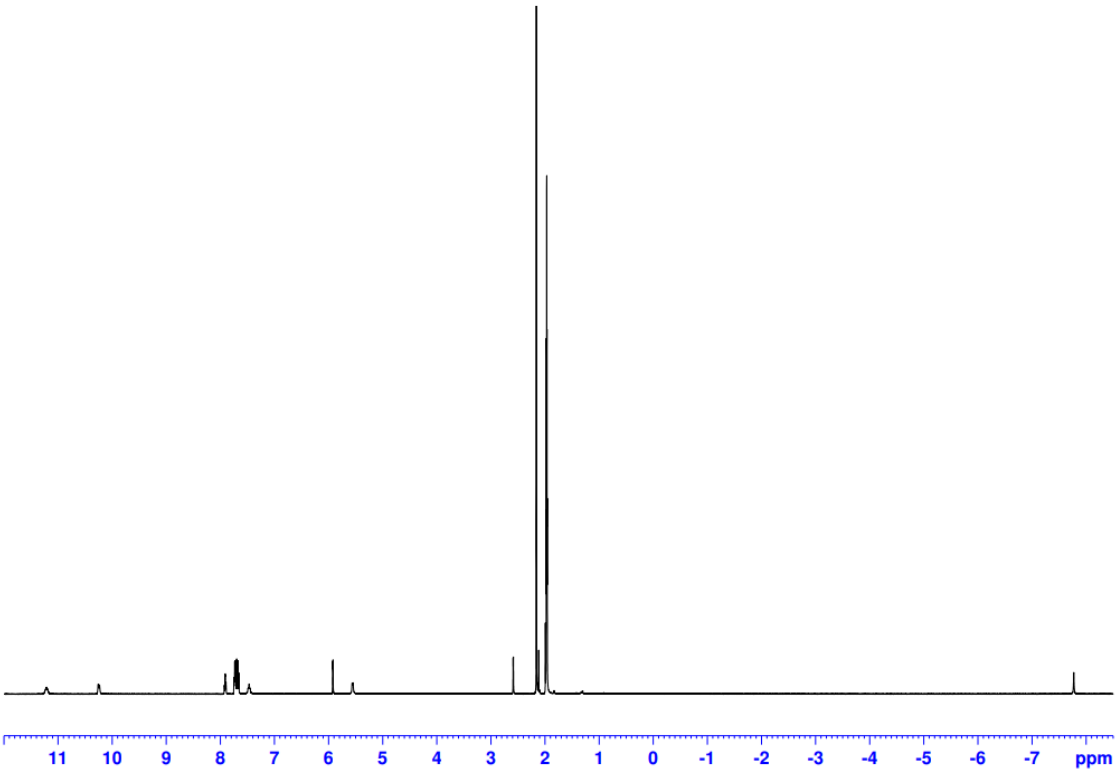

Figure 64. *^{1}H NMR spectrum of the complex [Δ-(**L1**)$_2$.Eu][PPh$_4$] in MeCN-d$_3$*

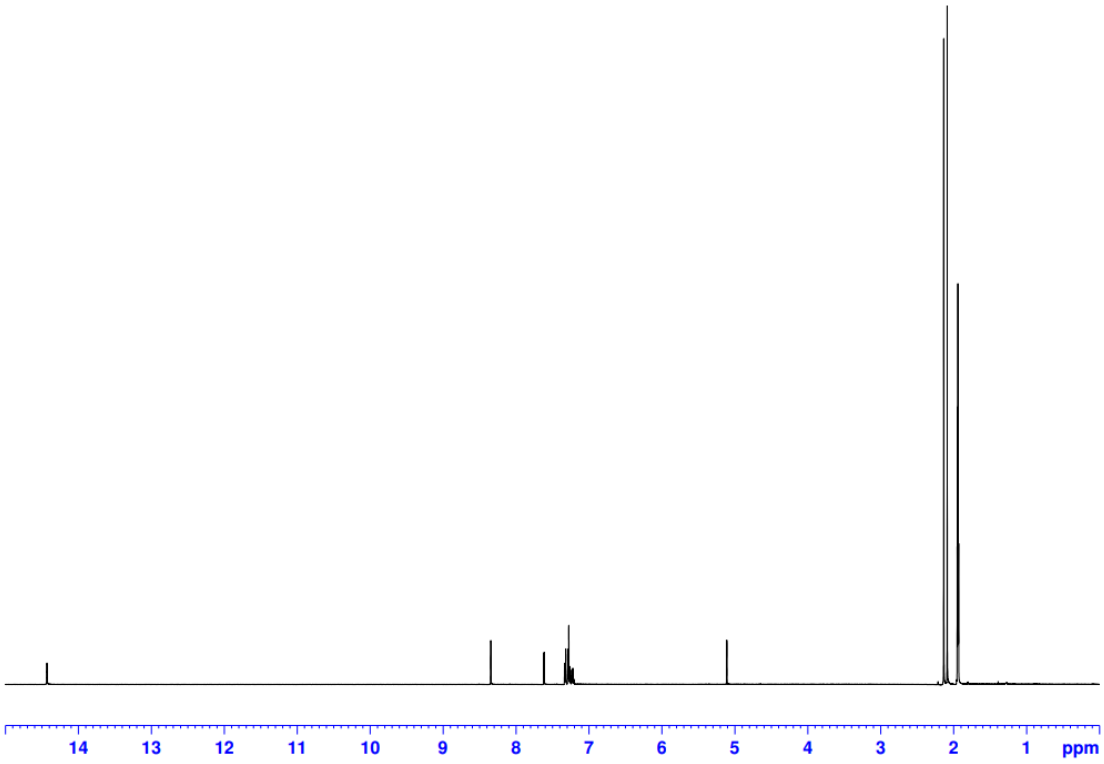

Figure 65. *^{1}H NMR spectrum of the ligand (S,S)-**L2** in MeCN-d_3.*

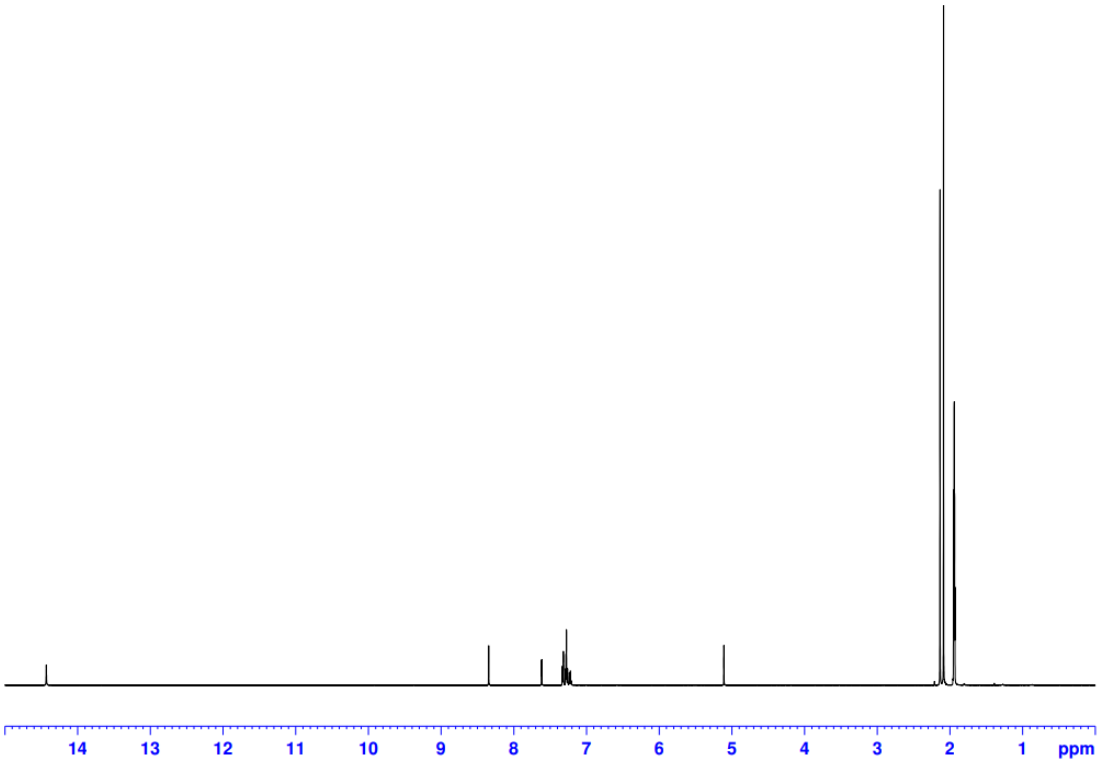

Figure 66. *^{1}H NMR spectrum of the ligand (R,R)-**L2** in MeCN-d_3.*

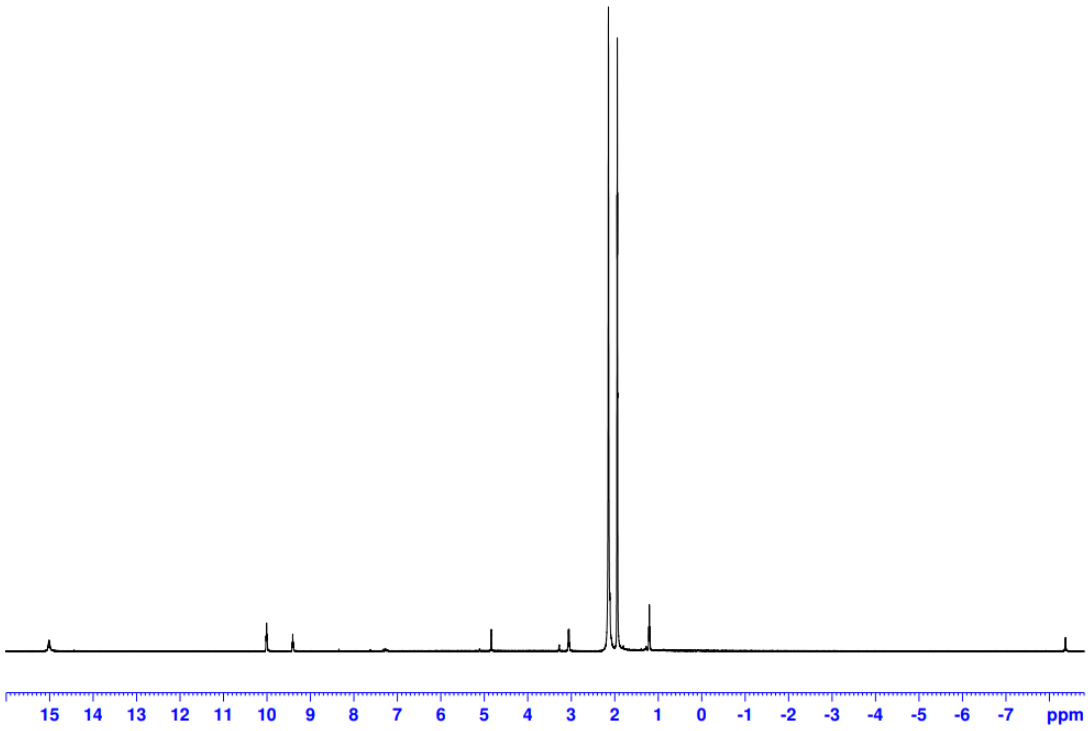

Figure 67. *^{1}H NMR spectrum of the complex [Λ-(**L2**)$_2$.Eu][Et$_3$NH] in MeCN-d$_3$.*

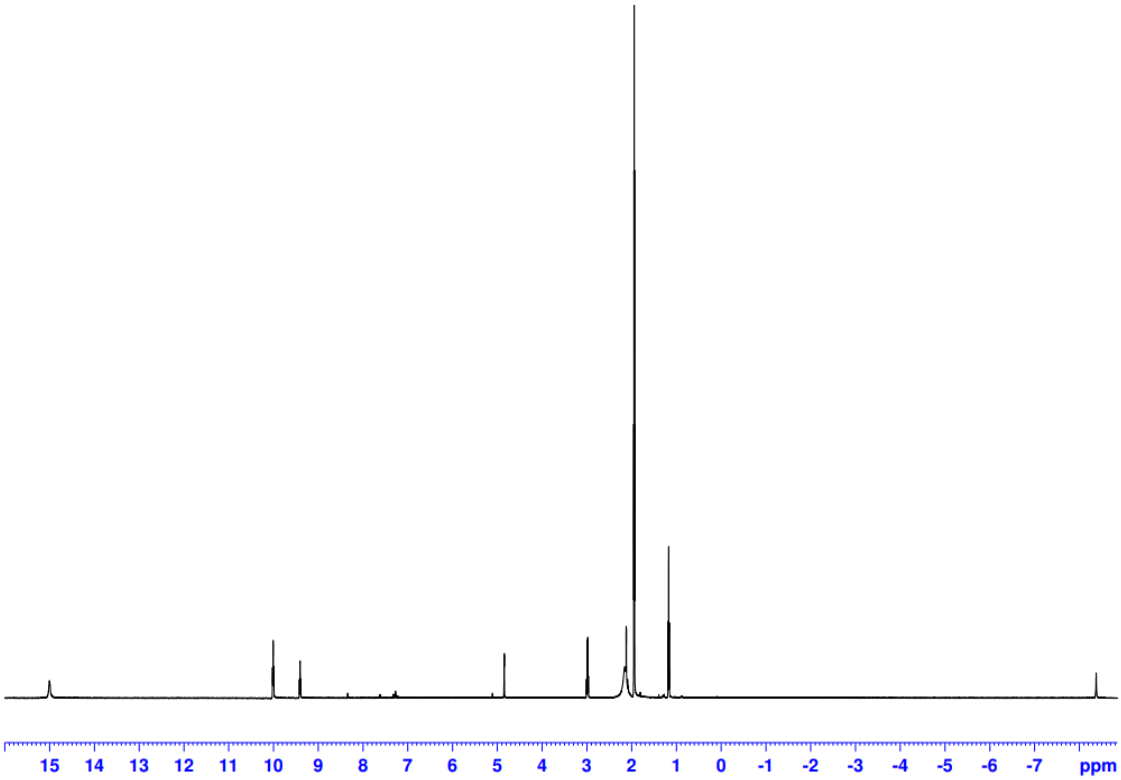

Figure 68. *^{1}H NMR spectrum of the complex [Δ-(**L2**)$_2$.Eu][Et$_3$NH] in MeCN-d$_3$.*

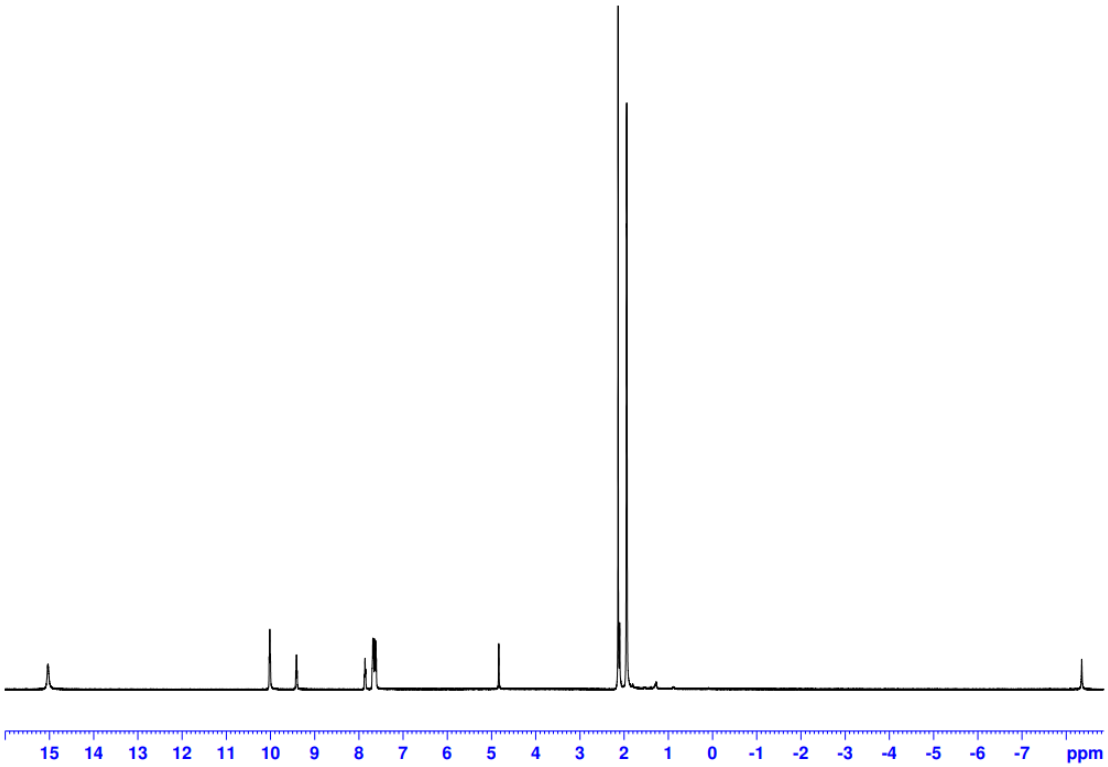

Figure 69. *^{1}H NMR spectrum of the complex [Λ-(**L2**)$_2$.Eu][PPh$_4$] in MeCN-d$_3$.*

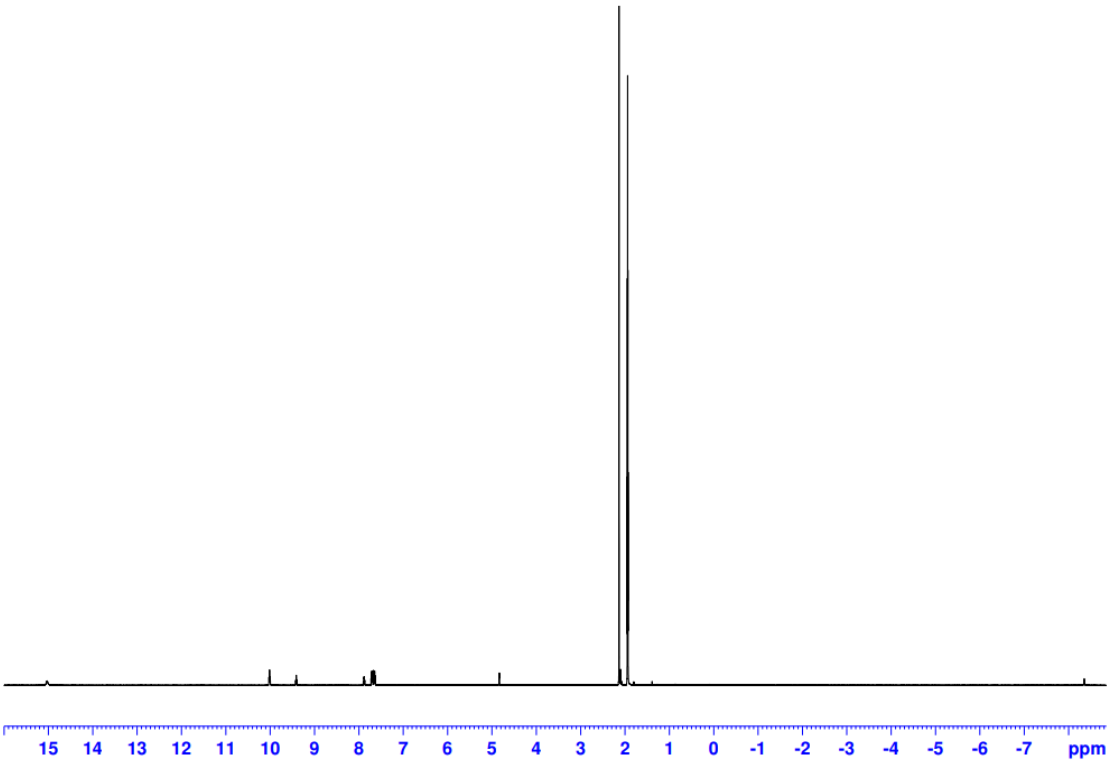

Figure 70. *^{1}H NMR spectrum of the complex [Δ-(**L2**)$_2$.Eu][PPh$_4$] in MeCN-d$_3$.*

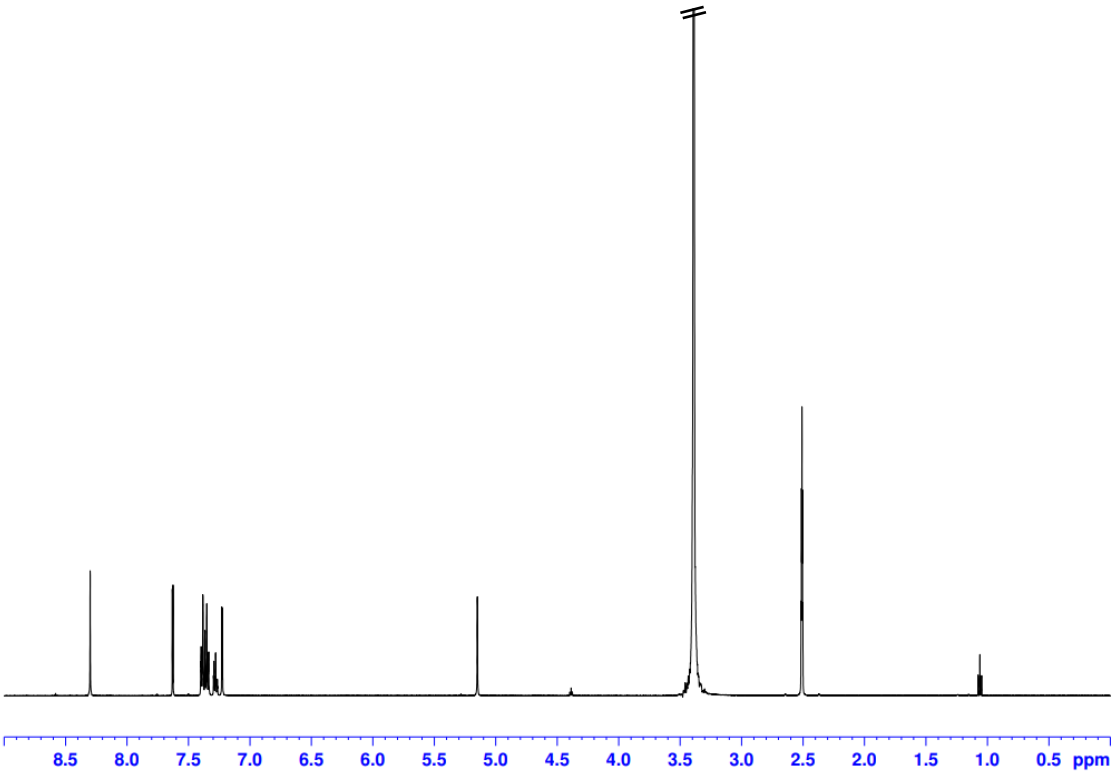

Figure 71. *^{1}H NMR spectrum of the ligand (S,S)-**L2** in DMSO-d_6.*

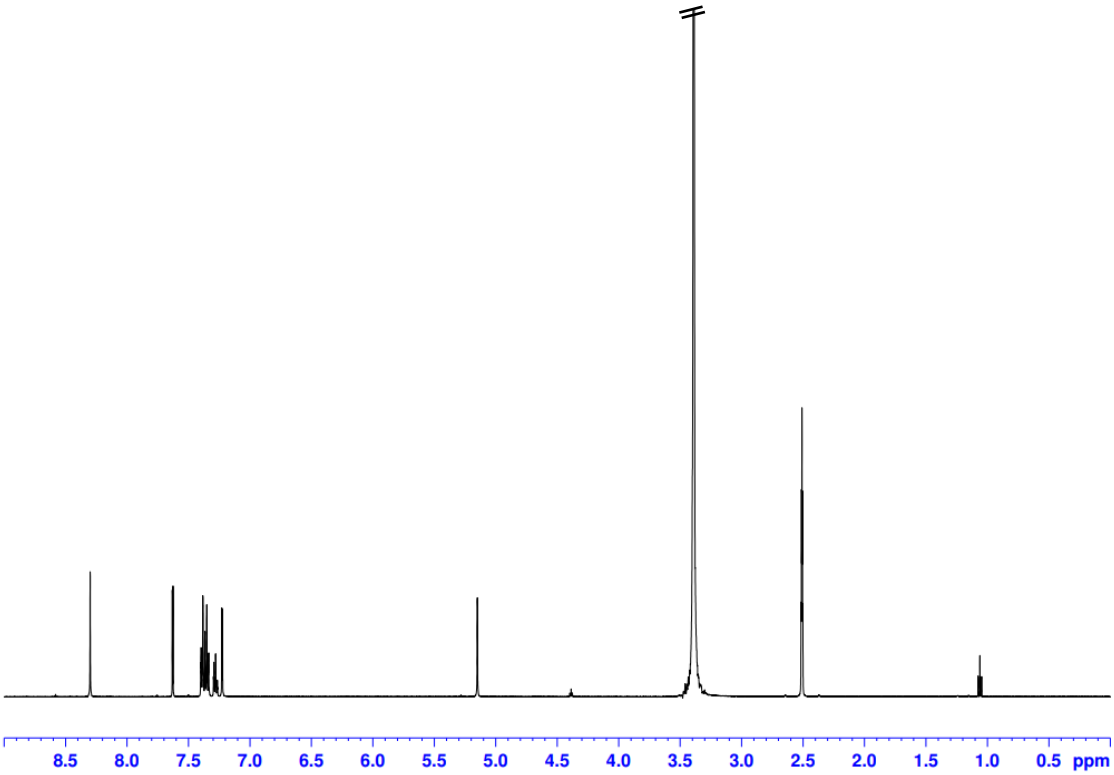

Figure 72. *^{1}H NMR spectrum of the ligand (R,R)-**L2** in DMSO-d_6.*

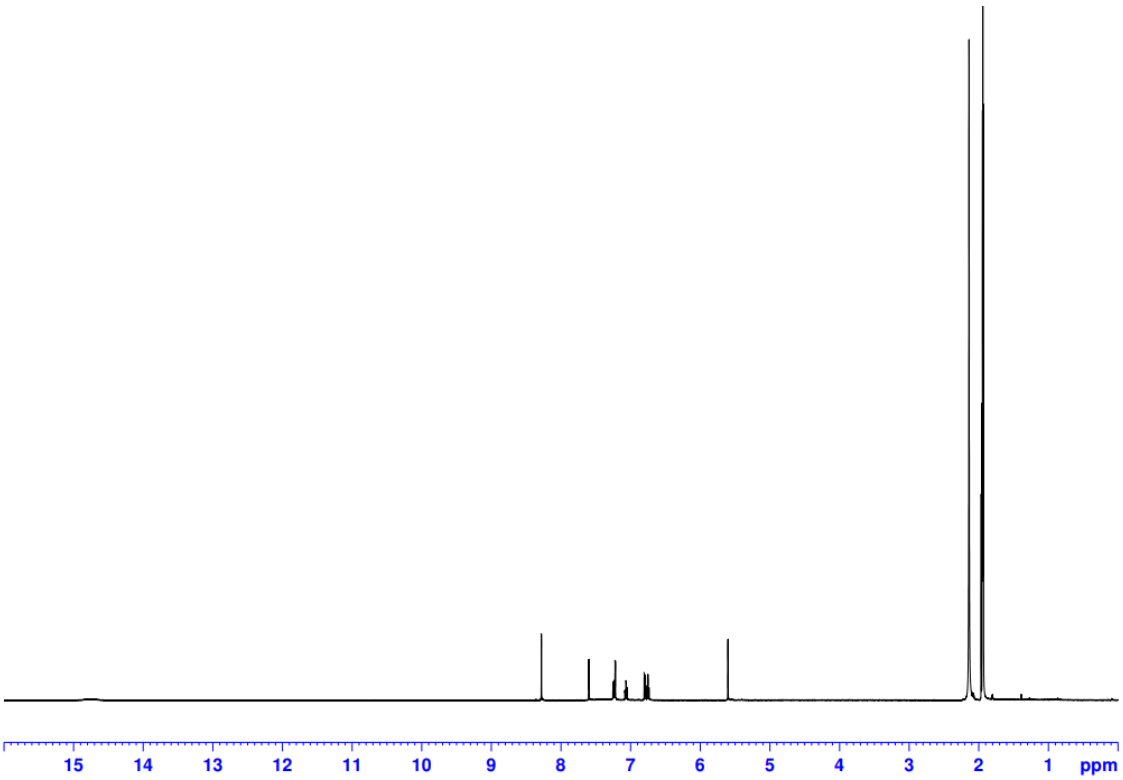

Figure 73. *^{1}H NMR spectrum of the ligand (R,R)-**L3** in MeCN-d_3.*

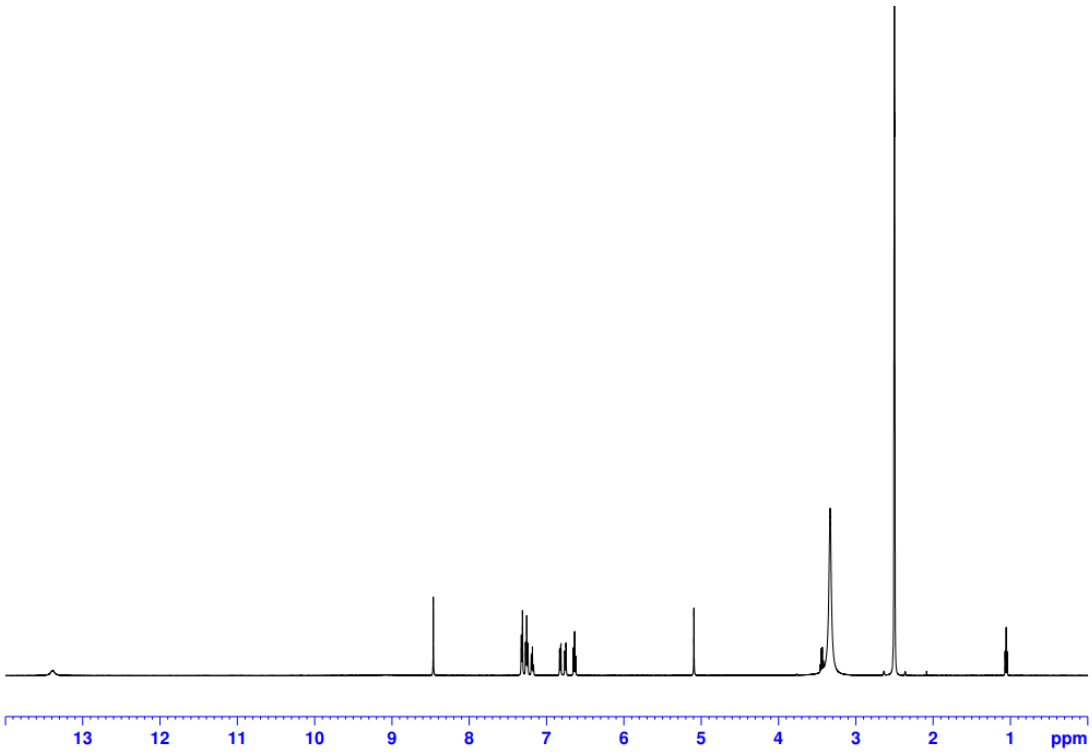

Figure 74. *^{1}H NMR spectrum of the ligand (R,R)-**I1** in DMSO-d_6.*

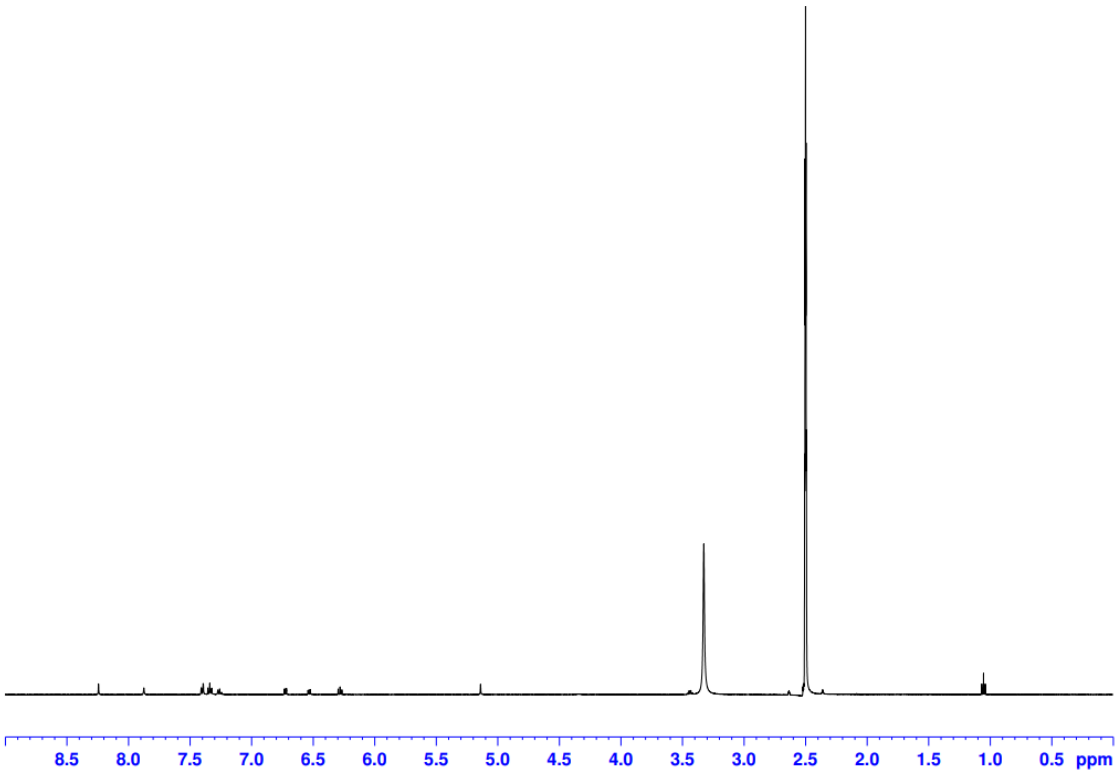

Figure 75. *^{1}H NMR spectrum of the complex [(R,R)-**I1**.Zn] in DMSO-d_6.*

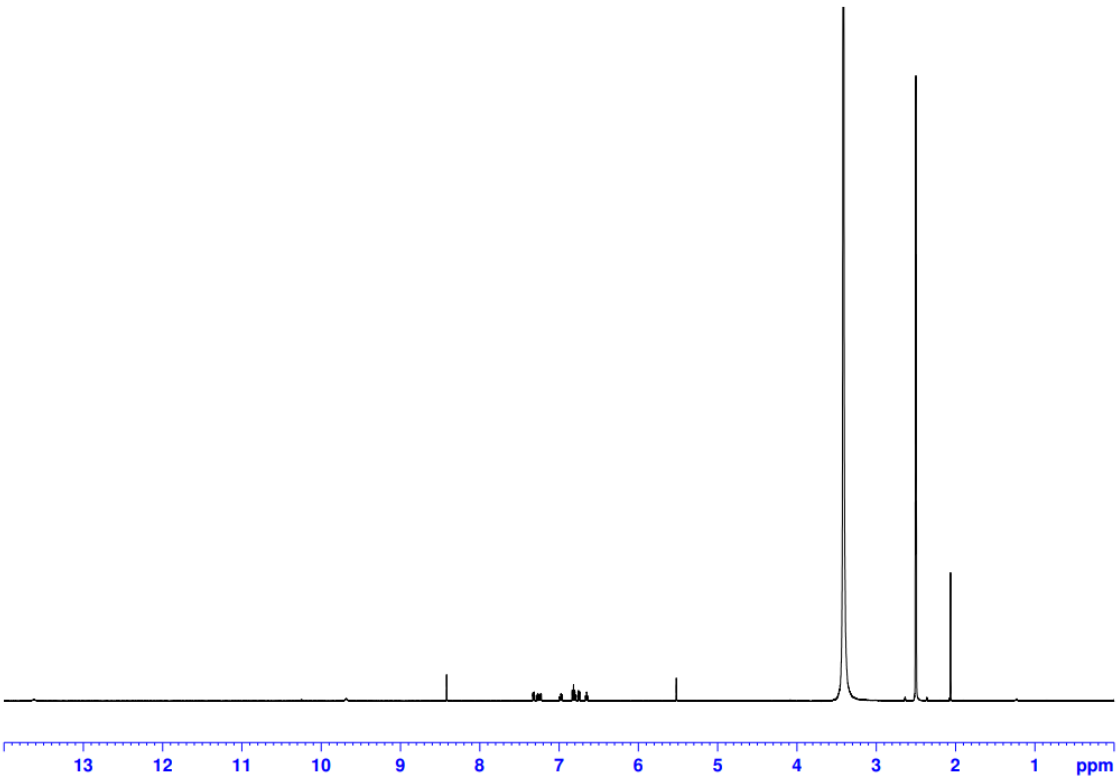

Figure 76. *^{1}H NMR spectrum of the ligand (R,R)-**I2** in DMSO-d_6.*

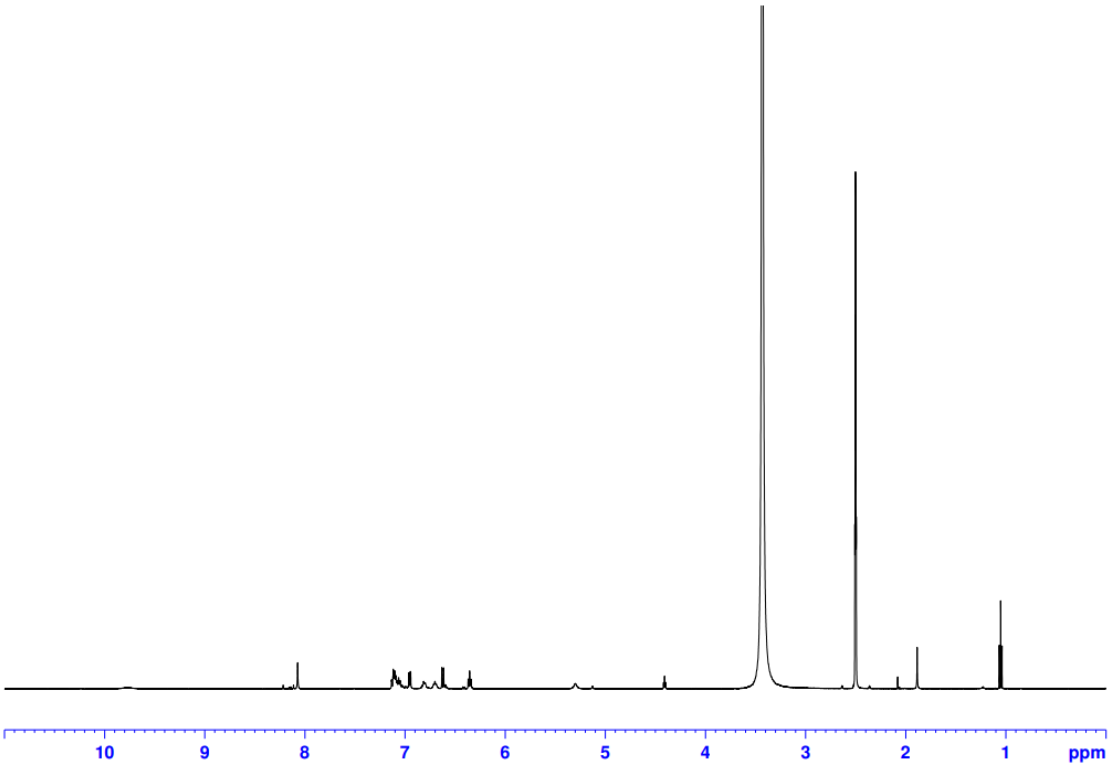

Figure 77. *^{1}H NMR spectrum of the complex [(R,R)-**I2**.Zn] in DMSO-d_6.*

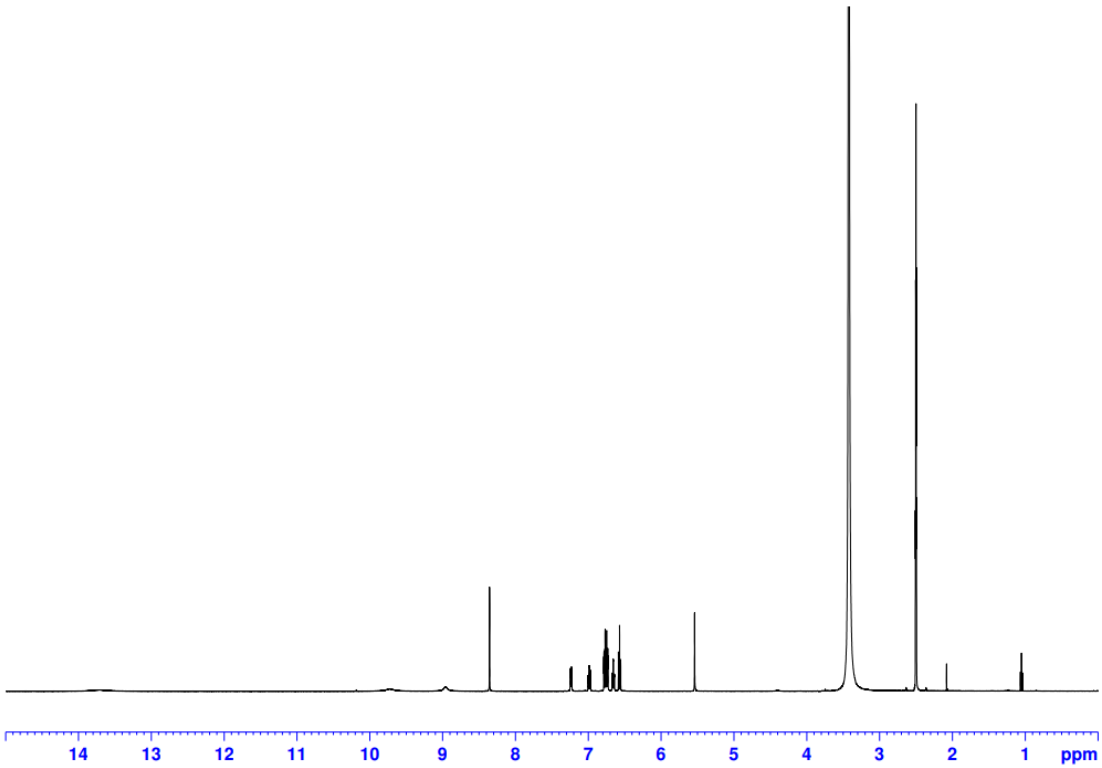

Figure 78. *^{1}H NMR spectrum of the ligand (R,R)-**I3** in DMSO-d_6.*

Coefficient:

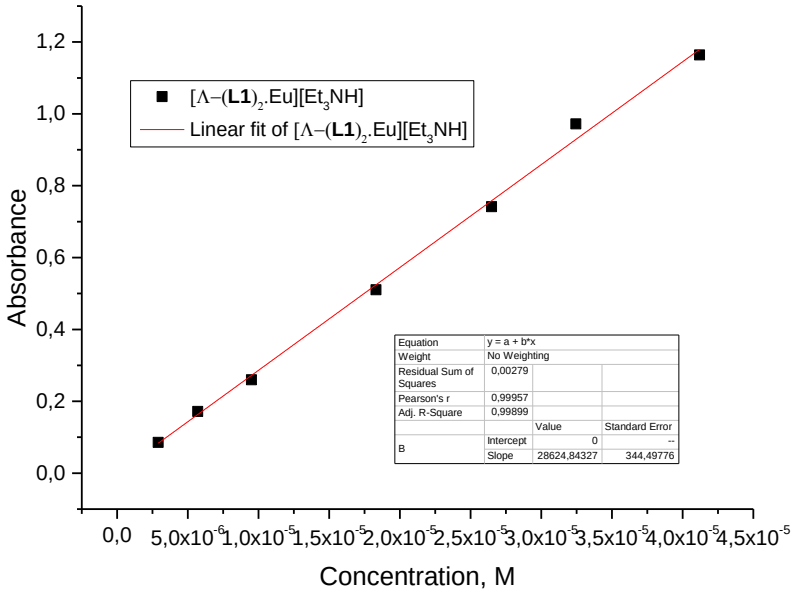

Figure 79. *Plot corresponding to the calculation of the molar absorption coefficient of Λ-(**L1**)₂.Eu][Et₃NH].*

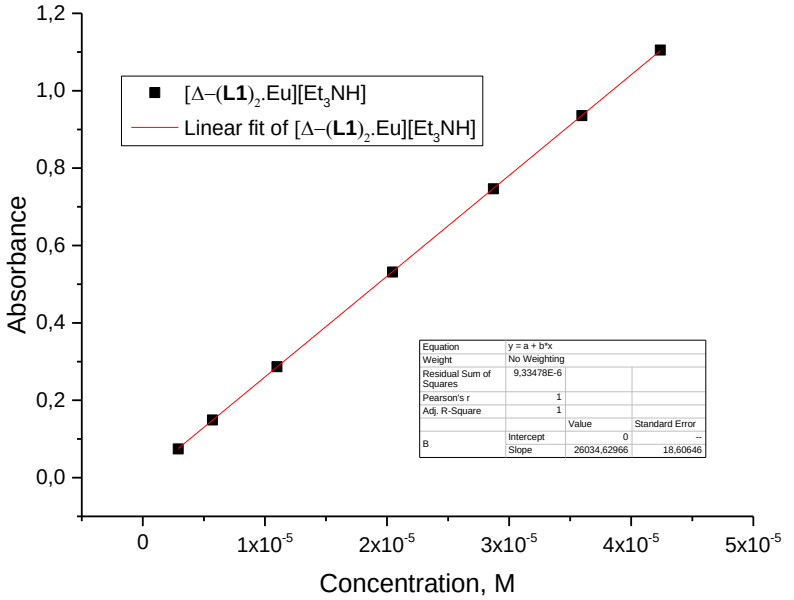

Figure 80. *Plot corresponding to the calculation of the molar absorption coefficient of Δ-(**L1**)₂.Eu][Et₃NH].*

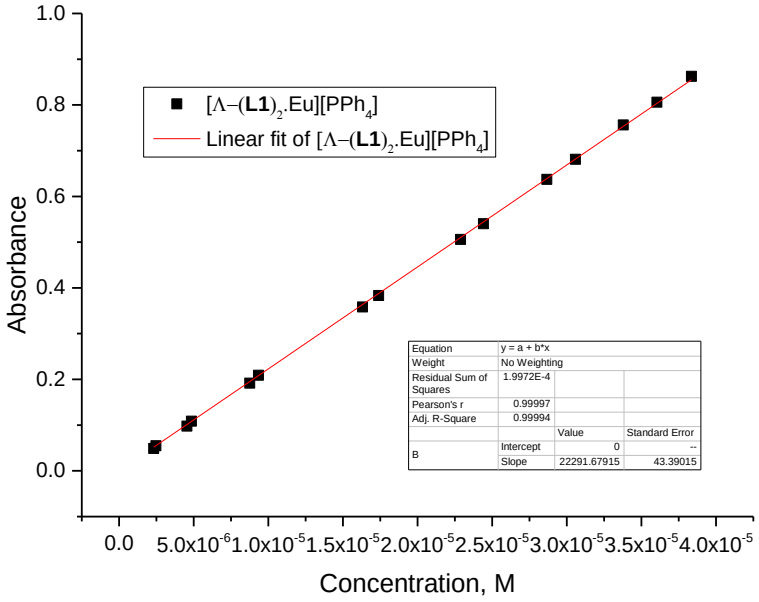

Figure 81. *Plot corresponding to the calculation of the molar absorption coefficient of Λ-(**L1**)₂.Eu][PPh₄].*

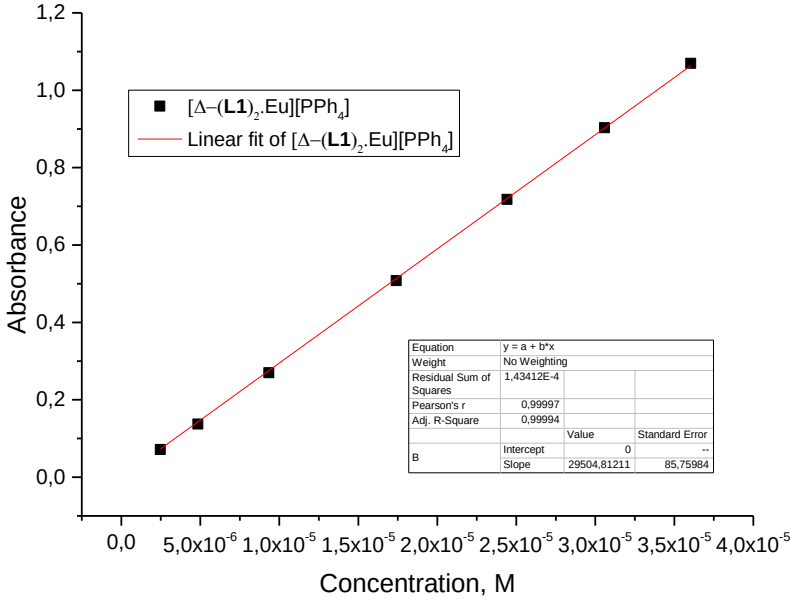

Figure 82. *Plot corresponding to the calculation of the molar absorption coefficient of Δ-(**L1**)₂.Eu][PPh₄].*

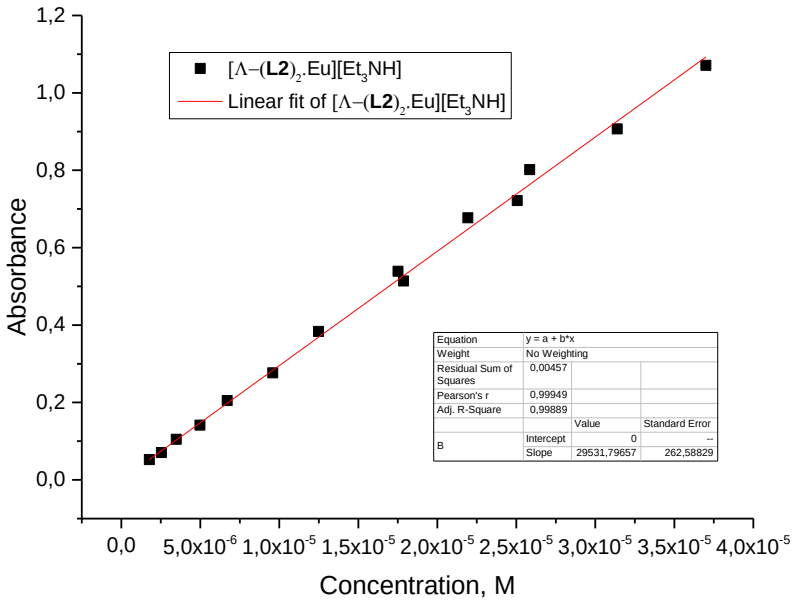

Figure 83. *Plot corresponding to the calculation of the molar absorption coefficient of Λ-(**L2**)₂.Eu][Et₃NH].*

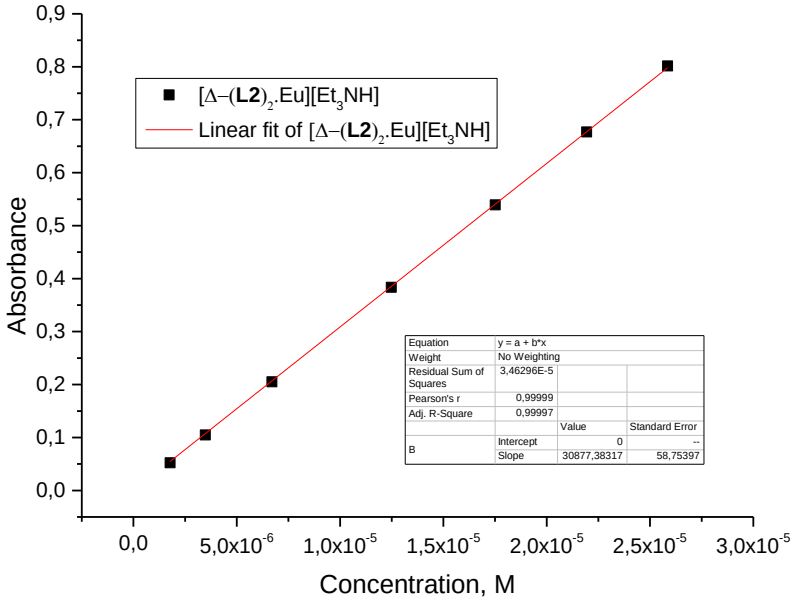

Figure 84. *Plot corresponding to the calculation of the molar absorption coefficient of Δ-(**L2**)₂.Eu][Et₃NH].*

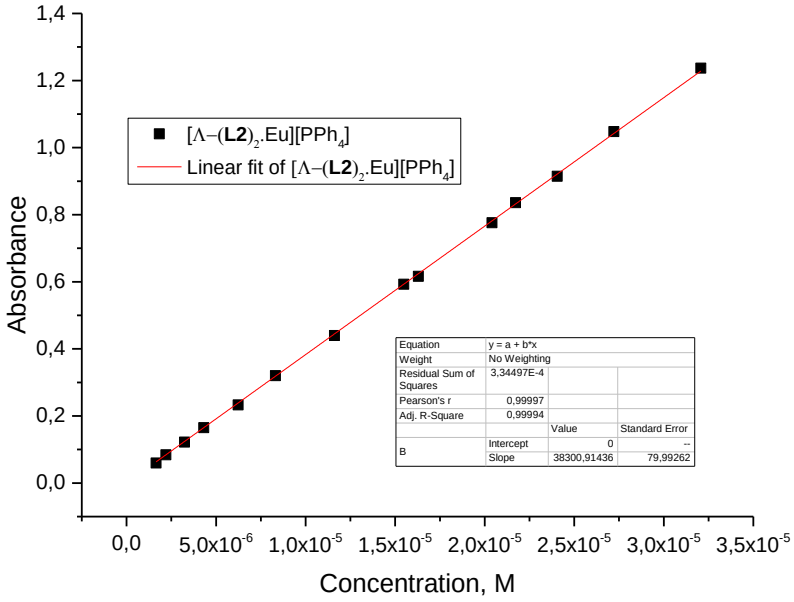

Figure 85. *Plot corresponding to the calculation of the molar absorption coefficient of Λ-(**L2**)₂.Eu][PPh₄].*

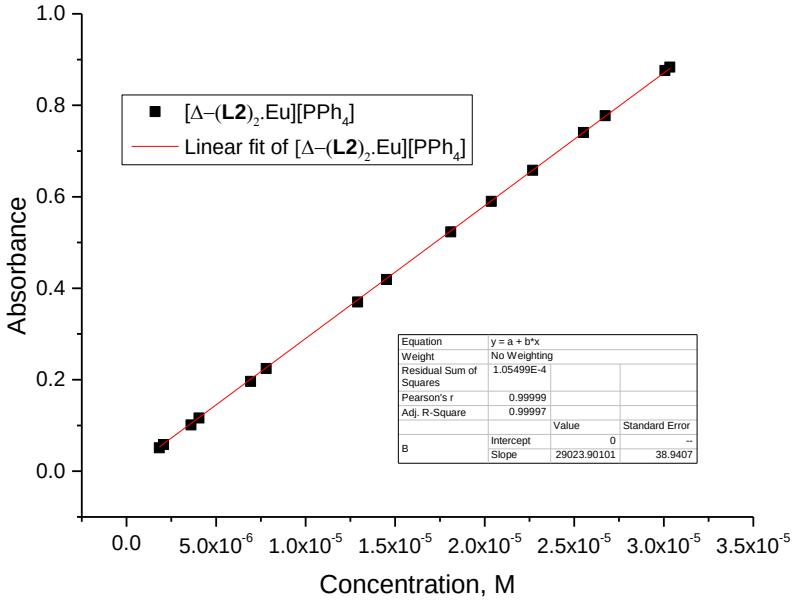

Figure 86. *Plot corresponding to the calculation of the molar absorption coefficient of Δ-(**L2**)₂.Eu][PPh₄].*

Lifetimes:

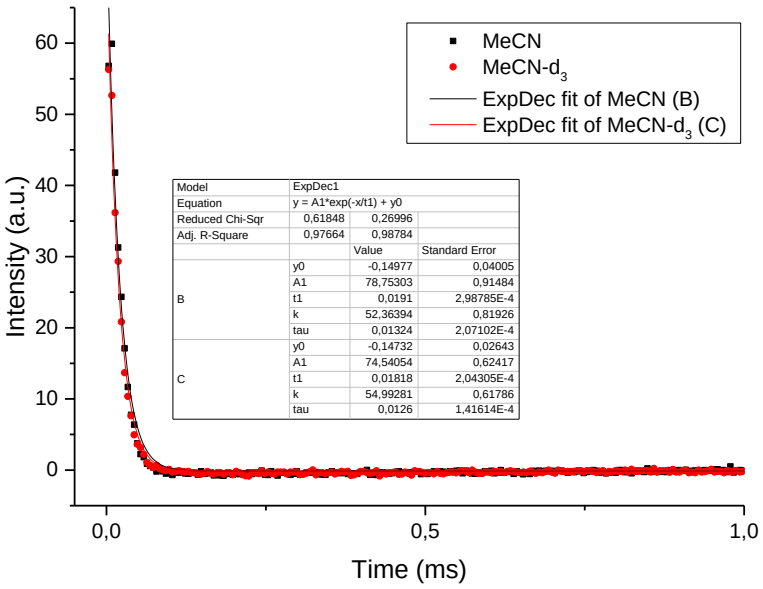

Model	ExpDec1		
Equation	y = A1*exp(-x/t1) + y0		
Reduced Chi-Sqr	0,61848	0,26996	
Adj. R-Square	0,97664	0,98784	
		Value	Standard Error
B	y0	-0,14977	0,04005
	A1	78,75303	0,91484
	t1	0,0191	2,98785E-4
	k	52,36394	0,81926
	tau	0,01324	2,07102E-4
C	y0	-0,14732	0,02643
	A1	74,54054	0,62417
	t1	0,01818	2,04305E-4
	k	54,99281	0,61786
	tau	0,0126	1,41614E-4

Figure 87. *Representative spectrum of the decays of the lifetimes of Λ-(**L1**)$_2$.Eu][Et$_3$NH] in deuterated and non-deuterated acetonitrile.*

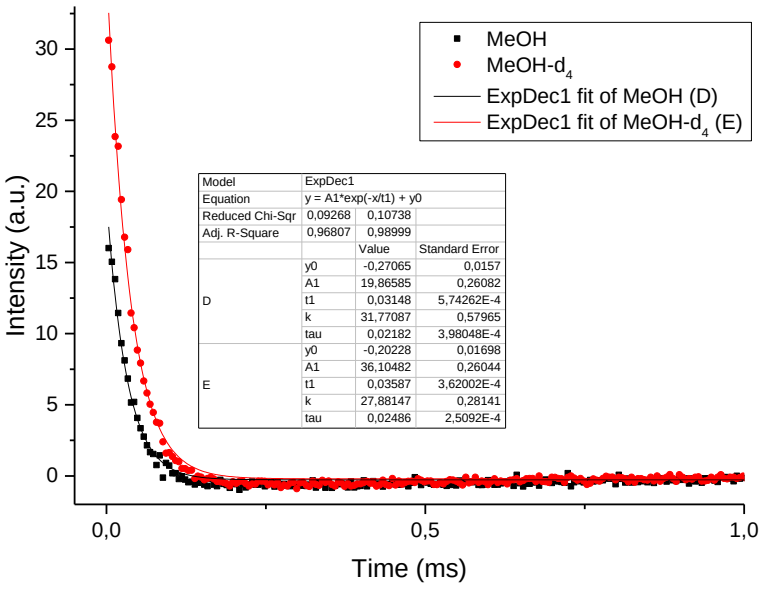

Model	ExpDec1		
Equation	y = A1*exp(-x/t1) + y0		
Reduced Chi-Sqr	0,09268	0,10738	
Adj. R-Square	0,96807	0,98999	
		Value	Standard Error
D	y0	-0,27065	0,0157
	A1	19,86585	0,26082
	t1	0,03148	5,74262E-4
	k	31,77087	0,57965
	tau	0,02182	3,98048E-4
E	y0	-0,20228	0,01698
	A1	36,10482	0,26044
	t1	0,03587	3,62002E-4
	k	27,88147	0,28141
	tau	0,02486	2,5092E-4

Figure 88. *Representative spectrum of the decays of the lifetimes of Λ-(**L1**)$_2$.Eu][Et$_3$NH] in deuterated and non-deuterated methanol.*

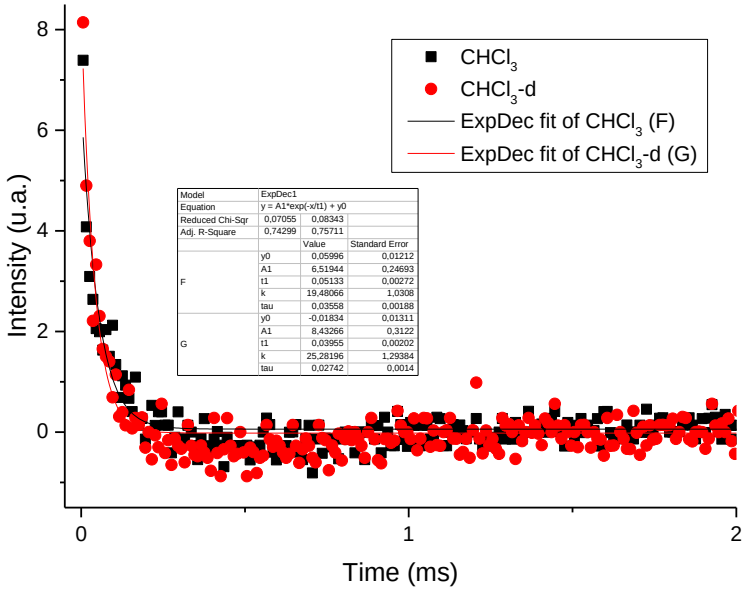

Model	ExpDec1		
Equation	y = A1*exp(-x/t1) + y0		
Reduced Chi-Sqr	0,07055	0,08343	
Adj. R-Square	0,74299	0,75711	
		Value	Standard Error
F	y0	0,05996	0,01212
	A1	6,51944	0,24693
	t1	0,05133	0,00272
	k	19,48066	1,0308
	tau	0,03558	0,00188
G	y0	-0,01834	0,01311
	A1	8,43266	0,3122
	t1	0,03955	0,00202
	k	25,28196	1,29384
	tau	0,02742	0,0014

Figure 89. *Representative spectrum of the decays of the lifetimes of Λ-(**L1**)$_2$.Eu][Et$_3$NH] in deuterated and non-deuterated chloroform.*

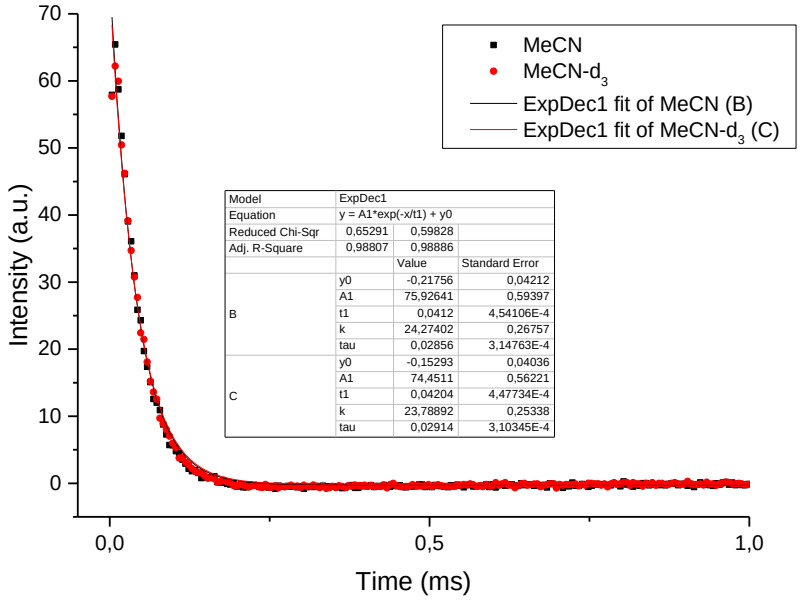

Model	ExpDec1		
Equation	y = A1*exp(-x/t1) + y0		
Reduced Chi-Sqr	0,65291	0,59828	
Adj. R-Square	0,98807	0,98886	
		Value	Standard Error
B	y0	-0,21756	0,04212
	A1	75,92641	0,59397
	t1	0,0412	4,54106E-4
	k	24,27402	0,26757
	tau	0,02856	3,14763E-4
C	y0	-0,15293	0,04036
	A1	74,4511	0,56221
	t1	0,04204	4,47734E-4
	k	23,78892	0,25338
	tau	0,02914	3,10345E-4

Figure 90. *Representative spectrum of the decays of the lifetimes of Λ-(**L2**)$_2$.Eu][Et$_3$NH] in deuterated and non-deuterated acetonitrile.*

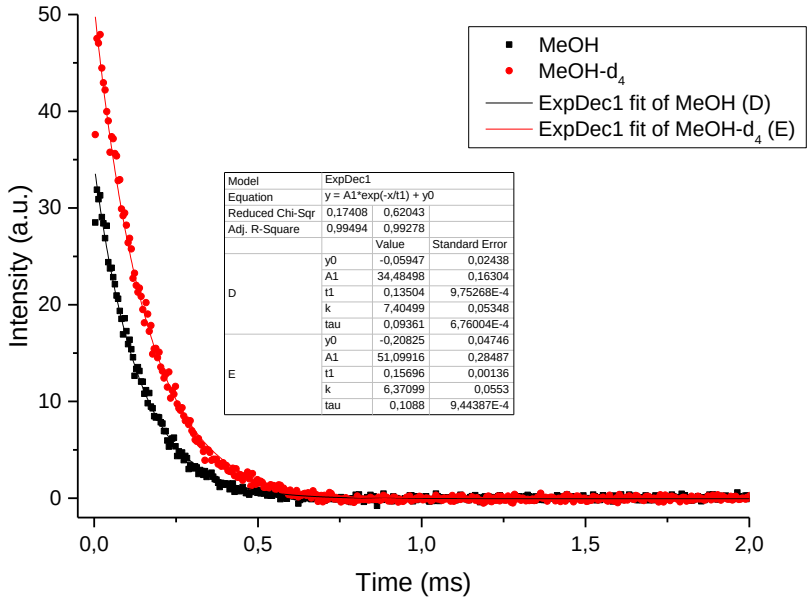

Model	ExpDec1		
Equation	y = A1*exp(-x/t1) + y0		
Reduced Chi-Sqr	0,17408	0,62043	
Adj. R-Square	0,99494	0,99278	
		Value	Standard Error
D	y0	-0,05947	0,02438
	A1	34,48498	0,16304
	t1	0,13504	9,75268E-4
	k	7,40499	0,05348
	tau	0,09361	6,76004E-4
E	y0	-0,20825	0,04746
	A1	51,09916	0,28487
	t1	0,15696	0,00136
	k	6,37099	0,0553
	tau	0,1088	9,44387E-4

Figure 91. *Representative spectrum of the decays of the lifetimes of Λ-(**L2**)$_2$.Eu][Et$_3$NH] in deuterated and non-deuterated methanol.*

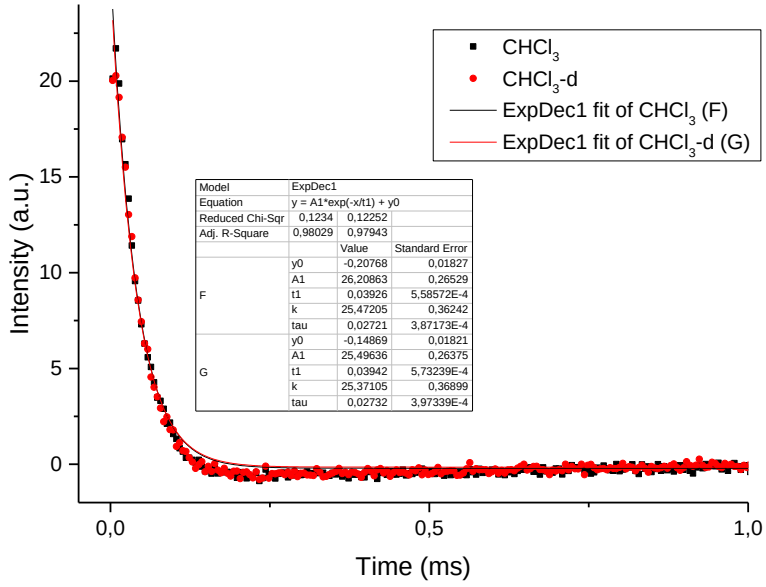

Model	ExpDec1		
Equation	y = A1*exp(-x/t1) + y0		
Reduced Chi-Sqr	0,1234	0,12252	
Adj. R-Square	0,98029	0,97943	
		Value	Standard Error
F	y0	-0,20768	0,01827
	A1	26,20863	0,26529
	t1	0,03926	5,58572E-4
	k	25,47205	0,36242
	tau	0,02721	3,87173E-4
G	y0	-0,14869	0,01821
	A1	25,49636	0,26375
	t1	0,03942	5,73239E-4
	k	25,37105	0,36899
	tau	0,02732	3,97339E-4

Figure 92*. Representative spectrum of the decays of the lifetimes of Λ-(**L2**)$_2$.Eu][Et$_3$NH] in deuterated and non-deuterated chloroform.*